Studies on Nonlinear Dispersive Water Waves

Thesis by

Wendong Qu

In Partial Fulfillment of the Requirements

for the Degree of

Doctor of Philosophy

California Institute of Technology

Pasadena, California

June 2000

(Submitted May 17, 2000)

© 2000
Wendong Qu
All Rights Reserved

Acknowledgements

My sincere thanks and respect go to my advisor, Professor Theodore Yao-Tsu Wu, for his valuable guidance throughout my graduate study, his introduction and encouragement to this versatile research field of nonlinear wave, and his enthusiasm and insight in scientific development. I have been greatly benefited from his experience, guidance and his previous work in this field. I gratefully acknowledge the many contributions Dr. Wu has made to my personal and scientific development.

Special thanks are due to Dr. Thomas Yizhao Hou for his friendly help in the computation and many valuable discussions on my research studies. I would also like to thank Dr. Norden E. Huang for his help on my personal and scientific development.

I am very grateful to Professors Christopher E. Brennen, Thomas K. Caughey, Thomas Y. Hou, Anthony Leonard and Fredric Raichlen, who served on my committee, and my thanks go to all professors who have ever taught me in Caltech.

I am deeply indebted to the past and present "family" members of the Engineering Science group for many helpful discussions and collaboration, especially to Dr. John Kao, Dr. Zheng Shen, Dr. Tao Wang and Dr. Hua Liu. Their friendship made my graduate study at Caltech colorful and meaningful.

My special thanks are due to my parents and my brother for all they did for me.

I dedicate this thesis to my wife, Lily, for her love and support.

I appreciate the enjoyment my little son Alexander brings to me, my love to him is for ever.

Abstract

This study investigates the phenomena of evolution of two-dimensional, fully nonlinear, fully dispersive, incompressible and irrotational waves in water of uniform depth in single and in double layers. The study is based on an exact fully nonlinear and fully dispersive (FNFD) wave model developed by Wu (1997, 1999a). This FNFD wave model is first based on two exact equations involving three variables all pertaining to their values at the water surface. Closure of the system of model equations is accomplished either in differential form, by attaining a series expansion of the velocity potential, or in integral form by adopting a boundary integral equation for the velocity field.

A reductive perturbation method for deriving asymptotic theory for higher-order solitary waves is developed using the differential closure equation of the FNFD wave theory. Using this method, we have found the leading 15th-order solitary wave solutions. The solution is found to be an asymptotic solution which starts to diverge from the 12th-order so that the 11th-order solution appears to provide the best approximation to the fully nonlinear solitary waves, with a great accuracy for waves of small to moderately large amplitudes.

Two numerical methods for calculating unsteady fully nonlinear waves, namely, the FNFD method and the Point-vortex method, are developed and applied to compute evolutions of fully nonlinear solitary waves. The FNFD method, which is based on the integral closure equation of Wu's theory, can provide good performance on computation of solitary waves of very large amplitude. The Point-vortex method using the Lagrange markers is very efficient for computation of waves of small to moderate amplitudes, but has intrinsic difficulties in computing waves of large amplitudes. These two numerical methods are applied to carry out a comparative study of interactions between solitary waves.

Capillary-gravity solitary waves are investigated both theoretically and numeri-

cally. The theoretical study based on the reductive perturbation method provides asymptotic theories for higher-order capillary-gravity solitary waves. A stable numerical method (FNFD) for computing exact solutions for unsteady capillary-gravity solitary waves is developed based on the FNFD wave theory. The results of the higher-order asymptotic theories compare extremely well with those given by the FNFD method for waves of small to moderate amplitudes.

A numerical method for computing unsteady fully nonlinear interfacial waves in two-layer fluid systems is developed based on the FNFD model. The subcritical and supercritical cases can be clearly distinguished by this method, especially for waves of amplitudes approaching the maximum attainable for the fully nonlinear theory.

Contents

List of Figures

List of Tables

Chapter 1 Introduction

The phenomena of water waves have attracted great attention from people of all ages and the subject's extent and diversity are enormous. The different types of waves in water, such as ripples on a quiet pond, breaking waves on a beach, billows on a stormy sea, geophysical waves and devastating tsunamis, are truly extensive. The salient features of the wave properties can often be perceived qualitatively with attentive naked eyes. Of the various wave phenomena found in nature, water waves have the distinction in exhibiting some basic properties that can rarely be matched by other kinds of waves. First, dispersive effects on water waves make their (phase) velocity vary with their wavelength, which in turn may differ considerably from the (group) velocity at which wave energy propagates. In deep water, the group velocity varies from three-halves of phase velocity for ripples to one-half the phase velocity for gravity waves. For long waves, the length of which is large compared to water depth, the dispersive effects, though slight in this case, can accumulate, in time, to noticeable margin as shown by the length increment of tsunami waves propagating across the Pacific. In addition, water waves can give conspicuous displays of the nonlinear effects (making linear superposition of solutions no longer a solution) as is evident in breaking roll waves on the beach. However, with the dispersive (wave-separating) and nonlinear (wave-focusing) effects kept in a proper balance, moderately steep waves are found to propagate on shallow water, keeping permanent in shape. This was first discovered by John Scott Russell (1844) who observed in August 1837. In what he claimed to be the happiest day of his life, he saw a boat, drawn along a narrow channel by a pair of horses, suddenly stopped. A single, hump-like mass of water detached itself from the boat and continued its course at eight to nine miles an hour without change of form or diminution of speed. In recent decades of the colorful modern history of pure and applied mathematics, physics, engineering science, biology and other disciplines, the same type of weakly nonlinear and weakly dispersive wave phenomena, now known

under the blanket term of *solitons*, seem to occur almost universally.

Different fundamental theories have been developed to interpret and predict the properties of water waves. These theories may be classified according to the specific regimes of the key physical parameters involved and on which regime they are based. Of the rich ensemble of physical parameters involved, two key parameters are essential, namely

$$\alpha = a/h \ , \qquad \epsilon = h/\lambda \ , \tag{1.1}$$

which represent, respectively, the nonlinear and dispersive effects for characterizing waves of amplitude a and typical length λ in water of typical depth h. Theoretical modeling of water waves becomes greatly more difficult when additional relevant factors are considered such as the extension from two to three spatial dimensions and another from uniform (h =const.) to nonuniform medium (with h varying in space and time). In fact, it takes decades of efforts to progress from a simple case to a more general one. Nevertheless, needs for generalizations do exist for various reasons. And in this respect, the nonlinearity factor α, the dispersion factor ϵ, and the medium geometry (nondimensional h, whether uniform or varying in space and time) can be said as the *three primary parameters* for modeling water waves. In addition, there are other parameters including the Froude number $F = U/\sqrt{gh}$ (for measuring the gravity effect ρgh relative to the inertial effect ρU^2 for motions with typical velocity U of fluid of density ρ under gravity acceleration g), the Weber number $U/\sqrt{\gamma/l}$, (for scaling the surface tension effect $\rho\gamma/l$ relative to the inertia effect, γ being the kinematic surface tension), the specific fluid density variation $\Delta\rho/\rho$ for density-stratified fluids, and perhaps also the frame rotation effect for rotating flows, etc. These parameters need be considered when their effects play a role in the problem in question. It is in this framework and scope that modeling of water waves is constituted, as has been much illuminated by Lin & Clark (1959), J.D. Cole (1968) and Sir James Lighthill (1978).

This study is focused on incompressible irrotational two-dimensional waves in water of uniform depth in a single layer and in double layers. Two classes of classical

theory, the weakly nonlinear and weakly dispersive (WNWD) wave theory, and the fully nonlinear and weakly dispersive (FNWD) wave theory for shallow water waves have been developed in literature, as recently reviewed by WU (1999a).

The WNWD theory was developed by the pioneering works of Boussinesq (1871, 1872), Rayleigh (1876) and Korteweg & de Vries (1895) for interpreting the solitary wave discovered by Russell (1844). Boussinesq (1872) found that the assumption of $\alpha = O(\epsilon^2) \ll 1$ provides a well balanced role between the nonlinear and dispersive effects for solitary waves to exist. Based on this assumption, Laitone (1960) used the method of Friedrichs (1948) to develop a solitary wave theory to second-order. Chappelear (1962) and Grimshaw (1971) further extended it to third-order. From a different approach, Fenton (1972) found a solution for solitary wave up to the ninth-order by assuming a series expansion for the wave elevation, with the coefficients numerically calculated. This solution has been subsequently further numerically extended by Longuet-Higgins & Fenton (1974) to 14th-order. So far no exact asymptotic theory by systemic analytic expansion has been known to exist for the solitary wave of order higher than the third.

For unidirectional waves of the Korteweg-de Vries (KdV) family in particular, the original KdV equation has been shown by Zabusky & Kruskal (1965) to possess remarkable properties implying that the KdV equation admits not only one, but N solitary waves, for $N = 1, 2, \cdots$, of arbitrary amplitudes, propagating and interacting on one real line and conserves all their entities, for which properties the term *soliton* is coined for such solitary waves.

The subject of water waves with parameters within the regime of the FNWD class has been of considerable interest in various aspects. The first order theory is known as Airy's model which has a certain range of validity in subcritical and supercritical regimes but fails in supporting solitary waves of permanent form in the transcritical regime. This shortcoming is due to a mismatched account on the balance between the effects of nonlinearity and dispersion. For modeling long waves of finite amplitude in layered media, Green & Naghdi (1976) assumed $\alpha = O(1)$ and $\epsilon \ll 1$, so that ϵ is the only small parameter adopted in deriving the Green-

Naghdi model. Along this direction, recent advances have been made by Ertekin et al. (1984, 1986), Choi (1995), Choi & Camassa (1996), and others for modeling nonlinear and dispersive wave motions in a single-layer or two-layer fluid, with intent to achieve higher accuracy than existing models. This demonstrates that various theories can be sought by making analysis based on different parametric regimes to obtain different approximations to serve as differing theoretical models, provided they be duly validated under the original premises.

The literature on numerical computation of unsteady gravity waves is rather extensive. A great number of previous studies can be categorized as the class of boundary-integral method using Lagrange's markers, including the works of Longuet-Higgins & Cokeket (1976), Vinje & Brevig (1981), Baker, Meiron & Orszag (1982), Roberts (1983), and Dold (1992). Beale, Hou & Lowengrub (1996) proved the convergence of a boundary integral method for deep water waves. Most of the numerical schemes for computing nonlinear shallow water waves found in literature can be applied for simulating evolution of shallow water waves of small to moderately large amplitudes. However, it is a great challenge to develop a stable and accurate numerical method for computing fully nonlinear unsteady solitary waves of large amplitude, especially for waves of amplitudes very close to that of the highest wave (which has an inner angle of 120° at the wave crest), due to a strong singularity at the crest.

A simpler but still challenging approach is to compute the fully nonlinear solitary waves of permanent shape. Cooker (1990) computed the exact stationary solitary wave solutions by using the method of Tanaka (1986). Wu & Kao (2000) obtained an exact solution for steady exact solitary wave with a high accuracy by evaluating more accurately the effects due to the irrational singularity of the asymptotic solution at the physical infinity.

There are nevertheless needs for modeling fully nonlinear, fully dispersive water wave phenomena, as for further developing the subject and for practical applications that would require the nonlinear and dispersive effects retained in the model to play their full exact physical roles. In a series of studies, Wu (1997, 1998a,b,c, 1999a, 2000) developed an exact inviscid theory for evaluating three-dimensional fully nonlinear,

fully dispersive (FNFD), incompressible, irrotational water waves in water of uniform or variable depth in single layer or in double layers. This exact theory is first built on two basic equations, one being the free-surface kinematic condition, and the other the horizontal momentum equation projected onto the free surface. These two partial differential equations are both exact but involve three unknowns, the horizontal velocity, $\hat{u}$, and the vertical velocity $\hat{w}$ at the free surface (in two horizontal dimensions) and the water surface elevation, ζ. Closure of the system is accomplished either in differential form by attaining a series expansion of the velocity potential or in integral form by adopting a boundary integral equation for the velocity field. This FNFD theory provides both analytical facilities and computational efficiency that a theoretical model can provide for resolving nonlinear water wave problems. In versatility, this theory can be approximated to various degrees of validity to agree with existing theories as special cases for predicting nonlinear dispersive water wave phenomena pertaining to their specific parametric regimes, as pointed out by Wu (1999a).

This study applies Wu's exact theory to theoretical and numerical investigation of various problems in two-dimensional shallow water waves. In chapter 2, Wu's FNFD model for describing the properties of evolution of nonlinear shallow water waves is reviewed for completeness of this thesis. The two exact equations are derived from the basic Euler equations. The closure of the system are accomplished in both differential form by performing a series expansion of the velocity potential and in integral form by adopting a boundary integral equation based on Cauchy's integral theorem for the velocity potential; either of them suffices to complete the set of modal equations.

The differential form of closure is used to derive higher-order asymptotic theories of solitary waves. Wu (2000) developed an asymptotic theory using the free surface elevation and horizontal velocity at the free surface as the basic unknowns, up to $O(\alpha^3)$ for solitary waves which are in agreement with the results of Korteweg-de Vries, Laitone, Chappelear and Grimshaw. He pointed out that regardless of the various basic velocity used as a variable (jointly with the unknown free surface elevation) in the derivation, such as the velocity on the bottom (used by Rayleigh (1871)) and the depth-mean velocity (used by Boussinesq (1871), Korteweg and de

Vries (1895), Green & Naghdi (1976) and Wu (1981)), different perturbation theories should provide the same solution for the free surface elevation. Finding the higher-order asymptotic solutions for solitary waves is an interesting problem because it will illustrate a theoretical proof of existence of the solitary wave to the Euler equations, at least in an asymptotic sense. However, the formidable algebra may be responsible for confining researchers from going further to orders higher than $O(\alpha^3)$. A reductive perturbation method is developed for pursuing asymptotic higher-order solitary wave solutions using the surface elevation and the bottom velocity as the basic unknowns based on the differential form of Wu's FNFD theory in chapter 3. This approach simplifies the derivation to a level that highter-order solution can be evaluated by a PC using a carefully designed Mathematica code. Solitary wave solutions have thus been found in this study up to $O(\alpha^{15})$. Comparisons between the results of the present FNFD theory and those of the higher-orders asymptotic theory indicate that the asymptotic solutions produce a sequence of increasingly improved approximations to the exact FNFD solution, with an increasing accuracy for solitary waves of moderately large to very large amplitudes, before the asymptotic series solution diverges at the 12th-order.

The integral closure equations provide an efficient way to develop a numerical method using the Euler mesh. In chapter 4 we provide two stable and efficient numerical schemes, namely, (i) the FNFD method using the integral closure and the Euler mesh for integration, and (ii) the Point-vortex method using the Lagrange markers, for computing evolution of unsteady fully nonlinear shallow water waves. The FNFD method using an Euler mesh is efficient and stable for computation of the asymptotic properties of solitary waves of amplitudes over nearly the whole range, even very close to the highest wave. In comparison, the Point-vortex method provides a good performance on computing interactions between solitary waves. Various aspects of these two numerical methods are studied to provide a compatible numerical method which is stable and convergent. We present the numerical results and an appraisal of the accuracy of both schemes in chapter 5.

With the accuracy established, we apply the numerical methods to study the in-

teractions between solitary waves in chapter 6. In chapter 7, we investigate capillary-gravity solitary waves under the effects of both gravity and surface tension. Solutions of higher-order asymptotic theories and numerical solutions of the FNFD theory are obtained and discussed. In chapter 8 we extend the numerical exact FNFD method to study interfacial waves in fluids of double layers. The numerical results of large-time asymptotic wave motion are found in excellent agreement with the fully nonlinear stationary solutions given by the method for steady wave motions.

Chapter 2 A fully nonlinear long-wave theory for modeling shallow water waves

2.1 The surface-projected basic equations

To facilitate evaluation of the general properties of free surface waves propagating in water of finite depth, we introduce the following model for describing the general class of fully nonlinear and fully dispersive (FNFD) water waves. We consider the motion of two-dimensional waves in water of uniform depth in a single layer. The fluid moves with velocity (u, v) referred to the (x, y)-coordinates fixed in the flow field bounded below by a rigid horizontal bottom at $y = -h$ and above by the free surface at $y = \zeta(x, t)$, measured from its rest level at $y = 0$ at time t as sketched in Figure 2.1. With the fluid assumed incompressible and inviscid, the motion satisfies the Euler equations of continuity, horizontal and vertical momentum as follows:

$$u_x + v_y = 0, \tag{2.1}$$

$$\frac{du}{dt} = u_t + u\, u_x + v\, u_y = -\frac{1}{\rho}\, p_x, \tag{2.2}$$

$$\frac{dv}{dt} = v_t + u\, v_x + v\, v_y = -\frac{1}{\rho}\, p_y - g, \tag{2.3}$$

where g is the gravitational acceleration, p the pressure and ρ the constant fluid density. Here the subscripts denote partial differentiation. We may assume that the ambient pressure on the free surface is gauged to zero and we ignore the surface tension for a moment to simplify our analysis. The capillary effect will be added on in chapter 7 to study specific problems. The boundary conditions are

$$\hat{v} = \zeta_t + \hat{u}\, \zeta_x, \quad \text{at} \quad y = \zeta(x, t), \tag{2.4}$$

$$\hat{p} = 0 \quad (\text{at} \quad y = \zeta(x, t)), \tag{2.5}$$

$$\underline{v} \;=\; 0 \quad (\text{at } \; y=-h) \tag{2.6}$$

where the hat and the underline bar denote variables at the free surface and at the bottom, respectively.

The momentum equations can be converted into an equation for $(\hat{u}, \zeta)$ as in Wu (1997). For an arbitrary flow variable $f(x,y,t)$, it assumes its free surface value

$$f(x, \zeta(x,t), t) = \hat{f}(x,t), \tag{2.7}$$

and we have for its derivatives, by the chain-rule, the following relations

$$\partial_t \hat{f}(x,t) = (\partial_t f + \frac{\partial f}{\partial y}\, \partial_t \zeta)\Big|_{y=\zeta}, \qquad \partial_x \hat{f}(x,t) = (\partial_x f + \frac{\partial f}{\partial y}\, \partial_x \zeta)\Big|_{y=\zeta}. \tag{2.8}$$

From the above relations we readily deduce, under condition (2.4), that

$$\begin{aligned} \frac{df}{dt}\Big|_{y=\zeta} &= \left(\frac{\partial f}{\partial t} + u\,\frac{\partial f}{\partial x} + v\,\frac{\partial f}{\partial y}\right)_{y=\zeta} \\ &= \hat{f}_t + \hat{u}\;\hat{f}_x - \left[\frac{\partial f}{\partial y}\;(\zeta_t + \hat{u}\;\zeta_x - \hat{v})\right]_{y=\zeta} \\ &= (\partial_t + \hat{u}\;\partial_x)\;\hat{f} = \hat{D}\hat{f}, \end{aligned} \tag{2.9}$$

with operator $\hat{D}$ defined as

$$\hat{D} = \partial_t + \hat{u}\,\partial_x. \tag{2.10}$$

Using these relations, we can project the horizontal momentum equation (2.2) onto the free surface so that

$$\rho\,\hat{D}\hat{u} = -\partial_x p\Big|_{y=\zeta} = -(\partial_x \hat{p} - \frac{\partial p}{\partial y}\Big|_{y=\zeta}\;\zeta_x). \tag{2.11}$$

Combining this equation with the vertical momentum equation (2.3) and conditions (2.4) and (2.5), we have the momentum equations projected onto the free surface as

$$\hat{u}_t + \hat{u}\;\hat{u}_x + [g + \hat{D}^2\zeta]\;\zeta_x = 0. \tag{2.12}$$

This provides an equation for $(\hat{u}, \zeta)$ at the free surface. Although (2.12) involves, superficially, only the variables pertaining to the water surface, it actually has incorporated the vertical momentum equation as well as the kinematic and dynamic conditions at the free surface to yield this equation of an overall equilibrium as pointed out by Wu (1997). Moreover, it is exact. In addition, the kinematic condition at the free surface is as before,

$$\hat{v} = \hat{D}\zeta = \zeta_t + \hat{u}\,\zeta_x. \tag{2.13}$$

So far we have two exact equations that can facilitate modeling time-evolving, two-dimensional, fully nonlinear and fully dispersive water waves, one being the free-surface kinematic condition (2.13) involving $(\hat{u}, \hat{v}, \zeta)$, and the other being the surface projected momentum equation (2.12) for $(\hat{u}, \zeta)$. Closure of this system now requires to find a third equation that relates the three variables $(\hat{u}, \hat{v}, \zeta)$. When it is so closed, the new system will comprise the basic variables $(\hat{u}, \hat{v}, \zeta)$, which are of $(1+1)$-dimensions in (x, t) instead of the $(2+1)$-dimensions in (x, y, t) for the underlying Euler system (2.1)-(2.3). Further, it is important to note that equations (2.12)-(2.13) hold valid regardless of whether or not the flow is irrotational. In this study, however, we shall only consider irrotational water waves so that there exists a velocity potential, $\phi(x, y, t)$, such that $u = \phi_x, v = \phi_y$, and, by (2.1), it satisfies the Laplace equation

$$\phi_{xx} + \phi_{yy} = 0. \tag{2.14}$$

With this equation, closure of (2.12) and (2.13) can be accomplished either in differential form by finding a series expansion of the velocity potential ϕ or in integral form by adopting a boundary integral equation pertaining to (2.14). The closure in differential form will be investigated in this section by performing a series expansion of the velocity potential. The equations will first be scaled to dimensionless form and a series expansion is performed to provide a closure to (2.12) and (2.13). The integral form can provide a method for directly performing numerical computations of exact solutions in the Euler context, as will be studied in section 2.2.

2.1.1 The basic equations in dimensionless form

The same dimensionless variables as those used in Wu (1979) for a single-layer system are adopted here to scale the basic equations in dimensionless form. In the following, * indicates a dimensionless variable, λ is a characteristic wavelength, $c = \sqrt{gh}$ is the wave speed of linear waves on water of depth h, and $\epsilon = h/\lambda$.

We scale the horizontal length by λ, the vertical length by h, time by λ/c, the velocity potential by $c\lambda$, and the velocities (u, v) are scaled by $(c, \epsilon c)$ since

$$v \sim u\,\epsilon \tag{2.15}$$

according to the continuity equation. Thus we have

$$\begin{aligned} &x = x^*\,\lambda, \quad (y, \zeta) = (y^*, \zeta^*)\,h, \quad t = t^*\,\lambda/c, \\ &\phi = \phi^*\,c\lambda, \quad u = u^*\,c, \quad v = \epsilon\,v^*\,c. \end{aligned} \tag{2.16}$$

Substituting (2.16) into (2.12)-(2.14), and omitting the superscript *, we obtain the Laplace equation in dimensionless form as

$$\phi_{yy} + \epsilon^2 \phi_{xx} = 0, \tag{2.17}$$

and the free-surface projected dynamic equation as

$$\hat{u}_t + \hat{u}\hat{u}_x + [1 + \epsilon^2 \hat{D}^2 \zeta]\zeta_x = 0. \tag{2.18}$$

The kinematic equation at the free surface remains unchanged, namely,

$$\hat{v} = \hat{D}\zeta = \zeta_t + \hat{u}\,\zeta_x. \tag{2.19}$$

The boundary condition at the bottom now becomes

$$\underline{v} = 0, \quad \text{at } y = -1. \tag{2.20}$$

2.1.2 The series expansion of ϕ; closure in differential form

We now seek a series solution of (2.17), (2.18) and (2.19) under condition (2.20). To begin with, we tacitly assume ϵ to be small ($0 < \epsilon \ll 1$), which applies to the general class of long waves (with $h \ll \lambda$), so that the velocity potential takes the following series form:

$$\phi(x, y, t; \epsilon) = \sum_{n=0}^{\infty} \phi_n(x, y, t)\ \epsilon^{2n}. \tag{2.21}$$

Substituting (2.21) into (2.17), we have

$$(\phi_0)_{yy} = 0, \quad (\phi_n)_{yy} = -(\phi_{n-1})_{xx}, \quad (n = 1, 2, 3, \ldots). \tag{2.22}$$

Integrating this set of recurrence equations and applying the boundary condition at the bottom, (2.20), we can write the solution for ϕ as:

$$\phi(x, y, t; \epsilon) = \sum_{n=0}^{\infty} (-1)^n\ \epsilon^{2n} \frac{(y+1)^{2n}}{(2n)!} \frac{d^{2n}}{dx^{2n}} \phi_0(x, t). \tag{2.23}$$

From this expression for ϕ, we can compute the horizontal velocity at the bottom as

$$\underline{u}(x, t) = \frac{d}{dx}\phi|_{y=-1} = \frac{d}{dx}\phi_0(x, t), \tag{2.24}$$

and the velocity conponents at the free surface by

$$\hat{u}(x, t) = \frac{d}{dx}\phi|_{y=\zeta} = \sum_{n=0}^{\infty} (-1)^n\ \epsilon^{2n} \frac{(\zeta+1)^{2n}}{(2n)!} \frac{d^{2n}}{dx^{2n}} \underline{u}(x, t), \tag{2.25}$$

$$\hat{v}(x, t) = \frac{1}{\epsilon^2}\frac{d}{dy}\phi|_{y=\zeta} = \sum_{n=1}^{\infty} (-1)^n\ \epsilon^{2n-2} \frac{(\zeta+1)^{2n-1}}{(2n-1)!} \frac{d^{2n-1}}{dx^{2n-1}} \underline{u}(x, t). \tag{2.26}$$

Here, $\hat{u}$ and $\hat{w}$ are unique functions of $(\underline{u}, \zeta)$ as determined by (2.25) and (2.26). Finally, by examining the validity of this solution, we find that the original assumption of ϵ being small can be relaxed provided $\underline{u}$ and all its derivatives exist and are bounded within the flow domain because then all the series in (2.23)-(2.26) converge absolutely and uniformly with an infinite radius of convergence. Upon substituting these relations for $\hat{u}$ and $\hat{v}$ into (2.18) and (2.19), we obtain the model equations for

evaluating fully nonlinear and fully dispersive gravity waves on water of uniform depth in terms of $(\underline{u}, \zeta)$. This model will be used to determine the solutions to higher-order for solitary waves in chapter 3.

2.2 Closure of the system in integral form

Instead of using a series solution of ϕ given above for closure, we may also adopt the solution expressed in terms of a boundary integral to close the basic equations (2.12) and (2.13). The integral closure equations are useful for direct applications to numerical computation.

For two-dimensional irrotational water waves, the complex velocity $w(z,t) = u(x,y,t) - iv(x,y,t)$ is an analytic function of the complex coordinate variable $z = x + i\,y$ at any time instant t, where $i = \sqrt{-1}$, and we have Cauchy's integral formula,

$$i\Omega(z)w(z,t) = \oint_{\partial\mathcal{D}} \frac{w(z',t)}{z'-z}dz', \tag{2.27}$$

where the contour is counterclockwise along the boundary $\partial\mathcal{D}$ of the flow domain $\mathcal{D}$, $\Omega = 2\pi$ for $z \in \mathcal{D}$, $\Omega = \pi$ for $z \in \partial\mathcal{D}$ (which is assumed to be a smooth contour), and $\Omega = 0$ for $z \ni \mathcal{D} + \partial\mathcal{D}$. Further, for $z \in \partial\mathcal{D}$, the integral assumes its Cauchy principal value.

By virtue of condition (2.20) for the special case of a horizontal bottom at hand, the flow domain $\mathcal{D}$ can be continued analytically by Schwarz's principle of symmetry,

$$w(z^* - 2i) = w^*(z), \tag{2.28}$$

with * denoting the complex conjugate, so that for z on the free surface,

$$u(x,\zeta) = u(x,-\zeta-2), \quad v(x,\zeta) = -v(x,-\zeta-2), \tag{2.29}$$

here with $\mathcal{D}$ continued to its extended domain

$$\mathcal{D}_e : (-2 - \zeta < y < \zeta, -\infty < x < \infty).$$

Consequently, we may revise the original boundary $\partial\mathcal{D}$ into $\partial\mathcal{D}_e$, the boundary of $\mathcal{D}_e$, thus curtailing the need of calculating velocity $\underline{u}(x) = u(x, -1)$ on the horizontal bottom. In fact, taking $\mathcal{D}_e$ either as a single cell in case of a periodic flow (e.g., cnoidal-type waves), or as the entire flow field of a local wave, so that its boundary $\partial\mathcal{D}_e$ consists of four parts as shown in Figure 2.2. The contributions from the two vertical paths cancel by virtue of the flow being periodic or assumed at rest at infinity. The remaining line integrals along the free surface and its image may be written, on account of the symmetry, as

$$\pi i\, w(\hat{z}) = \int_{-\infty}^{\infty} \frac{w(\hat{z'})}{\hat{z} - \hat{z'}} d\,\hat{z'} - \int_{-\infty}^{\infty} \frac{w^*(\hat{z'})}{\hat{z} - \hat{z'}^* + 2\,i} d\,\hat{z'}^*, \tag{2.30}$$

where $\hat{z} = x + i\,\zeta(x), w(\hat{z}) = \hat{u} - i\hat{v}$. Either the real, or, alternatively, the imaginary part of (2.30) is sufficient to provide the required closure equation to join (2.12) and (2.13) in constituting the complete model system.

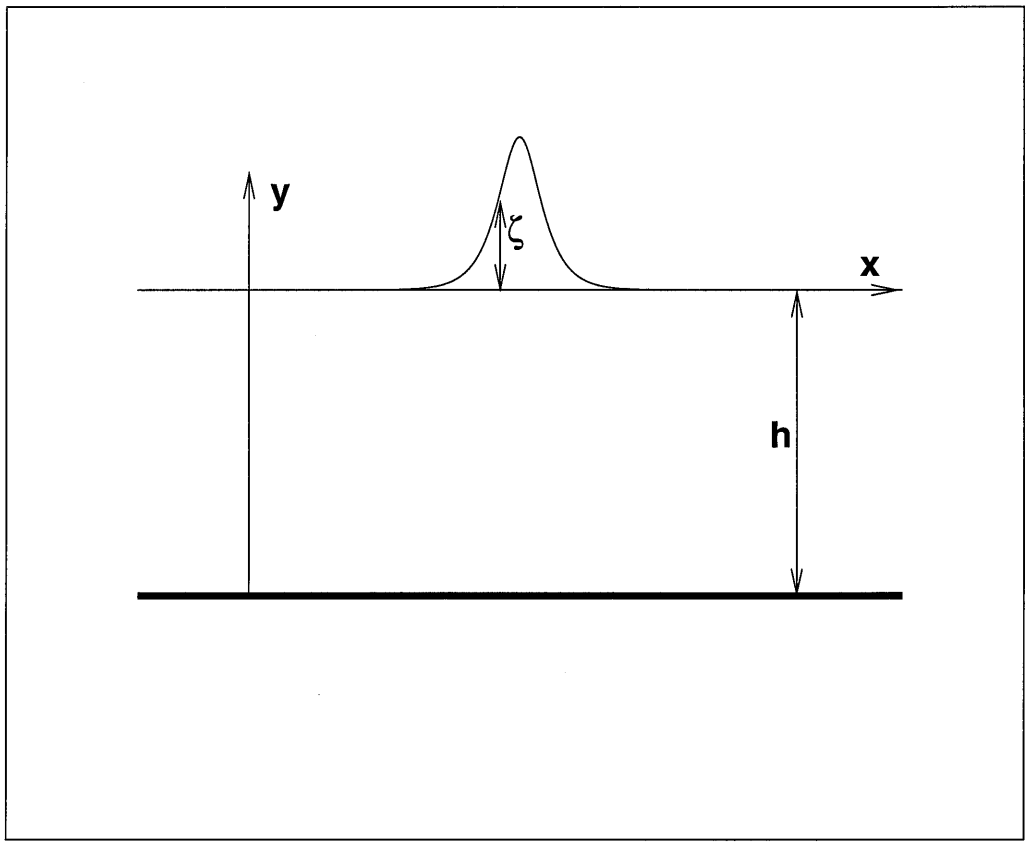

Figure 2.1: A sketch of a one-layer fluid system with a flat bottom.

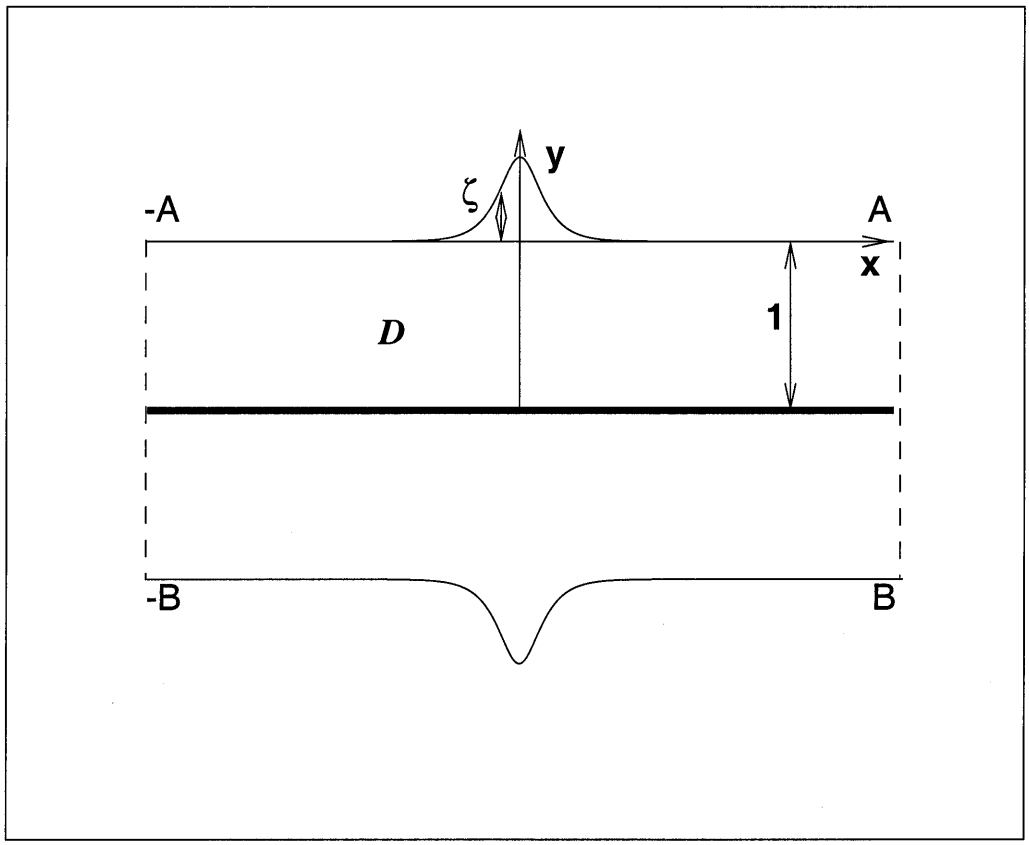

Figure 2.2: A sketch of the extended domain for a one-layer fluid system with a flat bottom.

Chapter 3 Higher-order solitary waves

The weakly nonlinear and weakly dispersive theory has been adopted to study solitary waves over a long history, Boussinesq (1872) and Rayleigh (1876) found the hyperbolic-secant-squared solution for the free surface elevation. Laitone (1960) used the method of Friedrichs's (1948) to obtain the second-order solution. Chappelear (1962) and Grimshaw (1970) found the third-order solution. In these studies, the free surface elevation and a different version of the velocity (such as the velocity on the bottom used by Rayleigh (1871), and the depth-mean velocity used by Boussinesq (1871) and Korteweg and de Vries (1895)) are used as the basic unknowns to establish the asymptotic theory. Wu (2000) provided a unified theory for evaluating fully nonlinear and full dispersive water waves which has the WNWD model as a special case. He recovered the first three-order solutions for solitary waves, using the surface elevation and the horizontal velocity at the free surface as the basic unknowns and yielding results in agreement with the previous contributions. Finding the properties of a higher-order asymptotic theory for solitary waves and studying the convergence of higher-order solutions to a fully nonlinear flow model is an interesting problem to which the answer could illustrate a theoretical proof of existence of solitary waves in asymptote to the Euler equations. For steady solitary waves, Fenton (1972) developed an exact operator equation to calculate the coefficients of an assumed series form of solution to give a ninth-order solution. With convergence improvement techniques, refined approximations were obtained numerically, including the solitary wave profile, wave speed, and other physical quantities. This solution has been subsequently further numerically extended by Longuet-Higgins & Fenton (1974) to 14th-order. So far no exact asymptotic theory by systematic analytic expansion has been known to exist for the solitary wave of order higher than the third. In this chapter, we study the higher-order solitary waves using the differential closure form developed in the last chapter. We provide a reductive perturbation method to construct exact higher-order

asymptotic solitary wave solutions in the parametric family of Boussinesq, namely, by ($\alpha = \epsilon^2$), see equation (3.3). This method can provide perturbation solutions to arbitrary higher order. A general solution is obtained up to $O(\alpha^{15})$ by applying this reductive perturbation method. As a result of great significance, the solution is found to be an asymptotic solution which starts to diverge from the 12th-order so that the 11th-order solution appears to provide the best approximation to the fully nonlinear solitary waves, nonetheless, with a great accuracy for waves of small to moderately large amplitudes.

3.1 The perturbation method

In modeling weakly nonlinear and weakly dispersive long waves in shallow water, it is known to be necessary to adopt two key parameters, namely

$$\alpha = \frac{a}{h}, \quad \epsilon = \frac{h}{\lambda}, \tag{3.1}$$

representing, respectively, the nonlinear and dispersive effects for characterizing a wave of amplitude a and typical length λ in water of rest depth h. Boussinesq (1872) found that the assumption of

$$\alpha = O(\epsilon^2) \ll 1 \tag{3.2}$$

provides a well balanced role between α and ϵ for solitary waves to exist. We will follow this assumption to find the leading and higher order solitary wave solutions, and achieve explicit results up to order $O(\alpha^{15})$. By assigning

$$\alpha = \epsilon^2, \tag{3.3}$$

we obtain the higher-order Boussinesq family model equations from (2.25), (2.26), (2.18) and (2.19) as follows:

$$\hat{u}(x,t) = \sum_{n=0}^{\infty} (-1)^n \, \alpha^n \frac{(\zeta+1)^{2n}}{(2n)!} \frac{d^{2n}}{dx^{2n}} \, \underline{u}(x,t), \tag{3.4}$$

$$\hat{v}(x,t) = \sum_{n=1}^{\infty} (-1)^n \, \alpha^{n-1} \frac{(\zeta+1)^{2n-1}}{(2n-1)!} \frac{d^{2n-1}}{dx^{2n-1}} \, \underline{u}(x,t), \tag{3.5}$$

$$\hat{u}_t + \hat{u}\hat{u}_x + [1 + \alpha \hat{D}^2 \zeta]\zeta_x = 0, \tag{3.6}$$

$$\hat{v} = \zeta_t + \hat{u}\,\zeta_x. \tag{3.7}$$

For waves of (1+1)-dimension in (x,t) progressing in a uniform medium and keeping permanent in shape, the flow is characterized by variables of the form

$$f(x,t) = f(\theta), \tag{3.8}$$

where θ is the *phase function* defined by

$$\theta = k\,(x - c\,t), \tag{3.9}$$

in which c is an undetermined wave velocity and k is the corresponding wave number. Both c and k are a part of the solution and they turn out to be amplitude dependent. In this moving frame fixed with the wave crest, we have

$$\frac{\partial}{\partial x} = k\,\frac{d}{d\theta}, \quad \frac{\partial}{\partial t} = -c\,k\,\frac{d}{d\theta}. \tag{3.10}$$

Applying these relations in (3.4)-(3.7), we obtain the following system of ordinary differential equations

$$(\hat{u}-c)\,\hat{u}' + \left\{1 + \alpha\,k^2\,\left[(\hat{u}-c)^2\,\zeta'' + \zeta'\,\hat{u}'\,(\hat{u}-c)\right]\right\}\,\zeta' = 0, \tag{3.11}$$

$$\hat{v} - k\,(\hat{u}-c)\,\zeta' = 0, \tag{3.12}$$

where the prime denotes the operator $d/d\theta$, and

$$\hat{u} = \sum_{n=0}^{\infty} (-1)^n \, \alpha^n \, \frac{(\zeta+1)^{2n}}{(2n)!} \, k^{2n} \, \underline{u}^{(2n)}, \tag{3.13}$$

$$\hat{v} = \sum_{n=1}^{\infty} (-1)^n \, \alpha^{n-1} \, \frac{(\zeta+1)^{2n-1}}{(2n-1)!} \, k^{2n-1} \, \underline{u}^{(2n-1)}. \tag{3.14}$$

In (3.11) we have made use of

$$\hat{D}^2\,\zeta = \hat{D}(\hat{D}\,\zeta) = k^2\,[(\hat{u}-c)d/d\theta]^2\;\;\zeta. \tag{3.15}$$

Equation (3.11) can be integrated once to yield

$$\zeta + \frac{\hat{u}^2}{2} - c\;\hat{u} + \alpha\;k^2\;\frac{(\hat{u}-c)^2}{2}\;(\zeta')^2 = 0, \tag{3.16}$$

where the integration constant vanishes for solitary waves by virtue of the rest conditions at infinity (or takes a certain constant for evaluating cnoidal waves). For the free surface elevation, ζ, and the bottom velocity, $\underline{u}$, we assume the following series expansion,

$$\zeta(\theta) \;=\; \sum_{n=1}^{\infty}\zeta_n(\theta)\;\alpha^n, \tag{3.17}$$

$$\underline{u}(\theta) \;=\; \sum_{n=1}^{\infty}u_n(\theta)\;\alpha^n. \tag{3.18}$$

Following Stokes, we further let k and c each assume a series expansion as

$$k \;=\; k_0\;K = k_0\;(1+\sum_{n=1}^{\infty}k_n\;\alpha^n), \tag{3.19}$$

$$c \;=\; \sum_{n=0}^{\infty}c_n\;\alpha^n. \tag{3.20}$$

Substituting these series expansions into (3.12)-(3.14) and (3.16), we obtain the following equations:

$$\hat{v} - (k_0\;(1+\sum_{n=1}^{\infty}k_n\;\alpha^n))\;(\hat{u} - (\sum_{n=0}^{\infty}c_n\;\alpha^n))\;\zeta' = 0, \tag{3.21}$$

$$\zeta + \frac{\hat{u}^2}{2} - (\sum_{n=0}^{\infty}c_n\;\alpha^n)\;\hat{u} + \alpha\;(k_0\;(1+\sum_{n=1}^{\infty}k_n\;\alpha^n))^2\;\frac{(\hat{u}-c)^2}{2}\;(\zeta')^2 = 0, \tag{3.22}$$

$$\hat{u} = \sum_{n=0}^{\infty}(-1)^n\;\alpha^n\;\frac{(\zeta+1)^{2n}}{(2n)!}\;(k_0\;(1+\sum_{n=1}^{\infty}k_n\;\alpha^n))^{2n}\;\underline{u}^{(2n)}, \tag{3.23}$$

$$\hat{v} = \sum_{n=1}^{\infty}(-1)^n\;\alpha^{n-1}\;\frac{(\zeta+1)^{2n-1}}{(2n-1)!}\;(k_0\;(1+\sum_{n=1}^{\infty}k_n\;\alpha^n))^{2n-1}\;\underline{u}^{(2n-1)}, \tag{3.24}$$

together with the series in (3.17) and (3.18). Grouping equations (3.21)-(3.24) to different orders of α, we obtain approximate representations, accurate to successive orders of α, of the exact model equations (2.25), (2.26), (2.18) and (2.19).

3.2 Higher-order asymptotic solutions for solitary waves

3.2.1 First order–$O(\alpha)$

We proceed to determine the solutions of (3.21)-(3.24), order by order. The leading order equations of (3.21)-(3.24) to $O(\alpha)$ are given by

$$\zeta_1 - c_0\, u_1 = 0, \tag{3.25}$$

$$c_0\, \zeta_1 - u_1 = 0, \tag{3.26}$$

or, in matrix form

$$\mathbf{L}_1 \begin{pmatrix} \zeta_1 \\ u_1 \end{pmatrix} = \begin{pmatrix} 0 \\ 0 \end{pmatrix}, \tag{3.27}$$

where

$$\mathbf{L}_1 = \begin{pmatrix} 1 & -c_0 \\ c_0 & -1 \end{pmatrix}. \tag{3.28}$$

For (ζ_1, u_1) to have nontrivial solutions, we must have

$$\det \mathbf{L}_1 = \det \begin{pmatrix} 1 & -c_0 \\ c_0 & -1 \end{pmatrix} = 0, \tag{3.29}$$

i.e.,

$$c_0^2 = 1, \tag{3.30}$$

of which we take

$$c_0 = 1 \tag{3.31}$$

for considering right-going waves (or $c_0 = -1$ for left-going waves). We thus have

$$u_1 = \zeta_1, \tag{3.32}$$

and for the velocity at the free surface, we find by combining (3.32) with (3.23) and (3.24),

$$\hat{u} = \alpha\, u_1 + O(\alpha^2) = \alpha\, \zeta_1 + O(\alpha^2), \tag{3.33}$$

$$\hat{v} = -k_0\, \alpha\, u_1' + O(\alpha^2) = -k_0\, \alpha\, \zeta_1' + O(\alpha^2). \tag{3.34}$$

The equation for solving ζ_1 will come from the next step (see equation (3.38)).

3.2.2 Second Order–$O(\alpha^2)$

The second-order perturbation equations are found as

$$\mathbf{L}_2 \begin{pmatrix} \zeta_2 \\ u_2 \end{pmatrix} = \mathbf{f}_2, \tag{3.35}$$

where

$$\mathbf{L}_2 = \mathbf{L} = \begin{pmatrix} 1 & -1 \\ 1 & -1 \end{pmatrix} \quad (\text{with } c_0 = 1), \tag{3.36}$$

$$\mathbf{f}_2 = \begin{pmatrix} f_{21} \\ f_{22} \end{pmatrix} = \begin{pmatrix} c_1\, \zeta_1 - \frac{1}{2}\, \zeta_1^2 - \frac{1}{2}\, k_0^2\, \zeta_1'' \\ -c_1\, \zeta_1 + \zeta_1^2 - \frac{1}{6}\, k_0^2\, \zeta_1'' \end{pmatrix}. \tag{3.37}$$

Equation (3.35) is an inhomogeneous equation. The homogeneous equation of (3.35) is the same as (3.27), which has a singular matrix.

Applying Fredholm's alternative theorem, for (ζ_2, u_2) to be solvable, we required that $f_{21} = f_{22}$, which yields

$$-2c_1\, \zeta_1 + \frac{3}{2}\, \zeta_1^2 + \frac{1}{3}\, k_0^2\, \zeta_1'' = 0. \tag{3.38}$$

The above equation can be integrated once to give

$$-c_1\,\zeta_1^2+\frac{1}{2}\,\zeta_1^3+\frac{1}{6}\,k_0^2\,(\zeta_1')^2=0, \tag{3.39}$$

where the integration constant vanishes for ζ to fall off exponentially toward infinity. In addition, we have the boundary condition, by the assumed symmetry of $\zeta(-\theta)=\zeta(\theta)$, that at the wave crest, where $\theta=0$, $\zeta_1(0)=1$, $\zeta_1'(0)=0$, by which c_1 is determined from (3.38) to give

$$c_1=1/2. \tag{3.40}$$

Solving (3.39) with $c_1=1/2$ and the condition that ζ falls off at infinity, we obtain

$$\zeta_1=\mathrm{sech}^2(\theta), \tag{3.41}$$

with

$$k_0=\sqrt{3}/2. \tag{3.42}$$

This is Korteweg-de Vries's(1895) solitary wave. Consequently, we obtain the first order solution as

$$u_1 = \zeta_1=\mathcal{S}, \tag{3.43}$$

$$\hat{u} = \alpha\,\mathcal{S}+O(\alpha^2), \tag{3.44}$$

$$\hat{v} = \sqrt{3}\,\alpha\,\mathcal{S}\,\mathcal{T}+O(\alpha^2), \tag{3.45}$$

in which we denote

$$\mathcal{S} = \mathrm{sech}^2(\theta),$$

$$\mathcal{T} = \tanh(\theta), \tag{3.46}$$

to simplify the notation. Finally, by (3.35), u_2 and ζ_2 are related by

$$u_2=\zeta_2+\zeta_1/2-\zeta_1^2+\zeta_1''/8. \tag{3.47}$$

This relation is needed for the solution in the next step.

3.2.3 The higher-order solutions

The third-order equations can be obtained by substituting the designated series expansions into (3.21)-(3.24), collecting all the terms of $O(\alpha^3)$ and using the solutions of the first two orders, yielding

$$\mathbf{L}_3 \begin{pmatrix} \zeta_3 \\ u_3 \end{pmatrix} = \mathbf{f}_3 = \begin{pmatrix} f_{31} \\ f_{32} \end{pmatrix}, \tag{3.48}$$

where $\mathbf{L}_3 = \mathbf{L}$, the same as (3.36), and

$$\begin{aligned} f_{31} &= -(2+3\,k_1)\;{\zeta_1}^2/2 + {\zeta_1}^3 - 3\,\zeta_1^{(4)}/128 + \zeta_1\;(1/4 + c_2 + k_1 - \zeta_2 + \zeta_1''/4) \\ &\quad + \left(8\,\zeta_2 + 6\,(\zeta_1')^2 - 5\,\zeta_1'' - 16\,k_1\,\zeta_1'' - 6\,\zeta_2''\right)/16, \qquad (3.49) \\ f_{32} &= {\zeta_1}^2/2 - (c_2\,\zeta_1) - {\zeta_1}^3 - 7\,\zeta_1^{(4)}/640 + (4\,\zeta_1 - 1)\;\zeta_2/2 \\ &\quad + (\zeta_1')^2/4 - (1+4\,k_1)\;\zeta_1''/16 - \zeta_2''/8. \qquad (3.50) \end{aligned}$$

The solvability condition for (3.48) requires that $f_{31} = f_{32}$, which yields

$$\zeta_2''/4 + (3\;\zeta_1 - 1)\zeta_2 = Z_2(\theta; c_2, k_1), \tag{3.51}$$

where

$$\begin{aligned} Z_2(\theta; c_2, k_1) &= 2\,{\zeta_1}^3 - 3\;(1+k_1)\;{\zeta_1}^2/2 - \zeta_1^{(4)}/80 + \zeta_1\;(1 + 8\,c_2 + 4\,k_1 + \zeta_1'')/4 \\ &\quad + \left((\zeta_1')^2 - 2\;(1+3\,k_1)\;\zeta_1''\right)/8. \qquad (3.52) \end{aligned}$$

Upon substituting the first order solution, we have

$$Z_2(\theta; c_2, k_1) = -(\frac{19}{20} + 2\;k_1 - 2\;c_2)\;\mathcal{S} + 3\;(1+k_1)\;\mathcal{S}^2 - \frac{3}{2}\;\mathcal{S}^3. \tag{3.53}$$

Equation (3.51) is an inhomogeneous ordinary differential equation of which $y_1 = \zeta_1'$ is a complementary solution (of the corresponding homogeneous equation), as can be verified with using (3.38). We can also find another complementary solution of (3.51) by applying the formula

$$y_2 = y_1(x) \int^x d\,x'/y_1^2(x'), \tag{3.54}$$

which gives

$$y_2 = -\frac{1}{64}\,\mathrm{sech}^2(\theta)\,\tanh(\theta)\,(60\,\theta - 32\,\coth(\theta) + 16\,\sinh(2\,\theta) + \sinh(4\,\theta))\,. \tag{3.55}$$

With these two complementary solutions y_1 and y_2, we can solve (3.51) by using Lagrange's method to obtain

$$\zeta_2 = y_p + C_1\,y_1 + C_2\,y_2, \tag{3.56}$$

where $C_1,\ C_2$ are constants and y_p is a particular solution,

$$y_p = \mathrm{sech}^4(\theta)\,\left[21 + 40\,c_2 + \cosh(2\,\theta)\,(-9 + 40\,c_2)\right]/40 + y_\theta, \tag{3.57}$$

$$y_\theta = \theta\,\mathrm{sech}^4(\theta)\,(19 + 40\,k_1 - 40\,c_2)\,\sinh(2\,\theta)/40. \tag{3.58}$$

Since y_2 goes to infinity exponentially as $|x|$ approaches infinity and y_1 is an anti-symmetric function of θ, we see that the symmetric property of the problem and the boundary condition that ζ_2 falls off at infinity clearly require that $C_1 = C_2 = 0$. From the condition $\zeta_2(0) = 0$, which follows from the definition of the wave amplitude that $\zeta(0) = \alpha$, we get

$$c_2 = -\frac{3}{20}. \tag{3.59}$$

As y_θ in y_p decays slower than ζ_1, so if we further invoke that ζ_2 decays no slower than ζ_1 toward infinity, y_θ must vanish identically, which gives

$$k_1 = -\frac{5}{8}. \tag{3.60}$$

We therefore have

$$\zeta_2 = -\frac{3}{4}(\mathcal{S}-\mathcal{S}^2), \tag{3.61}$$

$$u_2 = \mathcal{S}/4-\mathcal{S}^2, \tag{3.62}$$

and

$$\hat{u} = \alpha\,\mathcal{S}-5\,\alpha^2\,(\mathcal{S}-\mathcal{S}^2)/4+O(\alpha^3), \tag{3.63}$$

$$\hat{v} = \sqrt{3}\,\mathcal{T}\left(\alpha\,\mathcal{S}-\alpha^2\,(7\mathcal{S}-4\mathcal{S}^2)/8\right)+O(\alpha^3). \tag{3.64}$$

This is Laitone's (1960) solitary wave of second order. We can further derive a relation between u_3 and ζ_3 from (3.48) by substituting the above solutions into f_{32} or f_{31} as

$$u_3 = \zeta_3+\mathrm{sech}^4(\theta)\,(59+47\,\cosh(2\theta)-22\cosh(4\theta))/160. \tag{3.65}$$

This relation will be needed for the solution of $O(\alpha^4)$.

We now continue to find further higher-order solutions. Suppose that the solution has been determined up to $(\zeta_{n-1}, u_{n-1}, c_{n-1}, k_{n-2})$ for $n \geq 3$. This is accomplished by considering the n-th order equations, such as (3.48) for $n = 3$, and u_n has been related to ζ_n by

$$u_n = \zeta_n + g_n(\zeta_1, \cdots, \zeta_{n-1}), \tag{3.66}$$

such as (3.65) for $n = 3$, which reduces the two unknowns, namely, ζ_n and u_n, to one, since $g_n(\zeta_1, \cdots, \zeta_{n-1})$ is a known function. To solve the unknown function ζ_n, we proceed by induction, to consider the $(n+1)$st-order problem, which is determined to be of the form

$$\mathbf{L}_m \begin{pmatrix} \zeta_m \\ u_m \end{pmatrix} = \mathbf{f}_m = \begin{pmatrix} f_{m1} \\ f_{m2} \end{pmatrix} \qquad (m = n+1), \tag{3.67}$$

where $\mathbf{L}_m = \mathbf{L}$ of (3.36), $(m = n+1, n \geq 3)$ and (with $m = n+1$) $f_{n+1,1}$ and $f_{n+1,2}$ involves $(\zeta_1, \cdots, \zeta_n, u_1, \cdots, u_n)$, of which only u_n and ζ_n are unknown. At this order

$(m = n + 1)$, the solvability condition for (3.67) yields two equations that can be written as

$$f_{n+1,1} = f_{n+1,2}, \tag{3.68}$$

$$u_{n+1} = \zeta_{n+1} + g_{n+1}(\zeta_1, \cdots, \zeta_n). \tag{3.69}$$

Of these two equations, (3.68) insures the (3.67) to be solvable by requiring the two equations in (3.67) to be identical, and leaving one of them to be represented by (3.69). It has been found that (3.68) provides, like what has been illustrated by (3.51) for $n = 2$, a second-order differential equation for the single unknown ζ_n, after having used (3.66), of the following form:

$$\frac{1}{4}\zeta_n'' + (3\ \zeta_1 - 1)\zeta_n = Z_n(\zeta_1, \cdots, \zeta_{n-1}; c_n, k_{n-1}), \tag{3.70}$$

where $Z_n(\zeta_1, \cdots, \zeta_{n-1}; c_n, k_{n-1})$ involves $(\zeta_1, \cdots, \zeta_{n-1})$, the known solutions of the previous orders, and two unknown parameters c_n and k_{n-1}. That (3.70) holds valid for $n = 3, 4, \cdots$ because the coefficient factors for ζ_n and u_n, the terms of the highest order in (3.67) (with $m = n+1, n+2, \cdots$) are the same and the unknown parameters c_n and k_{n_1} enter (3.70) in the same manner as for the previous lower orders. Under all the same conditions as specified for the case $n = 3$, (3.70) can be solved to give ζ_n, c_n and $k_{n-1}(n \geq 3)$, in a manner entirely the same as illustrated in detail for $n = 2$.

Along this approach, the equation for solving (ζ_{n+1}, u_{n+1}) again comes from considering the $(n+2)$nd-order problem, for which the perturbation equations are again found to be (3.67) with $m = n+2$. The solvability condition for (ζ_{n+2}, u_{n+2}) involved in (3.67) is also found to yield the same two equations as (3.68) and (3.69), only with $n + 1$ replaced by $n + 2$. In this way, the inductive procedure can be carried further, except the algebra soon becomes formidable.

With a considerable amount of algebra derivation performed on a personal computer by using the Mathematica code which is listed in appendix A, we have succeeded in determining several successive leading higher-order solutions with accuracy up to

order $O(\alpha^{15})$ for solitary wave, of which we present the final results as follows:

$$
\begin{aligned}
\zeta_1 &= \mathcal{S}, \\
\zeta_2 &= -3(\mathcal{S}-\mathcal{S}^2)/4, \\
\zeta_3 &= (5\mathcal{S}-151\mathcal{S}^2+101\mathcal{S}^3)/80, \\
\zeta_4 &= -(32836\mathcal{S}-93128\mathcal{S}^2+112393\mathcal{S}^3-52101\mathcal{S}^4)/24000, \\
\zeta_5 &= (2917368\mathcal{S}-11683724\mathcal{S}^2+20013610\mathcal{S}^3 \\
&\quad -17906339\mathcal{S}^4+6659085\mathcal{S}^5)/1568000, \\
\zeta_6 &= -(1210872368\mathcal{S}-6249544064\mathcal{S}^2+14638442224\mathcal{S}^3 \\
&\quad -18866232488\mathcal{S}^4+13372133045\mathcal{S}^5-4105671085\mathcal{S}^6)/470400000, \\
\zeta_7 &= \frac{78263417033\,\mathcal{S}}{22638000000}-\frac{3094446826693\,\mathcal{S}^2}{135828000000} \\
&\quad +\frac{4635672338551\,\mathcal{S}^3}{67914000000}-\frac{10592199978011\,\mathcal{S}^4}{90552000000} \\
&\quad +\frac{26185456824781\,\mathcal{S}^5}{217324800000}-\frac{22060716178577\,\mathcal{S}^6}{310464000000}+\frac{641898267187\,\mathcal{S}^7}{34496000000}, \\
\zeta_8 &= \frac{-4595761996453\,\mathcal{S}}{980980000000}+\frac{15837237746581\,\mathcal{S}^2}{420420000000} \\
&\quad -\frac{1639571505368813\,\mathcal{S}^3}{11771760000000}+\frac{3548497975278001\,\mathcal{S}^4}{11771760000000} \\
&\quad -\frac{3874470304190711\,\mathcal{S}^5}{9417408000000}+\frac{334383022700383\,\mathcal{S}^6}{941740800000} \\
&\quad -\frac{38791575861419\,\mathcal{S}^7}{215255040000}+\frac{14856972755777\,\mathcal{S}^8}{358758400000}, \\
\zeta_9 &= \frac{6012057610748687\,\mathcal{S}}{971170200000000}-\frac{82356788521753915 3\,\mathcal{S}^2}{13596382800000000} \\
&\quad +\frac{7337762410742701999\,\mathcal{S}^3}{27192765600000000}-\frac{12909766370832092947\,\mathcal{S}^4}{18128510400000000} \\
&\quad +\frac{26496135954083452807\,\mathcal{S}^5}{21754212480000000}-\frac{6146113078456594781\,\mathcal{S}^6}{4439635200000000} \\
&\quad +\frac{63588950416860407731\,\mathcal{S}^7}{62154892800000000}-\frac{2374720426192371311\,\mathcal{S}^8}{5273748480000000} \\
&\quad +\frac{158703473516597379\,\mathcal{S}^9}{1757916160000000}, \\
\zeta_{10} &= \frac{-310079433650349323\,\mathcal{S}}{37822664880000000}+\frac{2473186175218720024 37\,\mathcal{S}^2}{2600308210500000000} \\
&\quad -\frac{1043312687394127219 01\,\mathcal{S}^3}{208024656840000000}+\frac{3276519369834474001 1081\,\mathcal{S}^4}{20802465684000000000}
\end{aligned}
$$

$$
\begin{aligned}
&-\frac{302809138961851981367\mathcal{S}^5}{92868150375000000}+\frac{771669987295758309025567\mathcal{S}^6}{166419725472000000000}\\
&-\frac{24103993990685635666351\mathcal{S}^7}{5283165888000000000}+\frac{111872053959635337853993\mathcal{S}^8}{36982161216000000000}\\
&-\frac{2218670303725981510183\mathcal{S}^9}{1793074483200000000}+\frac{711386192020122827249\mathcal{S}^{10}}{2988457472000000000},\\
\zeta_{11} &= \frac{58565881437681402143627\mathcal{S}}{5449615631460000000000}-\frac{17560673606750211706169879\mathcal{S}^2}{11989154389212000000000}\\
&+\frac{10799796212574031101050364 1\mathcal{S}^3}{11989154389212000000000}\\
&-\frac{33036021270973081224856501\mathcal{S}^4}{9990961991010000000000}\\
&+\frac{19381802903279576414683584 1\mathcal{S}^5}{23978308778424000000000}-\frac{85943265909385488932472869\mathcal{S}^6}{6228132150240000000000}\\
&+\frac{22729162844521735743833257 97\mathcal{S}^7}{13701890730528000000000}-\frac{57989073746689013810132406 7\mathcal{S}^8}{4262810449497600000000}\\
&+\frac{55011261333691931368083079 3\mathcal{S}^9}{78698039067648000000000}-\frac{34757283162717036103487 3\mathcal{S}^{10}}{185827719168000000000}\\
&+\frac{2979392970179667260449\mathcal{S}^{11}}{1946766581760000000},\\
\zeta_{12} &= \frac{-25977155068872536912989141\mathcal{S}}{17983731583818000000000000}+\frac{18997841266459139776474291\mathcal{S}^2}{85636817065800000000000}\\
&-\frac{37703569474833916416016881 19\mathcal{S}^3}{23978308778424000000000000}+\frac{35394051608772186162132343\mathcal{S}^4}{5320630646100000000000}\\
&-\frac{15081255530194977153653260279\mathcal{S}^5}{79927695928080000000000}+\frac{40547122029260233646303394781\mathcal{S}^6}{10657026123744000000000000}\\
&-\frac{23417602135768891364697379305 7\mathcal{S}^7}{41105672191584000000000000}+\frac{40355081492675140691563777517\mathcal{S}^8}{5994577194606000000000000}\\
&-\frac{20519344355270014787874436669 57\mathcal{S}^9}{30692235236382720000000000}+\frac{31626252885795886124429513 7133\mathcal{S}^{10}}{59023529300736000000000000}\\
&-\frac{11616231996979025468581432 03\mathcal{S}^{11}}{40882098216960000000000}+\frac{31210040402884924933497423\mathcal{S}^{12}}{4542455357440000000000},\\
\zeta_{13} &= \frac{21173669158070385359834313017 81\mathcal{S}}{95547565904825034000000000000}\\
&-\frac{17764412456746574694982138447 3\mathcal{S}^2}{53528048125952400000000000000}\\
&+\frac{11376185668309607448251456882747 9\mathcal{S}^3}{42465584846588904000000000000}\\
&-\frac{98719299150339384461109981722514 17\mathcal{S}^4}{76438052723860027200000000000}\\
&+\frac{27374529340091234477379602558970 7\mathcal{S}^5}{65331668994752160000000000000}\\
&-\frac{27400072762642333871301240201287 77\mathcal{S}^6}{28310389897725936000000000000}
\end{aligned}
$$

$$+\frac{685502060308298792432974569285662 11\mathcal{S}^7}{43678887270777158400000000000}$$
$$-\frac{230597158401261710739147685440268 1\mathcal{S}^8}{16845851839969152000000000000}$$
$$-\frac{319994578780307564515574341985 41\mathcal{S}^9}{33615305258895360000000000}$$
$$+\frac{732051067846105446874612653724081633\mathcal{S}^{10}}{14824349619172853760000000000000}$$
$$-\frac{517864189757491109745117046957758 13\mathcal{S}^{11}}{76022305739347968000000000000}$$
$$+\frac{892154079053997239593257442018793\mathcal{S}^{12}}{20272614863826124800000000000}$$
$$-\frac{757702067741455922345687426709 41\mathcal{S}^{13}}{67575382879420416000000000000},$$

$$\zeta_{14} = \frac{-9914944520052034929875503893 1\mathcal{S}}{16332917248688040000000000000}$$
$$+\frac{130532283853537267743346335032 3\mathcal{S}^2}{26321643499951800000000000000}$$
$$-\frac{149890862277456331905279236492 21\mathcal{S}^3}{33525461720991240000000000000}$$
$$+\frac{527020223097790551075078570743 29\mathcal{S}^4}{21666114717647400000000000000}$$
$$-\frac{455112072112602693061346863675788 649\mathcal{S}^5}{50958701815906684800000000000000}$$
$$+\frac{605902417762216376866154143802306 221\mathcal{S}^6}{25479350907953342400000000000000}$$
$$-\frac{257486502985572724811229204350168 99\mathcal{S}^7}{49235460691697280000000000000}$$
$$+\frac{139396067670897468055101782988841 23487\mathcal{S}^8}{10191740363181336960000000000000}$$
$$-\frac{968792589661484115641732084185364 13\mathcal{S}^9}{21177642313104076800000000000}$$
$$+\frac{153007620437110819474990892850354 75799\mathcal{S}^{10}}{12353624682644044800000000000}$$
$$-\frac{264408515207858750535802430336701 2623\mathcal{S}^{11}}{1235362468264404480000000000}$$
$$+\frac{166250050593391674270954088631399 0621\mathcal{S}^{12}}{76022305739347968000000000000}$$
$$-\frac{813956989367676036459810330026423 033\mathcal{S}^{13}}{67575382879420416000000000000}$$
$$+\frac{620635992342093993449909048902039 47\mathcal{S}^{14}}{22525127626473472000000000000},$$

$$\zeta_{15} = \frac{480679968338849799680888066043886 427\mathcal{S}}{11370160342674179046000000000000000}$$

$$
\begin{aligned}
&-\frac{1785377216671669330715893860542806501\mathcal{S}^2}{2274032068534835809200000000000000}\\
&+\frac{8347688324284894241997564883054795393\mathcal{S}^3}{1137016034267417904600000000000000}\\
&-\frac{2029901402103607082844379198872303097 01\mathcal{S}^4}{4548064137069671618400000000000000}\\
&+\frac{4773276455768964884363445562543452411 37\mathcal{S}^5}{2598893792611240924800000000000000}\\
&-\frac{1961013849774983679843053474722691419827 7\mathcal{S}^6}{3638451309655737294720000000000000}\\
&+\frac{4513025407887164451395762372181295069931\mathcal{S}^7}{5197787585222481849600000000000000}\\
&+\frac{1360911218351718236290810452773906511625 43\mathcal{S}^8}{3638451309655737294720000000000000}\\
&-\frac{2640645212198251629451462442933714614712 3\mathcal{S}^9}{6127917995209662812160000000000000}\\
&+\frac{1034684864579926140282328640455613950308211 7\mathcal{S}^{10}}{5292292814044708792320000000000000}\\
&-\frac{1138157080578488380158360650362746310969 9\mathcal{S}^{11}}{2255879289874129920000000000000}\\
&+\frac{3574606001659914568240385348269834050875309\mathcal{S}^{12}}{4565899682705238958080000000000000}\\
&-\frac{1125673650977626221150662168015496518210 51\mathcal{S}^{13}}{1560991344514611609600000000000000}\\
&+\frac{7654632625745923216178882904795231770 93\mathcal{S}^{14}}{2108351945837916979200000000000}\\
&-\frac{5792630668093676094411683013893005078 81\mathcal{S}^{15}}{7529828377992560640000000000000},
\end{aligned}
\tag{3.71}
$$

and

$$
\begin{aligned}
u_1 &= \mathcal{S},\\
u_2 &= \mathcal{S}/4-\mathcal{S}^2,\\
u_3 &= \frac{-19\,\mathcal{S}}{40}-\frac{\mathcal{S}^2}{5}+\frac{6\,\mathcal{S}^3}{5},\\
u_4 &= \frac{-943\,\mathcal{S}}{2625}+\frac{7157\,\mathcal{S}^2}{6000}+\frac{151\,\mathcal{S}^3}{750}-\frac{197\,\mathcal{S}^4}{125},\\
u_5 &= \frac{61891\,\mathcal{S}}{588000}+\frac{338399\,\mathcal{S}^2}{588000}-\frac{318823\,\mathcal{S}^3}{147000}-\frac{8891\,\mathcal{S}^4}{36750}+\frac{13438\,\mathcal{S}^5}{6125},\\
u_6 &= \frac{-27895737\,\mathcal{S}}{215600000}-\frac{6090013\,\mathcal{S}^2}{14700000}-\frac{12457867\,\mathcal{S}^3}{14700000}
\end{aligned}
$$

$$+\frac{13671151\,\mathcal{S}^4}{3675000}+\frac{71773\,\mathcal{S}^5}{183750}-\frac{295102\,\mathcal{S}^6}{91875},$$

$$u_7 = \frac{44954076523\,\mathcal{S}}{588588000000}-\frac{2342717291\,\mathcal{S}^2}{16978500000}+\frac{46539081023\,\mathcal{S}^3}{33957000000}$$
$$+\frac{226064327\,\mathcal{S}^4}{176859375}-\frac{259280221\,\mathcal{S}^5}{42446250}-\frac{80856212\,\mathcal{S}^6}{75796875}+\frac{127483816\,\mathcal{S}^7}{25265625},$$

$$u_8 = \frac{-227324509157\,\mathcal{S}}{1471470000000}+\frac{249410423\,\mathcal{S}^2}{21560000000}+\frac{485243015347\,\mathcal{S}^3}{735735000000}$$
$$-\frac{29896015563173\,\mathcal{S}^4}{8828820000000}-\frac{19767139409\,\mathcal{S}^5}{12262250000}+\frac{148445086843\,\mathcal{S}^6}{18393375000}$$
$$+\frac{746928838\,\mathcal{S}^7}{140765625}-\frac{205847123\,\mathcal{S}^8}{21896875},$$

$$u_9 = \frac{6041201332267921\,\mathcal{S}}{66039573600000000}+\frac{491544641657249\,\mathcal{S}^2}{4532127600000000}-\frac{30936968270777\,\mathcal{S}^3}{94419325000000}$$
$$-\frac{3609115949220449\,\mathcal{S}^4}{2266063800000000}+\frac{935163163716097\,\mathcal{S}^5}{113303190000000}-\frac{3126148057731\,\mathcal{S}^6}{481731250000}$$
$$+\frac{590608127509\,\mathcal{S}^7}{41688281250}-\frac{2236629577529\,\mathcal{S}^8}{53647343750}+\frac{204822459482\,\mathcal{S}^9}{7315546875},$$

$$u_{10} = \frac{-7412231802809876437\,\mathcal{S}}{45171068342400000000}-\frac{1148554214829763649\,\mathcal{S}^2}{20802465684000000000}$$
$$-\frac{73291718527021177\,\mathcal{S}^3}{260030821050000000}+\frac{1932388545406550471\,\mathcal{S}^4}{1300154105250000000}$$
$$+\frac{251046425037987727 3\,\mathcal{S}^5}{472783311000000000}-\frac{69732639412783842331\,\mathcal{S}^6}{1300154105250000000}$$
$$+\frac{260524552562296559\,\mathcal{S}^7}{1289835421875000}-\frac{149850874195751467\,\mathcal{S}^8}{347263382812500}$$
$$+\frac{890305415130853\,\mathcal{S}^9}{1954296093750}-\frac{6134359551506462\,\mathcal{S}^{10}}{34200181640625},$$

$$u_{11} = \frac{3959812931862372436932461\,\mathcal{S}}{17983731583818000000000}-\frac{70514931596256248442829807 1\,\mathcal{S}^2}{28773970534108800000000000}$$
$$+\frac{3853095609484285544747151439\,\mathcal{S}^3}{28773970534108800000000000}-\frac{1447848635066743637971622287\,\mathcal{S}^4}{3197107837123200000000000}$$
$$+\frac{597845006830560029806244731\,\mathcal{S}^5}{5754794106821760000000}-\frac{39578750775670141140691585 63\,\mathcal{S}^6}{2348895553804800000000000}$$
$$+\frac{3201212297246515114231806007 9\,\mathcal{S}^7}{1644226887663360000000000}-\frac{2394741750267636453748360322 9\,\mathcal{S}^8}{1534611761819136000000000}$$
$$+\frac{5963644683523171445281355 3\,\mathcal{S}^9}{7377941162592000000000}-\frac{1592970882939174775697603\,\mathcal{S}^{10}}{681368303616000000000}$$
$$+\frac{5144298965617376988301\,\mathcal{S}^{11}}{1946766581760000000 0},$$

$$u_{12} = \frac{-2288418190090246814642656 3\,\mathcal{S}}{4136258264278140000000000 0}-\frac{2573521707927708946289747\,\mathcal{S}^2}{1438698526705440000000000 0}$$

$$
\begin{aligned}
&-\frac{71722800672587531774803\mathcal{S}^3}{17983731583818000000000000}-\frac{4699516649861117953206 29\mathcal{S}^4}{11989154389212000000000000}\\
&+\frac{13564935652277431175903 9\mathcal{S}^5}{17292049599825000000000}-\frac{5394372878231171617008560 89\mathcal{S}^6}{89918657919090000000000000}\\
&+\frac{65136292918139467190657899\mathcal{S}^7}{802845159991875000000 0}-\frac{1172315222083879243075111 87\mathcal{S}^8}{267615053330625000000 0}\\
&+\frac{91074886767526804160921 83\mathcal{S}^9}{78054390554765625000}-\frac{1467028899524757994475401 7\mathcal{S}^{10}}{90062758332421875000}\\
&+\frac{1113473017211252616343\mathcal{S}^{11}}{9747051767578125}-\frac{309435718604552534242\mathcal{S}^{12}}{9747051767578125},
\end{aligned}
$$

$$
\begin{aligned}
u_{13} = \;&\frac{24584875705808396914409338168 93\mathcal{S}}{76438052723860027200000000000}+\frac{32777840993854432746750576751\mathcal{S}^2}{36399072725647632000000000000}\\
&+\frac{18979465110480247595075975 09\mathcal{S}^3}{70775974744314840000000000}-\frac{3643084782185923116149877317 3\mathcal{S}^4}{19109513180965006800000000000}\\
&+\frac{42161977599056991872184571475 3\mathcal{S}^5}{15924594317470839000000000000}-\frac{3869479827484936256539116106747 3\mathcal{S}^6}{15924594317470839000000000000}\\
&+\frac{42067937938784718932113590434963\mathcal{S}^7}{85310326700736637500000000 0}-\frac{3266660645159438770463933086 3\mathcal{S}^8}{8308599589631250000000 0}\\
&+\frac{10020120210775470894971954095 27\mathcal{S}^9}{64629035379345937500000 0}-\frac{1880832915001033851700833899261 3\mathcal{S}^{10}}{56550405956927695312500 00}\\
&+\frac{14330717558019699810740406793 1\mathcal{S}^{11}}{3625026022879980468750 0}-\frac{8866731644789046583355785 19\mathcal{S}^{12}}{362502602287998046875}\\
&+\frac{24751607534653531604077924\mathcal{S}^{13}}{40278066920888671875},
\end{aligned}
$$

$$
\begin{aligned}
u_{14} = \;&\frac{-57646795713239023506979134757\mathcal{S}}{19764202384967040000000000 0}-\frac{2435808783341614934026367156510 9\mathcal{S}^2}{38219026361930013600000000000 0}\\
&-\frac{11616861946494308140181473583 77\mathcal{S}^3}{76438052723860027200000000000}-\frac{3526637208493216904470886850 61\mathcal{S}^4}{95547565904825034000000000000 0}\\
&+\frac{26823403785426143909172285370 7\mathcal{S}^5}{45716538710442600000000000 0}-\frac{2897701858499912283980382512891 47\mathcal{S}^6}{29858614345257823125000000000}\\
&+\frac{35542391795945085498853507182506701\mathcal{S}^7}{11943445738103129250000000000}\\
&-\frac{29250506262963232197494477279677181\mathcal{S}^8}{85310326700736637500000000 0}\\
&+\frac{52407650486877560530521175046386 99\mathcal{S}^9}{27144194859325293750000000 0}\\
&-\frac{67801737293544458517447250561582 51\mathcal{S}^{10}}{11310081191385539062500000 0}\\
&+\frac{60992312738563892922088581653209 7\mathcal{S}^{11}}{56550405956927695312500 00}\\
&-\frac{24347537149572958478954480551 73\mathcal{S}^{12}}{21750156137279882812500}
\end{aligned}
$$

$$
\begin{aligned}
u_{15} \;=\; & \frac{557602402869839465862092022403271336 81\mathcal{S}}{17585847996669396924480000000000000000} \\
& + \frac{33346135408891468503563107933007801\mathcal{S}^2}{56850801713370895230000000000000000} \\
& + \frac{51822935365189786746450513412001857\mathcal{S}^3}{45480641370696716184000000000000000} \\
& + \frac{75358651050621199090760629158956 9\mathcal{S}^4}{28425400856685447615000000000000000} \\
& + \frac{11443001581170274006227224934857 53\mathcal{S}^5}{85489927388527662000000000000000} \\
& - \frac{10970730166412325609693028761828848819\mathcal{S}^6}{28425400856685447615000000000000000} \\
& + \frac{36213266737539729062197280786399385781\mathcal{S}^7}{20303857754775319725000000000000} \\
& - \frac{52065524515382745865488234051237634622 9\mathcal{S}^8}{17765875535428404759375000000000} \\
& + \frac{51138528525707515811137785168897574559\mathcal{S}^9}{22207344419285505949218750000 0} \\
& - \frac{10068258210971163125437066945175729503 1\mathcal{S}^{10}}{10094247463311593613281250000 0} \\
& + \frac{19447798037958939475018401256838125 7\mathcal{S}^{11}}{76125546480479589843750000} \\
& - \frac{10789293331093624727890148300931844 81\mathcal{S}^{12}}{27214882866771453369140625 0} \\
& + \frac{12765469185453604609350042043641394\mathcal{S}^{13}}{34890875470219812011718 75} \\
& - \frac{80564036864696743616967945591 64\mathcal{S}^{14}}{4363457249762939453125} \\
& + \frac{17460237717895461514453876482 8\mathcal{S}^{15}}{445250739771728515625}.
\end{aligned}
\tag{3.72}
$$

The wave speed and the corresponding wave number are found to be

$$
\begin{aligned}
c \;=\; & 1 + \frac{\alpha}{2} - \frac{3\,\alpha^2}{20} + \frac{3\,\alpha^3}{56} - \frac{309\,\alpha^4}{5600} + \frac{12237\,\alpha^5}{616000} - \frac{3843597\,\alpha^6}{112112000} \\
& + \frac{54122199\,\alpha^7}{5605600000} - \frac{105542372307\,\alpha^8}{3811808000000} + \frac{36794935644933\,\alpha^9}{5069704640000000} \\
& - \frac{226367085036921\,\alpha^{10}}{6560794240000000} + \frac{421462952714394852 51\,\alpha^{11}}{897844691744000000000}
\end{aligned}
$$

$$\frac{-6646896436150796544437 1\,\alpha^{12}}{233439619853440000000000}+\frac{2801444532459206080407141\,\alpha^{13}}{1485524853612800000000000}$$
$$-\frac{22761113929487163369422890 71\,\alpha^{14}}{135394979514995200000000000}+\frac{1696699209029175156065547813782 79\,\alpha^{15}}{95055240030086336000000000000},$$
(3.73)

and

$$k=\frac{\sqrt{3}}{2}\,K \tag{3.74}$$

with

$$\begin{aligned}K &= 1-\frac{5\,\alpha}{8}+\frac{71\,\alpha^2}{128}-\frac{100627\,\alpha^3}{179200}+\frac{16259737\,\alpha^4}{28672000}-\frac{7606868327\,\alpha^5}{12615680000}\\
&+\frac{2295736286537\,\alpha^6}{3673686016000}-\frac{352070152840157\,\alpha^7}{524812288000000}+\frac{97977609247836695759\,\alpha^8}{139893963489280000000}\\
&-\frac{8083405107086958479894 1\,\alpha^9}{106319412251852800000000}+\frac{5476137529498985937055469 31\,\alpha^{10}}{65492757947141324800000000 0}\\
&\frac{-4126510583730329213200944737 1\,\alpha^{11}}{35443139594923540480000000000}+\frac{5561140407985801031237128721437717\,\alpha^{12}}{17545771825070949479219200000000 00}\\
&-\frac{1260486526833636924236609237538501 1\,\alpha^{13}}{61028771565464172101632000000000 0}\\
&+\frac{1166511052815111141875247523312809421566839\,\alpha^{14}}{56988666887830443908503961600000000000 00}.\end{aligned} \tag{3.75}$$

The horizontal and vertical velocity, $\hat{u}$ and $\hat{v}$, at the free surface can be easily found by substituting ζ, $\underline{u}$ and k into equations (3.23) and (3.24) as followings:

$$\begin{aligned}\hat{u} &= \sum_{i=1}^{15}\hat{u}_i\,\alpha^i,\\
\hat{v} &= \sum_{i=1}^{15}\hat{v}_i\,\alpha^i,\end{aligned} \tag{3.76}$$

with

$$\begin{aligned}\hat{u}_1 &= \mathcal{S},\\
\hat{u}_2 &= -5(\mathcal{S}-\mathcal{S}^2)/4,\\
\hat{u}_3 &= \frac{7\,\mathcal{S}}{5}-\frac{181\,\mathcal{S}^2}{80}+\frac{81\,\mathcal{S}^3}{80},\end{aligned}$$

$$\hat{u}_4 = \frac{-24247\,\mathcal{S}}{10500} + \frac{7133\,\mathcal{S}^2}{1500} - \frac{117343\,\mathcal{S}^3}{24000} + \frac{19717\,\mathcal{S}^4}{8000},$$

$$\hat{u}_5 = \frac{1968229\,\mathcal{S}}{588000} - \frac{6299449\,\mathcal{S}^2}{588000} + \frac{18566113\,\mathcal{S}^3}{1176000} - \frac{60318043\,\mathcal{S}^4}{4704000} + \frac{7039717\,\mathcal{S}^5}{1568000},$$

$$\hat{u}_6 = \frac{-1025829487\,\mathcal{S}}{215600000} + \frac{1156831673\,\mathcal{S}^2}{58800000} - \frac{95731739\,\mathcal{S}^3}{2400000} + \frac{5477656007\,\mathcal{S}^4}{117600000} - \frac{2898132199\,\mathcal{S}^5}{94080000} + \frac{868289447\,\mathcal{S}^6}{94080000},$$

$$\hat{u}_7 = \frac{485464036511\,\mathcal{S}}{73573500000} - \frac{9389235949061\,\mathcal{S}^2}{271656000000} + \frac{24557834890219\,\mathcal{S}^3}{271656000000} - \frac{25775626539427\,\mathcal{S}^4}{181104000000} + \frac{7451559431803\,\mathcal{S}^5}{54331200000} - \frac{23907683834627\,\mathcal{S}^6}{310464000000} + \frac{2050928559661\,\mathcal{S}^7}{103488000000},$$

$$\hat{u}_8 = \frac{-6684013529131\,\mathcal{S}}{735735000000} + \frac{12378279119963\,\mathcal{S}^2}{210210000000} - \frac{4509478377283301\,\mathcal{S}^3}{23543520000000} + \frac{26896191000483341\,\mathcal{S}^4}{70630560000000} - \frac{458004232347899\,\mathcal{S}^5}{941740800000} + \frac{56726638803047\,\mathcal{S}^6}{142688000000} - \frac{3129030529573391\,\mathcal{S}^7}{16144128000000} + \frac{15632609830171\,\mathcal{S}^8}{358758400000},$$

$$\hat{u}_9 = \frac{812016688229161861\,\mathcal{S}}{66039573600000000} - \frac{440253722638311941\,\mathcal{S}^2}{4532127600000000} + \frac{3465687373367774293\,\mathcal{S}^3}{9064255200000000} - \frac{33618651644029768609\,\mathcal{S}^4}{36257020800000000} + \frac{430759350459058007\,\mathcal{S}^5}{290056166400000} - \frac{2074369672798910203\,\mathcal{S}^6}{1294893600000000} + \frac{35321698432480341923\,\mathcal{S}^7}{31077446400000000} - \frac{855757535179651087\,\mathcal{S}^8}{1757916160000000} + \frac{511058488424380537\,\mathcal{S}^9}{5273748480000000},$$

$$\hat{u}_{10} = \frac{-746496831692783015983\,\mathcal{S}}{45171068342400000000} + \frac{107246136385333386019\,\mathcal{S}^2}{687684816000000000} - \frac{12129520455273052774951\,\mathcal{S}^3}{16641972547200000000} + \frac{17526534115042731234086 9\,\mathcal{S}^4}{83209862736000000000} - \frac{13605644772780379178834 23\,\mathcal{S}^5}{332839450944000000000} + \frac{18355346416893697334144 69\,\mathcal{S}^6}{332839450944000000000} - \frac{54795175457359600300397\,\mathcal{S}^7}{10566331776000000000} + \frac{24395472699396195870691 1\,\mathcal{S}^8}{73964322432000000000} - \frac{232722036357955677971 3\,\mathcal{S}^9}{1793074483200000000} + \frac{216591141412912862739 7\,\mathcal{S}^{10}}{8965372416000000000},$$

$$\hat{u}_{11} = \frac{39598129318623724369324 61\,\mathcal{S}}{17983731583818000000000} - \frac{70514931596256248442829 8071\,\mathcal{S}^2}{28773970534108800000000000} + \frac{38530956094842855447471514 39\,\mathcal{S}^3}{28773970534108800000000000} - \frac{14478486350667436379716222 87\,\mathcal{S}^4}{31971078371232000000000}$$

$$+\frac{597845006830560029806244731\mathcal{S}^5}{57547941068217600000000}-\frac{39578750775670141140691585 63\mathcal{S}^6}{234889555380480000000000}$$
$$+\frac{320121229724651511423180600 79\mathcal{S}^7}{16442268876633600000000000}-\frac{23947417502676364537483603229\mathcal{S}^8}{153461176181913600000000000}$$
$$+\frac{59636446835231714452813553\mathcal{S}^9}{737794116259200000000}-\frac{15929708829391747756976 03\mathcal{S}^{10}}{681368303616000000000}$$
$$+\frac{5144298965617376988301\mathcal{S}^{11}}{1946766581760000000},$$

$$\hat{u}_{12} = \frac{-24473266368123573887012343 41\mathcal{S}}{82725165285562800000000000}+\frac{13596254509530157076924079 97\mathcal{S}^2}{35967463167636000000000000}$$
$$-\frac{10560823416265922192718405827\mathcal{S}^3}{44267646975552000000000000}+\frac{10502997363249431655379217833\mathcal{S}^4}{11283910013376000000000000}$$
$$-\frac{71339242750948828197212467733 9\mathcal{S}^5}{28773970534108800000000000}+\frac{73014816077364442864651998 31\mathcal{S}^6}{153871500182400000000000}$$
$$-\frac{22229523910005808198043624793 71\mathcal{S}^7}{32884537753267200000000000}+\frac{52370551893724758317394412185 1\mathcal{S}^8}{69755080082688000000000000}$$
$$-\frac{87751960412838781830019299293\mathcal{S}^9}{12788431348492800000000000}+\frac{74631891677959496264481154597\mathcal{S}^{10}}{14755882325184000000000000}$$
$$-\frac{93930511236424705005796063\mathcal{S}^{11}}{3716554383360000000000}+\frac{24142917491923592052307651 7\mathcal{S}^{12}}{40882098216960000000000},$$

$$\hat{u}_{13} = \frac{32694590412237056000626350631903\mathcal{S}}{76438052723860027200000000000}-\frac{20924450210399274255609971638829\mathcal{S}^2}{36399072725647632000000000000}$$
$$+\frac{23443149432631947388410108360 5467\mathcal{S}^3}{56620779795451872000000000000}$$
$$-\frac{11267337157466165365555003932 1341151\mathcal{S}^4}{61150442179088021760000000000000}$$
$$+\frac{11451643807193190167958226636 8942829\mathcal{S}^5}{20383480726362673920000000000000}$$
$$-\frac{62946570959338703464221359697 916991\mathcal{S}^6}{50958701815906684800000000000000}$$
$$+\frac{17022072877355328314175413627 3990897\mathcal{S}^7}{87357774541554316800000000000000}$$
$$-\frac{45413074342212708749801470837 514143\mathcal{S}^8}{24707249365288089600000000000000}$$
$$-\frac{61310075394356430923325094334 0647\mathcal{S}^9}{21177642313104076800000000000}$$
$$+\frac{29273198395158331286570061364 5022139\mathcal{S}^{10}}{74121748095864268800000000000000}$$
$$-\frac{16792213409593898183176622973 84763\mathcal{S}^{11}}{29239348361287680000000000000}$$
$$+\frac{22828871552994554006359144593 80881\mathcal{S}^{12}}{60817844591478374400000000000}$$

$$\hat{u}_{14} = \frac{-\frac{64828537148212932117623845770341\mathcal{S}^{13}}{6757538287942041600000000000},}{\frac{-28062935695310418363004422935149 7\mathcal{S}}{3057522108954401088000000000000}} + \frac{5259468734781200244279061446664 3\mathcal{S}^{2}}{6042533812162848000000000000} - \frac{3305374928934236934808867358951099\mathcal{S}^{3}}{4703880167622155520000000000} + \frac{1080129906206941761439659178211999803\mathcal{S}^{4}}{3057522108954401088000000000000} - \frac{1491634068387502038030783462471781545 1\mathcal{S}^{5}}{1223008843581760435200000000000} + \frac{3767560146700092310265563411589956442 3\mathcal{S}^{6}}{1223008843581760435200000000000} - \frac{7712445994470895331061518094748214557 1\mathcal{S}^{7}}{1223008843581760435200000000000} + \frac{1758140830339918213402709938907063996 69\mathcal{S}^{8}}{1223008843581760435200000000000} - \frac{3833082953197734011408183632415251825 9\mathcal{S}^{9}}{8894609771503712256000000000000} + \frac{1665318215890991386308605657900820088 03\mathcal{S}^{10}}{1482434961917285376000000000000} - \frac{1137769521709575541872560695049552892 37\mathcal{S}^{11}}{5929739847669141504000000000000} + \frac{8902649223698782609560519954977133197\mathcal{S}^{12}}{4561338344360878080000000000} - \frac{2174788391176571594279052453147424349\mathcal{S}^{13}}{2027261486382612480000000000} + \frac{3247943818391240011541688389336741\mathcal{S}^{14}}{1325007507439616000000000000},$$

$$\hat{u}_{15} = \frac{\frac{10962764964778166621804942434308385757\mathcal{S}}{2198230999583674615560000000000000} - \frac{5021821354208839224220899327919907403 1\mathcal{S}^{2}}{3638451309655737294720000000000000} + \frac{4259953201858064919179145171553659425 81\mathcal{S}^{3}}{3638451309655737294720000000000000} - \frac{4794816252627412038575406831425732659321\mathcal{S}^{4}}{7276902619311474589440000000000000} + \frac{6345238261751847852329591123735860741\mathcal{S}^{5}}{2486979705848077440000000000000} - \frac{2082530920239239946104377847827429235247 41\mathcal{S}^{6}}{2910761047724589835776000000000000} + \frac{5101912764004216317624642072868353121712 3\mathcal{S}^{7}}{4158230068177985479680000000000000}}$$

$$+\frac{34952987241047225754655440887272513783853\mathcal{S}^8}{126554828161938688512000000000000000}$$
$$-\frac{3509085948202166385623304941171994928048 9\mathcal{S}^9}{909612827413934323680000000000000}$$
$$+\frac{188075413245515746957456432143744324140304 19\mathcal{S}^{10}}{10584585628089417584640000000000000000}$$
$$-\frac{95362075194461103287526321139991469481874 3\mathcal{S}^{11}}{20754089466841995264000000000000000}$$
$$+\frac{65108811845638539193304324069783665375286 83\mathcal{S}^{12}}{91317993654104779161600000000000000}$$
$$-\frac{33418897206856181559080785505002757576 39\mathcal{S}^{13}}{5090189166895472640000000000000}$$
$$+\frac{61116682390912441986341933727590593907\mathcal{S}^{14}}{184943153143676928000000000000}$$
$$-\frac{17573219163976070654648074309891279732 7\mathcal{S}^{15}}{250994279266418688000000000000000}, \tag{3.77}$$

and

$$\frac{\hat{v}_1}{\sqrt{3}\mathcal{T}} = \mathcal{S},$$
$$\frac{\hat{v}_2}{\sqrt{3}\mathcal{T}} = \frac{-7\mathcal{S}}{8}+\frac{\mathcal{S}^2}{2},$$
$$\frac{\hat{v}_3}{\sqrt{3}\mathcal{T}} = \frac{519\mathcal{S}}{640}-\frac{107\mathcal{S}^2}{80}+\frac{83\mathcal{S}^3}{80},$$
$$\frac{\hat{v}_4}{\sqrt{3}\mathcal{T}} = \frac{-4441387\mathcal{S}}{2688000}+\frac{345949\mathcal{S}^2}{96000}-\frac{63261\mathcal{S}^3}{16000}+\frac{4017\mathcal{S}^4}{2000},$$
$$\frac{\hat{v}_5}{\sqrt{3}\mathcal{T}} = \frac{277732577\mathcal{S}}{120422400}-\frac{92762599\mathcal{S}^2}{12544000}+\frac{144596329\mathcal{S}^3}{12544000}-\frac{23633677\mathcal{S}^4}{2352000}+\frac{1202053\mathcal{S}^5}{313600},$$
$$\frac{\hat{v}_6}{\sqrt{3}\mathcal{T}} = \frac{-88003766717\mathcal{S}}{27033600000}+\frac{135841253119\mathcal{S}^2}{10035200000}-\frac{73042724689\mathcal{S}^3}{2508800000}$$
$$+\frac{34129698809\mathcal{S}^4}{940800000}-\frac{318900271\mathcal{S}^5}{12544000}+\frac{129487867\mathcal{S}^6}{15680000},$$
$$\frac{\hat{v}_7}{\sqrt{3}\mathcal{T}} = \frac{42947742641840557\mathcal{S}}{9643425792000000}-\frac{6688436796201613\mathcal{S}^2}{278175744000000}+\frac{6126691999389691\mathcal{S}^3}{92725248000000}$$
$$-\frac{105181950775051\mathcal{S}^4}{965888000000}+\frac{15249326986367\mathcal{S}^5}{139087872000}$$
$$-\frac{6669092080429\mathcal{S}^6}{103488000000}+\frac{255078204461\mathcal{S}^7}{14784000000},$$
$$\frac{\hat{v}_8}{\sqrt{3}\mathcal{T}} = \frac{-337395569271572219\mathcal{S}}{55105290240000000}+\frac{1182962679572859973 1\mathcal{S}^2}{289302773760000000}$$

$$
\begin{aligned}
&-\frac{6697858989610979329\mathcal{S}^3}{48217128960000000}+\frac{5195398571702622739\mathcal{S}^4}{18081423360000000}\\
&-\frac{12567068982306689\mathcal{S}^5}{32875315200000}+\frac{49464485802512923\mathcal{S}^6}{150678528000000}\\
&-\frac{112443777758459\mathcal{S}^7}{658944000000}+\frac{5652359523149\mathcal{S}^8}{134534400000},\\
\frac{\hat{v}_9}{\sqrt{3}\mathcal{T}} &= \frac{568926381567171728639281\mathcal{S}}{69247511927193600000000}-\frac{5996567878975197694299 1\mathcal{S}^2}{891052543180800000000}\\
&+\frac{818853345904796270888 87\mathcal{S}^3}{297017514393600000000}-\frac{128755871835766794997 87\mathcal{S}^4}{18563594649600000000}\\
&+\frac{1709068247087725034737\mathcal{S}^5}{1485087571968000000}-\frac{424283835144527369993\mathcal{S}^6}{331492761600000000}\\
&+\frac{130232358574431805981\mathcal{S}^7}{142068326400000000}-\frac{1490269441513682321\mathcal{S}^8}{3955311360000000}\\
&+\frac{1156655489483444 91\mathcal{S}^9}{1757916160000000},\\
\frac{\hat{v}_{10}}{\sqrt{3}\mathcal{T}} &= \frac{-731085741801586756816408016 3\mathcal{S}}{66311417421480591360000000 0}+\frac{4702795562194697723772316939\mathcal{S}^2}{43625932514131968000000000}\\
&-\frac{1902132476289581411584380 19\mathcal{S}^3}{36354943761776640000000 0}+\frac{1066189958796514959646622947\mathcal{S}^4}{68165519553331200000000 0}\\
&-\frac{4700200530922088050907099\mathcal{S}^5}{1498143286886400000000}+\frac{2276230990960264763980812 1\mathcal{S}^6}{5164054511616000000000}\\
&-\frac{1443834788954992709842 51\mathcal{S}^7}{32202153984000000000}+\frac{1433421416895317292067 61\mathcal{S}^8}{42265327104000000000}\\
&-\frac{2144303206727164474993\mathcal{S}^9}{1195382988800000000}+\frac{430386406330241340097\mathcal{S}^{10}}{896537241600000000},\\
\frac{\hat{v}_{11}}{\sqrt{3}\mathcal{T}} &= \frac{3536791185313218497390866541008 33\mathcal{S}}{24137355941418935255040000000 00}\\
&-\frac{1699298189636330448202114378388 59\mathcal{S}^2}{10057231642257889689600000000 0}\\
&+\frac{3208981662069011638993934378522 33\mathcal{S}^3}{33524105474192965632000000000 0}\\
&-\frac{1575293656567483463940189209599 63\mathcal{S}^4}{47143273323083857920000000000}\\
&+\frac{3308586071411650103091491529511\mathcal{S}^5}{41905131842741207040000000 0}\\
&-\frac{2712177806903512410316444915 29\mathcal{S}^6}{20786275715645440000000000}\\
&+\frac{3412179832284237076429557829781\mathcal{S}^7}{24052690470961152000000000 0}\\
&-\frac{1650699678055875843164826563 3\mathcal{S}^8}{24553788189106176000000 00}
\end{aligned}
$$

$$
\begin{aligned}
\frac{\hat{v}_{12}}{\sqrt{3}\mathcal{T}} = {} & -\frac{2159032653589245630257103403\mathcal{S}^9}{41972287502745600000000} \\
& + \frac{19429195831006989584203\mathcal{S}^{10}}{2186208460800000000} - \frac{2079056054717563971121\mathcal{S}^{11}}{589929267200000000}, \\
\frac{\hat{v}_{13}}{\sqrt{3}\mathcal{T}} = {} & \frac{-14786935689088217202757085065205173 7\mathcal{S}}{74021224887018068115456000000000000} \\
& + \frac{81475198644025140042835888943879 3\mathcal{S}^2}{31347215508336279552000000000000} \\
& - \frac{68332458109377616365442416795506777\mathcal{S}^3}{40228926569031558758400000000000} \\
& + \frac{34343486638887739643079332429444341\mathcal{S}^4}{50286158211289448448000000000000} \\
& - \frac{14118743058240094233512490691724203\mathcal{S}^5}{75429237316934172672000000000000} \\
& + \frac{61875552159013039253481538085881 3\mathcal{S}^6}{16541499411608371200000000000} \\
& - \frac{67906609899712292558194342100627\mathcal{S}^7}{10690084653760512000000000000} \\
& + \frac{35987991757513159846932796130339 27\mathcal{S}^8}{29464545826927411200000000000} \\
& - \frac{15833594509608886536335702718919 9\mathcal{S}^9}{65476768504283136000000000} \\
& + \frac{13917571572757299193161134482 13\mathcal{S}^{10}}{4197228750274560000000000} \\
& - \frac{18261250970627449015613142 71\mathcal{S}^{11}}{7433108766720000000000} \\
& + \frac{19206647042046539537316949\mathcal{S}^{12}}{262064732160000000000}, \\
\frac{\hat{v}_{13}}{\sqrt{3}\mathcal{T}} = {} & \frac{25704905851612500622725501768322839215587\mathcal{S}}{820747341547256339264176128000000000000} \\
& - \frac{96260974445755271710493816570060027299 7\mathcal{S}^2}{24427004212715962478100480000000000000} \\
& + \frac{16740207041824451754812753093331195948391\mathcal{S}^3}{56996343163003912448901120000000000000} \\
& - \frac{43127574871798823518071408486884236823357\mathcal{S}^4}{32060443029189700752506880000000000000} \\
& + \frac{13843788879058851495410616016941617912 33\mathcal{S}^5}{32882505670963795643596800000000000} \\
& - \frac{12125702232275903208330116883266881075 7\mathcal{S}^6}{13096586204734354882560000000000000} \\
& + \frac{29629412290043485326443370185514718837\mathcal{S}^7}{31456478639314855526400000000000000}
\end{aligned}
$$

$$
\begin{aligned}
&+\frac{2566033564138004096956114361105293050 1\mathcal{S}^{8}}{6325055837513750937600000000000}\\
&-\frac{6071479713612168723650389133322756811\mathcal{S}^{9}}{240954508095761940480000000000}\\
&+\frac{6021916566648129077131831294308861297 7\mathcal{S}^{10}}{948758375627062640640000000000}\\
&-\frac{3104374330253092959949022752912041 61\mathcal{S}^{11}}{368592997524111360000000000}\\
&+\frac{4456169982598820984606597219204 83\mathcal{S}^{12}}{77971595630100480000000000}\\
&-\frac{2431664598189525055104019684926 23\mathcal{S}^{13}}{155943191260200960000000000},\\
\frac{\hat{v}_{14}}{\sqrt{3}\mathcal{T}} &= \frac{-8319859627786591386631890027594341505567 1\mathcal{S}}{937996961768292959159058432000000000000}\\
&+\frac{4432454692251456021207665307755279107092 61\mathcal{S}^{2}}{7461339468611421266037964800000000000000}\\
&-\frac{6795735436491722729755649521247308318187 17\mathcal{S}^{3}}{136791223591209389877362688000000000000}\\
&+\frac{3896353187043465128362893305274905594504 9\mathcal{S}^{4}}{151765410789063672201216000000000000}\\
&-\frac{4665429250304435491583067973649305881084157\mathcal{S}^{5}}{5129670884670352120401100800000000000}\\
&+\frac{5233846041253957357398193603446576075891763\mathcal{S}^{6}}{213736286861264671683379200000000000}\\
&-\frac{7530701396238518336085756595136706555094 7\mathcal{S}^{7}}{88078140190081595473920000000000}\\
&+\frac{1780796232318389720578459635496928784936 91\mathcal{S}^{8}}{29467318960652298485760000000000}\\
&-\frac{1013571396875631707145820702108390028793 7\mathcal{S}^{9}}{2891454097149143285760000000000}\\
&+\frac{2015278502638275580810156075935873878512 3\mathcal{S}^{10}}{16866815566703335833600000000000}\\
&-\frac{6269721189114466437147301016800490148 23\mathcal{S}^{11}}{265386958217360179200000000000}\\
&+\frac{6513545114152047336956814916488468193 9\mathcal{S}^{12}}{24327137836591349760000000000}\\
&-\frac{1509005776821584175626513104696244786 9\mathcal{S}^{13}}{935659147561205760000000000}\\
&+\frac{3784944594976306511263011239785441\mathcal{S}^{14}}{9464339338854400000000000},\\
\frac{\hat{v}_{15}}{\sqrt{3}\mathcal{T}} &= \frac{5706143274220312934579747573543997000037796534537\mathcal{S}}{90636770421746612057621498167296000000000000000}
\end{aligned}
$$

$$
\begin{aligned}
&-\frac{3630848478882402323218441747572852089709649898 3\mathcal{S}^2}{39067573457649401748974783692800000000000000} \\
&+\frac{10751373627190369070346268920034243555764016544 9\mathcal{S}^3}{13022524485883133916324927897600000000000000} \\
&-\frac{5821747613302852841564181348277819031797189937 9\mathcal{S}^4}{12208616705515438046554619904000000000000000} \\
&+\frac{3845567133758903163210137405644642247562004 7\mathcal{S}^5}{20339219834261454471561216000000000000000} \\
&-\frac{5129637752610321744059517256126073629981248636 7\mathcal{S}^6}{10173847254596198372128849920000000000000000} \\
&-\frac{6968994940205361498897470869960611444432751 27\mathcal{S}^7}{56626237038568822108323840000000000000000} \\
&+\frac{9614587068768616495944358846970859655369322129\mathcal{S}^8}{21677231366327127213342720000000000000000} \\
&-\frac{8710494365523021479357320271626847721384950884 7\mathcal{S}^9}{21195515113742079941935104000000000000000} \\
&+\frac{1444156847555482648922413976705986818745320326 9\mathcal{S}^{10}}{72257437887757090711142400000000000000} \\
&-\frac{1092874535830556222570937408989631740606959027\mathcal{S}^{11}}{19320170558223821045760000000000000000} \\
&+\frac{4676957685860179925823106309806523943795460 37\mathcal{S}^{12}}{48702929948855882219520000000000000000} \\
&-\frac{1663421162722474262825335822427684372040190 9\mathcal{S}^{13}}{17290981046931082444800000000000000} \\
&+\frac{2628629273938959570654770460633732847079\mathcal{S}^{14}}{50198855853283737600000000000000} \\
&-\frac{1996490965915301824795433165677326254 87\mathcal{S}^{15}}{16732951951094579200000000000000}.
\end{aligned}
\tag{3.78}
$$

Returning to dimensional form, we have the first 11th-order solitary wave solution, given by

$$\zeta = \sum_{n=1}^{15} \alpha^n \, \zeta_n(\theta') + O(\alpha^{16}), \tag{3.79}$$

$$\underline{u} = \sum_{n=1}^{15} \alpha^n \, u_n(\theta') + O(\alpha^{16}), \tag{3.80}$$

$$\hat{u} = \sum_{n=1}^{15} \alpha^n \, \hat{u}_n(\theta') + O(\alpha^{16}), \tag{3.81}$$

$$\hat{v} = \sum_{n=1}^{15} \alpha^n \, \hat{v}_n(\theta') + O(\alpha^{16}), \tag{3.82}$$

$$\tag{3.83}$$

where

$$\theta' = \frac{1}{2}\sqrt{3\,\alpha}\;K\;\frac{x-ct}{h}, \tag{3.84}$$

in which c and K are the same as (3.73) and (3.75).

It is found that for solitary waves the 14th-order solutions of Longuet-Higgins and Fenton (1974) and the present 15th-order solution by asymptotic expansion analysis are in complete agreement, with the same results for the wave speed to $O(\alpha^{14})$ and for the wave profiles to $O(\alpha^9)$, there being a lack of corresponding data for the latter. A result of great significance is the finding that the series expansion shows to diverge starting from the 12th-order term. Numerically, this implies that the present series expansion is not convergent, but can provide an optimum approximation at the 11th-order, with a maximum relative error generally negligible in comparison with the corresponding exact solution, except possibly when the wave amplitude is in a very small neighborhood of the highest solitary wave, as will be illustrated in the example provided in next section.

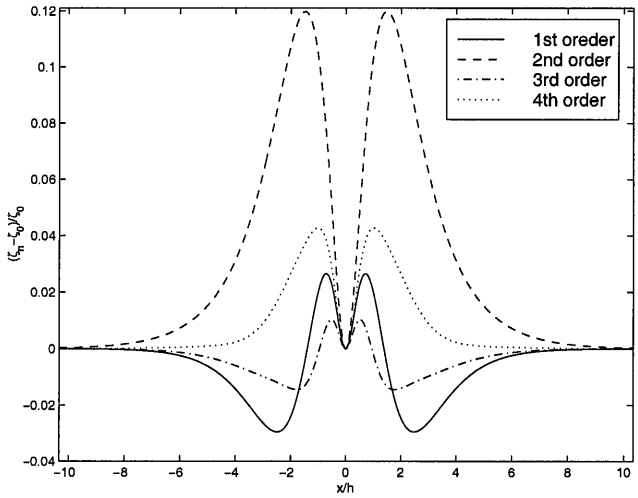

Figure 3.1a: Comparison between the free surface elevation of the fully nonlinear solution and that of the weakly nonlinear asymptotic solutions for solitary wave of amplitude $\alpha = 0.70$. ζ_0: The fully nonlinear solution computed by the method of Wu & Kao. ζ_n: n-th order asymptotic solution. Notice the different scales in Figures (3.1a)-(3.1d).

3.3 Comparison of the higher-order solutions with the fully nonlinear solutions

In this section, we compare the higher-order asymptotic solutions with the fully nonlinear solution for solitary waves. Wu & Kao (2000) have obtained numerical results for steady solitary waves using the fully nonlinear equations for the complex velocity potential. They analyzed the singular behavior of the analytic solution at physical infinity and had the singularity removed by introducing appropriate terms raised to irrational powers to the original power-series solution, yielding improved results which are limited by a maximum local error less than 10^{-8}. In Figures (3.1a)-(3.1d), we compare the asymptotic solutions to various orders with the fully nonlinear solution for solitary wave of amplitude $\alpha = 0.7$. The difference between the exact solution and the higher-order asymptotic solutions decreases with increasing order of the asymptotic approximation before the series diverges at 12th-order. The difference is almost undetectable at the 11th-order for waves with moderately large amplitudes such as shown in Figure (3.2) for $\alpha = 0.7$.

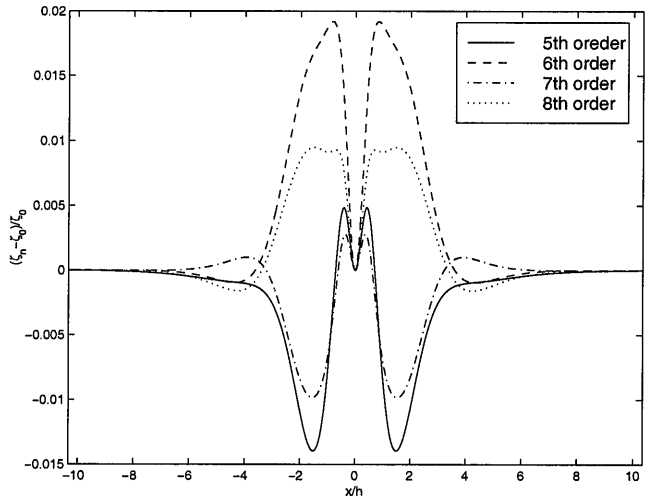

Figure 3.1b: Comparison between the free surface elevation of the fully nonlinear solution and that of the weakly nonlinear asymptotic solutions for solitary wave of amplitude $\alpha = 0.70$. ζ_0: The fully nonlinear solution computed by the method of Wu & Kao. ζ_n: n-th order asymptotic solution. Notice the different scales in Figures (3.1a)-(3.1d).

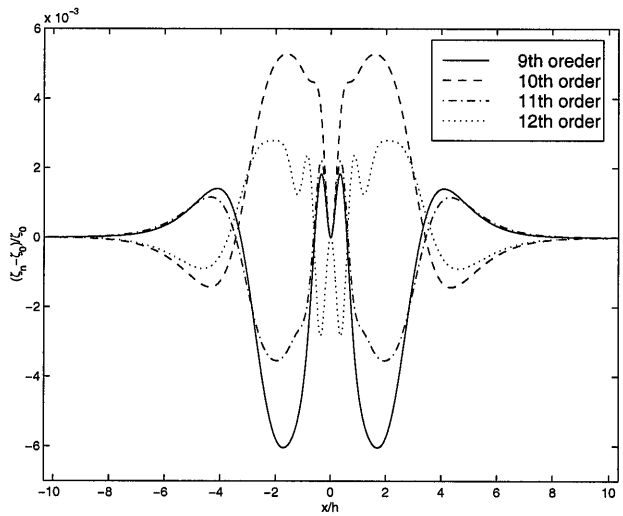

Figure 3.1c: Comparison between the free surface elevation of the fully nonlinear solution and that of the weakly nonlinear asymptotic solutions for solitary wave of amplitude $\alpha = 0.70$. ζ_0: The fully nonlinear solution computed by the method of Wu & Kao. ζ_n: n-th order asymptotic solution. Notice the different scales in Figures (3.1a)-(3.1d).

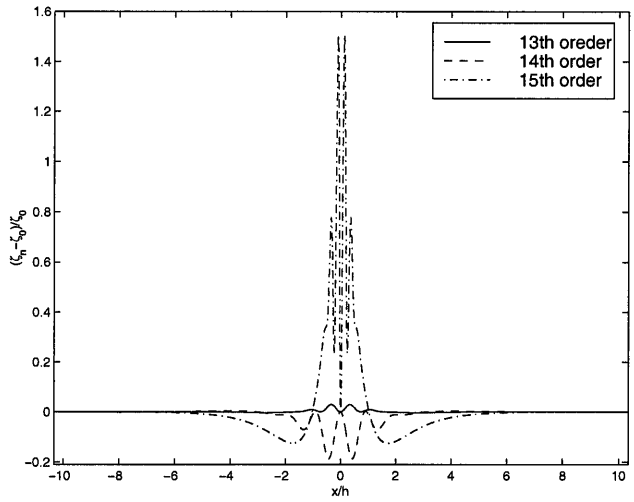

Figure 3.1d: Comparison between the free surface elevation of the fully nonlinear solution and that of the weakly nonlinear asymptotic solutions for solitary wave of amplitude $\alpha = 0.70$. ζ_0: The fully nonlinear solution computed by the method of Wu & Kao. ζ_n: n-th order asymptotic solution. Notice the different scales in Figures (3.1a)-(3.1d).

We use the infinity norm to measure the error of the nth-order asymptotic solution with respect to the fully nonlinear solution, i.e.,

$$error(\zeta_n) = \|\zeta^{(n)} - \zeta_0\|_\infty = \max_{x\in(-\infty,\infty)} |\zeta^{(n)}(x) - \zeta_0(x)| \tag{3.85}$$

where $\zeta^{(n)} = \sum_{i=1}^{n} \alpha^i \zeta_i$ is the nth-order asymptotic solution and ζ_0 is the exact solution. The numerical results of the error of the asymptotic solution accurate to successive orders for waves of various amplitudes are listed in table 3.1. The asymptotic series show to have a rapid convergent rate for waves of small amplitudes before the series diverges at 12th-order.

Variations of the wave speed of solitary wave with amplitude have been computed using (3.73). The relative error of the wave speed predicted by the asymptotic theory to various orders is defined as

$$err(c^{(n)}) = (c^{(n)} - c)/c \tag{3.86}$$

where $c^{(n)} = c_0 + \alpha\, c_1 + \cdots + \alpha^n\, c_n$ is the wave speed of the nth-order asymptotic

order	α							
	0.2001	0.3001	0.4001	0.5001	0.6000	0.7000	0.8095	$0.833199\cdots$
1	7.12e-3	1.40e-2	2.12e-2	2.76e-2	3.18e-2	4.00e-2	1.18e-1	1.42e-1
2	2.92e-3	1.01e-2	2.49e-2	5.06e-2	9.18e-2	1.55e-1	2.63e-1	2.88e-1
3	2.76e-4	1.30e-3	3.70e-3	7.83e-3	1.32e-2	1.76e-2	7.49e-2	9.86e-2
4	8.99e-5	6.88e-4	2.97e-3	9.47e-3	2.52e-2	6.06e-2	1.52e-1	1.78e-1
5	1.60e-5	1.75e-4	9.23e-4	3.24e-3	8.57e-3	1.77e-2	5.41e-2	7.75e-2
6	4.23e-6	6.60e-5	4.80e-4	2.26e-3	8.52e-3	2.84e-2	1.03e-1	1.29e-1
7	6.16e-7	2.09e-5	1.95e-4	1.09e-3	4.24e-3	1.25e-2	4.31e-2	6.60e-2
8	4.61e-7	7.26e-6	9.29e-5	6.50e-4	3.19e-3	1.41e-2	7.52e-2	1.01e-1
9	2.73e-7	2.27e-6	3.70e-5	3.28e-4	1.85e-3	7.49e-3	3.65e-2	5.90e-2
10	2.93e-7	7.80e-7	1.83e-5	1.88e-4	1.31e-3	6.90e-3	5.54e-2	8.02e-2
11	2.84e-7	2.30e-7	7.48e-6	9.50e-5	7.65e-4	4.21e-3	3.85e-2	6.11e-2
12	2.86e-7	2.53e-7	8.16e-6	1.18e-4	9.54e-4	4.62e-3	2.52e-2	3.94e-2
13	2.85e-7	6.84e-7	3.09e-5	5.83e-4	6.39e-3	4.83e-2	3.38e-1	5.00e-1
14	2.86e-7	1.97e-6	1.17e-4	2.75e-3	3.57e-2	3.00e-1	2.51	3.94
15	2.85e-7	6.71e-6	5.29e-4	1.54e-2	2.43e-1	2.55	23.2	36.0

Table 3.1: The relative errors of $|\zeta^{(n)} - \zeta_0|_{max}$, where $\zeta^{(n)}$ is nth order asymptotic solution of ζ and ζ_0 is the fully nonlinear solution, for various wave amplitude α.

solution and c is the exact solution given by Wu & Kao (2000). The numerical results for this error are listed in table 3.2 which indicates that the higher-order solutions agree well with the exact solution for waves of moderately high amplitudes before the series diverges.

Further, to test how well the higher-order asymptotic solutions approximate the fully nonlinear solitary wave, we use the solutions of different orders, all starting with the same initial wave of amplitude $\alpha = 0.6$ to compute its unsteady asymptotic limit using the method which we will discuss in the next chapter. The numerical evolutions of the free surface resulted from starting initially with the solution of a given order of the asymptotic theory generally exhibit how well the theory of that order approximates the corresponding fully nonlinear solution. If the initial wave profile and wave speed provided are taken from an exact solution, the free surface elevation should be expected to propagate with the shape remaining unchanged if the error is indiscernible. The results indicate the degree of a broad agreement between the higher-order asymptotic solutions up to 11th-order and the corresponding fully

order	α								
	0.1761	0.2867	0.4074	0.5252	0.5837	0.6970	0.8001	0.8114	0.8241
1	4.07e-3	1.01e-2	1.93e-2	3.09e-2	3.79e-2	5.51e-2	8.18e-2	8.69e-2	9.33e-2
2	-2.22e-4	-8.02e-4	-1.77e-3	-2.90e-3	-3.18e-3	-1.95e-3	7.64e-3	1.05e-2	1.44e-2
3	4.82e-5	3.13e-4	1.29e-3	3.44e-3	5.38e-3	1.22e-2	2.88e-2	3.26e-2	3.76e-2
4	-7.97e-7	-1.66e-5	7.58e-6	1.34e-5	2.32e-4	2.05e-3	1.14e-2	1.41e-2	1.79e-2
5	2.31e-6	1.74e-5	1.96e-4	6.62e-4	1.31e-3	4.61e-3	1.64e-2	1.95e-2	2.37e-2
6	1.37e-6	5.72e-7	6.36e-5	7.41e-5	2.24e-4	1.53e-3	9.45e-3	1.20e-2	1.54e-2
7	1.41e-6	1.93e-6	7.88e-5	1.61e-4	4.03e-4	2.13e-3	1.10e-2	1.37e-2	1.74e-2
8	1.39e-6	8.14e-7	6.11e-5	3.01e-5	1.04e-4	9.28e-4	7.42e-3	9.68e-3	1.28e-2
9	1.39e-6	8.98e-7	6.30e-5	4.81e-5	1.50e-4	1.15e-3	8.18e-3	1.05e-2	1.38e-2
10	1.39e-6	7.83e-7	5.93e-5	3.11e-6	2.24e-5	4.18e-4	5.31e-3	7.24e-3	9.93e-3
11	1.39e-6	8.28e-7	6.13e-5	3.53e-5	1.23e-4	1.11e-3	8.43e-3	1.09e-2	1.43e-2
12	1.39e-6	7.51e-7	5.63e-5	-6.72e-5	-2.34e-4	-1.82e-3	-6.72e-3	-7.04e-3	-7.37e-3
13	1.39e-6	8.98e-7	6.99e-5	2.89e-4	1.15e-3	1.17e-2	7.36e-2	8.93e-2	1.11e-1
14	1.39e-6	5.22e-7	2.05e-5	-1.38e-3	-6.05e-3	-7.23e-2	-4.99e-1	-6.07e-1	-7.57e-1
15	1.39e-6	1.67e-6	2.34e-4	7.92e-3	3.85e-2	5.49e-1	4.37	5.39	6.83

Table 3.2: The relative error of the wave speed, $(c^{(n)}/c - 1)$, where $c^{(n)}$ is the wave speed of the nth-order asymptotic solution and c is the wave speed of the fully nonlinear solution.

nonlinear solution.

In most of the cases, the solutions of the 5th-order asymptotic theory can provide a very good approximation to fully nonlinear waves with a relative error of $O(10^{-2})$ for waves of amplitudes up to 0.7.

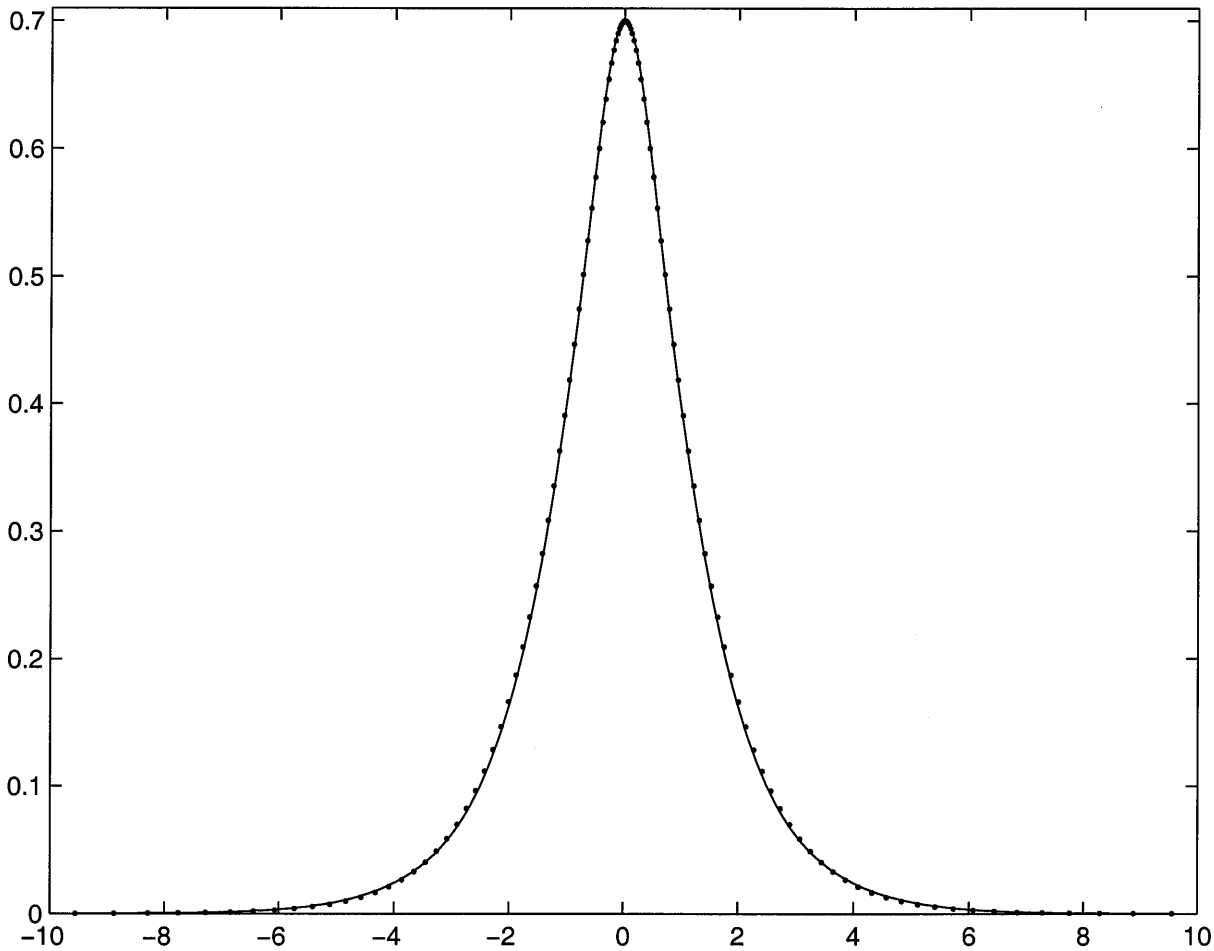

Figure 3.2: Comparison between the free surface elevation of the fully nonlinear theory and that of a higher-order weakly nonlinear theory for solitary wave of amplitude $\alpha = 0.70$. Dotted line: fully nonlinear theory, solid line: the 11th asymptotic theory.

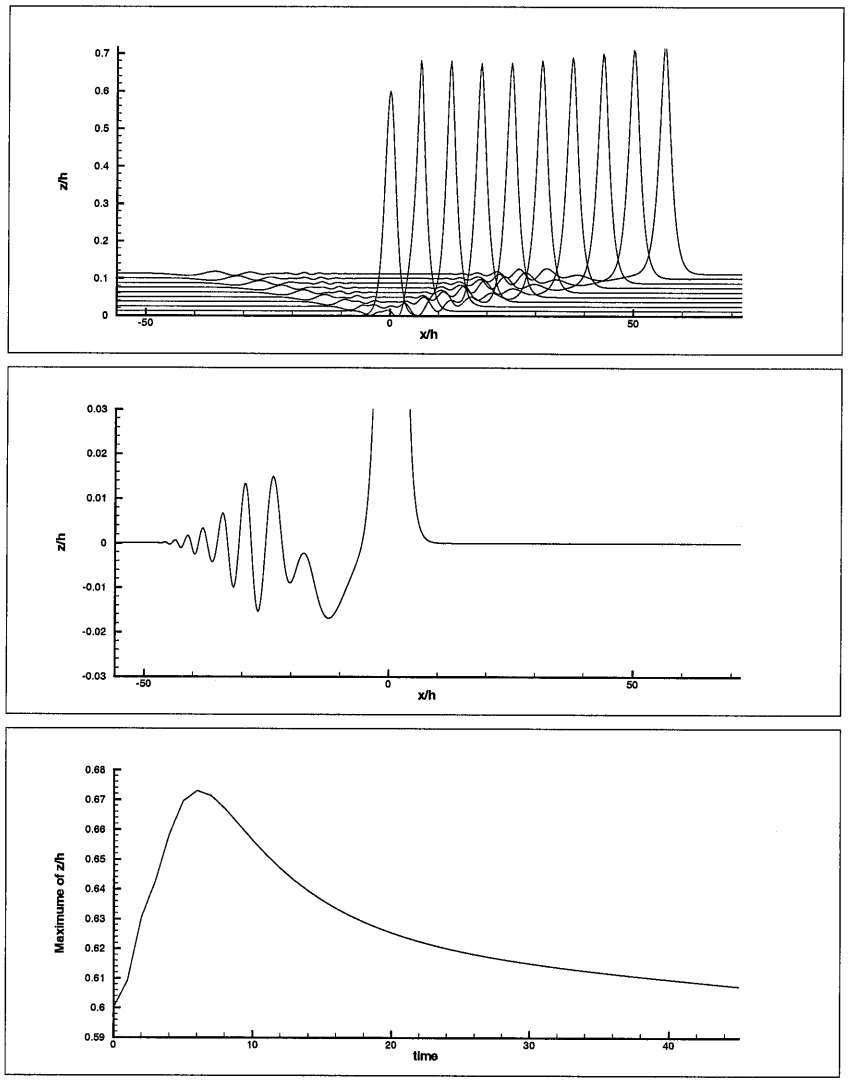

Figure 3.3a: Evolution of the free surface elevation computed by the time-marching method for the unsteady fully nonlinear theory started with the free surface elevation and initial wave speed and computed by the 1st-order asymptotic theory for a solitary wave of amplitude 0.6 as the initial condition. Top: The history of the free surface elevation from t=0s to t=45s. The time interval between two crests is 5s. Middle: Magnified view of the free surface elevation at t=45. Bottom: Variation of the wave crest height with time.

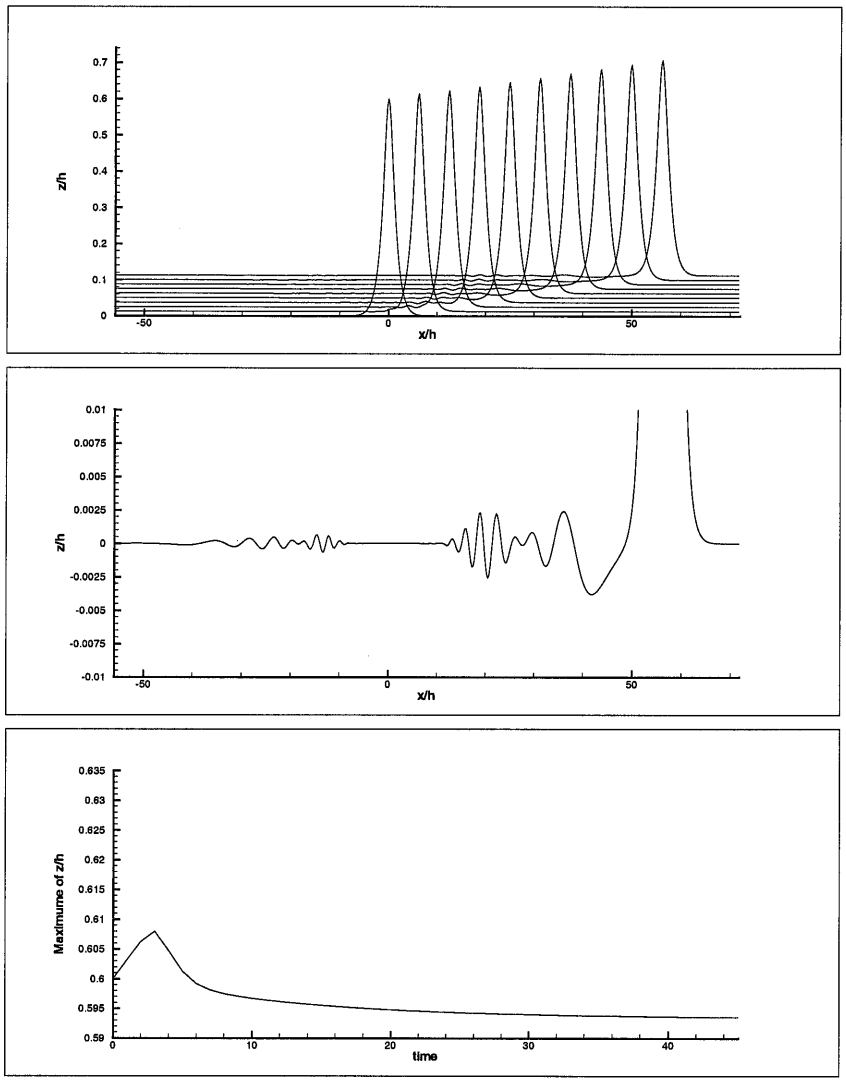

Figure 3.3b: Evolution of the free surface elevation computed by the time-marching method for the unsteady fully nonlinear theory started with the free surface elevation and initial wave speed and computed by the 5th-order asymptotic theory for a solitary wave of amplitude 0.6 as the initial condition. Top: The history of the free surface elevation from t=0s to t=45s. The time interval between two crests is 5s. Middle: Magnified view of the free surface elevation at t=45. Bottom: Variation of the wave crest height with time.

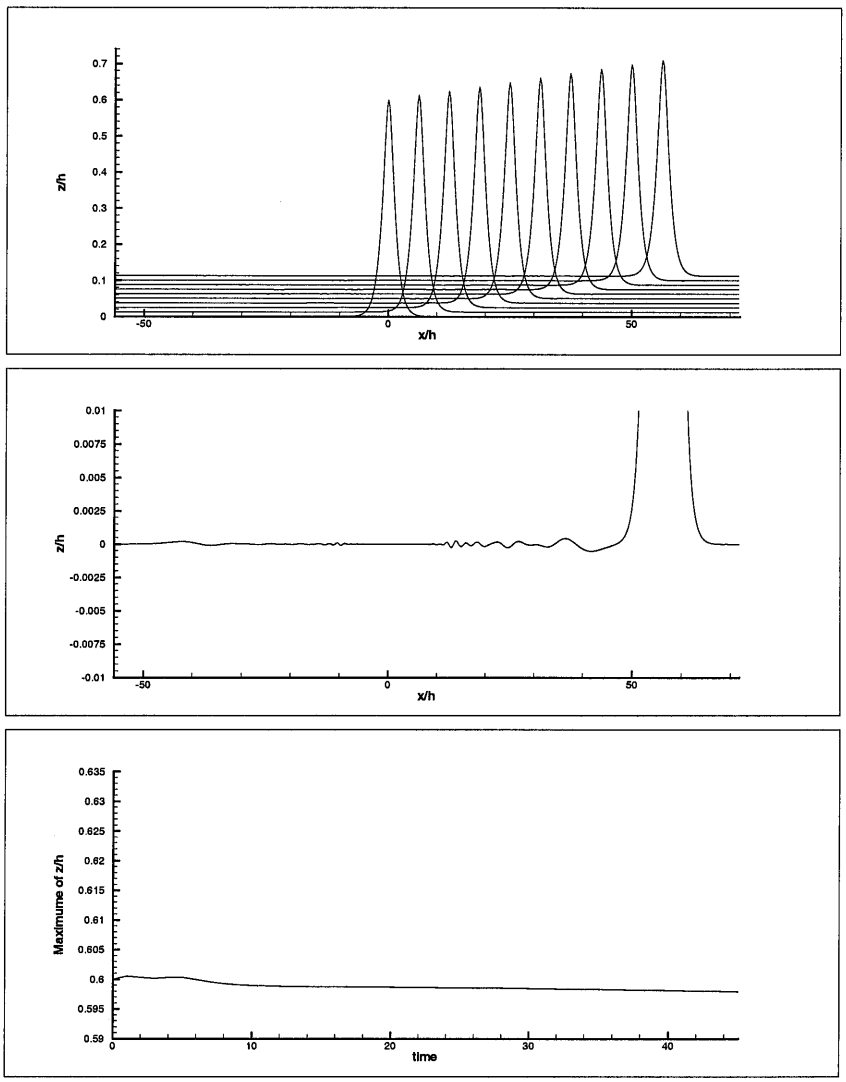

Figure 3.3c: Evolution of the free surface elevation computed by the time-marching method for the unsteady fully nonlinear theory started with the free surface elevation and initial wave speed and computed by the 11th-order asymptotic theory for a solitary wave of amplitude 0.6 as the initial condition. Top: The history of the free surface elevation from t=0s to t=45s. The time interval between two crests is 5s. Middle: Magnified view of the free surface elevation at t=45. Bottom: Variation of the wave crest height with time.

Chapter 4 Numerical scheme for fully nonlinear shallow water waves

In this chapter, two boundary integral methods, the FNFD and the Point-vortex methods, are developed for computing time-dependent, fully nonlinear, two-dimensional shallow water gravity waves. Boundary integral methods have been used extensively for calculation of various sorts of flow motions, especially those with free interfaces. The key feature of boundary integral method is that only the quantities on the boundary surface of a flow domain need to be computed. Among the variants, the Lagrange markers are commonly used for performing computations. The Lagrange markers method can provide automatically adaptive mesh, a method which is efficient, but has a disadvantage that the markers invariably tend to move together to cause clustering about boundary points of large curvature of the local surface, such as at the crest of a large wave. In such case, the calculation must be stopped and the markers be duly rearranged by some interpolation method to facilitate continuing computation.

The FNFD method is based on the integral closure equations mentioned in chapter 2 using an Euler-like mesh to avoid the problem of clustering. The FNFD method is very stable and efficient for computation of the asymptotic properties of solitary waves of large amplitude, even those very close to that of the highest wave which has an inner angle of 120° at the wave crest. In addition, to take the advantage of using the adaptive mesh for comparison with the FNFD method, we perform parallel computations by employing the Point-vortex method with using the Lagrange markers. The latter method is an extension of the method of Beale, Hou and Lowengrub (1996) for deep water waves. We modify their scheme by adding a bottom-effect term for computing fully nonlinear shallow water waves. The Point-vortex method will be used to compute waves of moderately large amplitude, especially for the computation of wave-wave interactions.

4.1 The FNFD numerical method

4.1.1 The basic equations for unsteady fully nonlinear shallow water waves

For the purpose of computation, it is advantageous to project the flow velocity into components proportional to local tangential and normal components. Viewed in these coordinates, as found earlier (e.g., Beale et al. 1996), the most singular terms cancel out to the highest order retained in the theory, and the behavior of the linearized equations qualitatively resemble that for the case near equilibrium. So we adopt a pair of new variables at the free surface,

$$u_s = \hat{u} + \hat{v}\ \zeta_x, \qquad u_n = \hat{v} - \hat{u}\ \zeta_x, \tag{4.1}$$

which has the inversion

$$\hat{u} = \frac{u_s - u_n\ \zeta_x}{R^2}, \qquad \hat{v} = \frac{u_n + u_s\ \zeta_x}{R^2}, \tag{4.2}$$

where

$$R^2 = 1 + \zeta_x^2 = \hat{z}_x\ \hat{z}_x^* \qquad (\hat{z}_x = \frac{d\,\hat{z}}{d\,x} = 1 + i\ \zeta_x), \tag{4.3}$$

and * denotes the complex conjugate so that u_s/R and u_n/R are the tangential and (outward) normal components of the flow velocity at the free surface. The complex velocity, written in term of u_s and u_n, becomes

$$\hat{w} = \hat{u} - i\ \hat{v} = \frac{u_s - i\ u_n}{\hat{z}_x}. \tag{4.4}$$

With the new unknowns (ζ, u_s, u_n), (2.12), (2.13) and (2.30) can be rearranged to produce a set of exact model equations as

$$\zeta_t = u_n \tag{4.5}$$

$$(u_s)_t = -\left[\zeta + \frac{1}{2R^2}\ (u_s^2 - u_n^2 - 2u_s u_n \zeta_x)\right]_x \tag{4.6}$$

$$\pi u_n(x,t) = \Re \int_{-\infty}^{\infty} \left[\frac{\hat{z}_x(x)}{\hat{z}(x) - \hat{z}(x')} \right] [u_s(x') - i\, u_n(x')] dx' - \Re \int_{-\infty}^{\infty} \left[\frac{\hat{z}_x(x)}{\hat{z}(x) - \hat{z}^*(x') + 2i} \right] [u_s(x') + i u_n(x')] dx', \quad (4.7)$$

where $\hat{z}_x(x) = d\hat{z}(x)/dx$ and only the real part of the (complex) integral equation (2.30) is adopted. The final form of (4.5) is obvious, since ζ_t/R is the (outward) normal component of the velocity of the free water surface. To obtain (4.6), we may make use of (2.13) and

$$\hat{D}^2\zeta = \hat{D}\hat{v} = \hat{v}_t + \hat{u}\ \hat{v}_x \quad (4.8)$$

to rearrange (2.12) as

$$(u_s)_t = (\hat{u} + \hat{v}\ \zeta_x)_t = -\frac{\partial}{\partial x}[\zeta + \frac{1}{2}(\hat{u}^2 - \hat{v}^2) + \hat{u}\ \hat{v}\ \zeta_x],$$

which is readily converted to (4.6) by using (4.1). Equation (4.7) follows from using (4.4) in (2.30) and taking its real component. In this system, (4.5) and (4.6) give the time evolution of ζ and u_s, while (4.7) closes the system. Equation (4.7) is a Fredholm integral equation of the second kind, which is well known for its convergence and efficiency in numerical computation for solution. We shall call the model consisted of equations (4.5)-(4.7) the FNFD wave model and use it to study the behavior of solitary-like waves that result from evolution of waves initially localized.

Stability analysis of the linearized system: the dispersion relationship

We next perform a linear stability analysis of the basic model equations. The result is of value for it can provide a reference criterion for constructing convergent numerical schemes for efficient computational applications. Assuming (ζ, u_s, u_n) to be sufficiently smooth and small in magnitude, all of order $O(\epsilon) \ll 1$, we find the linearized version of system (4.5)-(4.7) as

$$\zeta_t = u_n \quad (4.9)$$

$$(u_s)_t = -\zeta_x \quad (4.10)$$

$$\pi u_n(x) = \int_{-\infty}^{\infty} \left[\frac{1}{x-x'} - \frac{(x-x')}{(x-x')^2+4} \right] u_s(x')dx' - \int_{-\infty}^{\infty} \frac{2u_n(x')}{(x-x')^2+4} dx'. \tag{4.11}$$

We introduce the Fourier transform of $f(x)$ denoted by its calligraphic uppercase character as

$$\mathcal{F}(k) = \int_{-\infty}^{\infty} e^{-i\ k\ x} f(x)dx, \tag{4.12}$$

with the inversion

$$f(x) = \frac{1}{2\pi} \int_{-\infty}^{\infty} e^{i\ k\ x} \mathcal{F}(k)dk. \tag{4.13}$$

$f(x)$	$\mathcal{F}(k)$
$\partial f / \partial x$	$i\ k\ \mathcal{F}(k)$
$1/x$	$-i\ \pi\ \mathrm{sgn}(k)$
$x/(x^2+a^2)$	$-i\ \pi\ \mathrm{sgn}(k)\ e^{-\lvert ka \rvert}$
$a/(x^2+a^2)$	$\pi\ e^{-\lvert ka \rvert}$

Table 4.1: Some Fourier transform relations.

Applying the Fourier transformation to the linear system (4.9)-(4.11) and using the relations in table (4.1) for the integrals, which are all in convolution form, we obtain

$$\mathcal{Z}_t = \mathcal{U}_n, \tag{4.14}$$

$$(\mathcal{U}_s)_t = -i\ k\ \mathcal{Z}, \tag{4.15}$$

$$\mathcal{U}_n = -i\ \mathcal{U}_s\ \mathrm{sgn}(k) \tanh(|k|). \tag{4.16}$$

The eigenvalues of the above system, determined with all the variables taking a factor $\exp(\lambda t)$, are readily found to be given by the following equation

$$\lambda^2 = -k \tanh(k). \tag{4.17}$$

This is the linear dispersion relation derived from the basic model equations and is in agreement with the classical linear water wave theory. We further note that this rela-

tion plays such crucial roles in analysis of numerical stability that the corresponding numerical scheme is necessary to be compatible with it.

4.1.2 A convergent numerical method for evaluating unsteady fully nonlinear water waves

We proceed to derive a numerical scheme for applying the model equations (4.5)-(4.7) to compute fully nonlinear time-evolving water waves. The numerical algorithm includes choosing an optimum difference operator for evaluating the derivatives, finding a quadrature rule to perform the integration, selecting filters to remove errors due to the discretization and ensure the convergence and stability of the calculation as well as the accuracy of the result while keeping the physical information intrinsically unaffected. There are various ways to discretize system (4.5)-(4.7) based on different choices. However, the selections must be made all conjointly to attain a convergent and accurate numerical method. We shall follow the approach of Hou (1995) and Beale et al. (1996), who have shown, for free-surface flows in general (involving high-order accurate singular boundary integrals as in the present case), that valid numerical methods must satisfy certain compatibility conditions (between the choice of quadrature rule for the singular integral and that of the discrete derivatives) in order to be stable, and violation of these compatibility conditions will lead to numerical instability. This compatibility requirement ensures that the balance of the terms at the continuous level is preserved at the discrete level.

A numerical method for localized waves in infinite domain

We perform the numerical computation in a region, $-L \leq x' \leq L$, with the length of this region $2L$ taken to be large enough for the water surface elevation to fall off, from a localized (solitary-like) wave centered at the origin, to a negligible height at the two ends (at $x' = \pm L$). To simplify the discretization of equations (4.5)-(4.7), we scale the physical region to a computational region, $-\pi \leq x \leq \pi$, by using a scaling factor π/L. Upon finishing the computation with using the mesh generated

for the computational region, we can convert the result to the physical space just by inverse scaling. From here on, x' and x denote the coordinate in the physical and the computational regions, respectively. We generate a uniformly distributed mesh by discretizing the x-coordinate in the computational region with $2N$ equally spaced points $x_j = jh$ $(h = \pi/N, j = -N+1, \cdots, N)$. To make choice on the difference operator, quadrature rule and filters, we shall employ the discrete Fourier transform,

$$\tilde{u}_k = h \sum_{j=-N+1}^{N} u(x_j) e^{-i\ k\ j\ 2\pi/(2N)}, \qquad (k = -N+1, \cdots, N), \tag{4.18}$$

with the following inversion formula:

$$u(x_j) = \frac{1}{2\pi} \sum_{k=-N+1}^{N} \tilde{u}_k e^{i\ k\ j\ 2\pi/(2N)}. \tag{4.19}$$

Notice that $\tilde{u}_k$ is periodic in k with period $2N$. A discrete derivative operator may be expressed in terms of the discrete Fourier transform as

$$(D_{\tilde{h}} f)_k = i\ k\ \rho(kh) \tilde{f}_k, \qquad (k = -N+1, \cdots, N), \tag{4.20}$$

where the weighting factor $\rho(kh)$ depends on the choice of the difference operator. For a few commonly used discrete difference operators, we refer them to Beale et al. (1996) and cite them in the following list. For the second-order centered difference operator, we have

$$\rho_2(kh) = \frac{\sin(kh)}{kh} \geq 0; \tag{4.21}$$

for the fourth-order centered differencing,

$$\rho_4(kh) = \frac{8\sin(kh) - \sin(2kh)}{6kh} \geq 0; \tag{4.22}$$

and for the cubic spline approximation,

$$\rho_c(kh) = \frac{\sin(kh)}{kh} \frac{3}{2 + \cos(kh)} \geq 0. \tag{4.23}$$

Alternatively, we may choose the spectral derivative operator, with

$$\rho_s(kh) = 1, \tag{4.24}$$

for obtaining a spectrally accurate (of infinite order) approximation.

Filtering or smoothing of free-surface variable $\zeta(x)$ can be performed by multiplying its Fourier transform $\tilde{\zeta}_k$ by $p(kh)$,

$$\tilde{\zeta}_k^p = p(kh)\tilde{\zeta}_k, \tag{4.25}$$

where the superscript p denotes the weighting function of the filter which should have its value equal to one for most of the relevant frequencies and decay rapidly for frequencies at the very high end.

With this background clarified, we now derive the numerical scheme for computation of equations (4.5)-(4.7) by applying the alternating trapezoidal rule to discretize the singular integral on the free surface and the regular trapezoidal rule to discretize the regular integral on the image of the free surface. In this manner, we convert model equations (4.5)-(4.7) into discrete equations, for $m = -N+1, \cdots, N$, as

$$(\zeta_m)_t = u_{nm}, \tag{4.26}$$

$$(u_{sm})_t = -D_h \left[\zeta_m + \frac{u_{sm}^2 - u_{nm}^2 - 2\, u_{sm}\, u_{nm}\, D_h\zeta_m}{2(1+(D_h\zeta_m)^2)} \right]_m, \tag{4.27}$$

$$\begin{aligned} \pi u_{nm} &= \sum_{j=-N+1}^{N,(j-i)\ odd} \Re\left[\left(\frac{D_h \hat{z}_m^p}{\hat{z}_m^p - \hat{z}_j^p} \right) (u_{sj} - i u_{nj}) \right] 2h \\ &- \sum_{j=-N+1}^{N} \Re\left[\left(\frac{D_h \hat{z}_m^p}{\hat{z}_m^p - \hat{z}_j^{p*} + 2i} \right) (u_{sj} + i\, u_{nj}) \right] h. \end{aligned} \tag{4.28}$$

Here $h = \pi/N$, $\zeta_j(t)$, $u_{sj}(t)$ and $u_{nj}(t)$ denote the discrete representation of $\zeta(x,t)$, $u_s(x,t)$ and $u_n(x,t)$ at $x = jh$, respectively, and the superscript p denotes the filtered variables.

When the two boundaries at $x' = \pm L$ are taken to be open boundaries (connected

to still water outside), we adopt a radiation condition to invoke that

$$\frac{\partial \zeta}{dt} = \pm c_0 \frac{\partial \zeta}{dx'} \qquad (x' = \pm L) \tag{4.29}$$

where $c_0 = \sqrt{gh} = 1$ is the linear wave speed for water of uniform depth, and the $\pm$ signs are vertically ordered. Basically, this radiation condition lets all linear waves go out of the boundary to avoid numerical instability problems caused by non-physically reflected waves. This condition has been found sufficiently effective in retaining an overall high accuracy provided that L is taken large enough to let only waves of very small amplitudes reach the boundary during the time period of computation. For the purpose of computing the almost highest nonlinear unsteady waves, it is generally necessary to let the dominant waves propagate over a long distance to reach their permanent form asymptotically from any given initial condition. The window-shift technique used by Wu & Wu (1982) to follow the dominant waves of interest is adopted in this scheme.

A numerical method for periodic waves

As an alternative, we assume that the flow is periodic in x, with period $2L$. This periodic extension provides many advantages for developing a designed numerical scheme. With the solutions assumed periodic, we may use the spectral differential operator which provides a very high accuracy. The boundary condition becomes very easy to deal with under periodicity, especially for studying the evolution of unidirection waves, since outgoing waves simply reappear periodically in the computation region. In this manner, the asymptotic properties of a wave can be investigated over a long time of computation within a physical region of a relatively short length. The error caused by this periodic extension is within the same range as that caused by truncating an infinite physical region to a finite one. The error can be neglected provided that L is taken to be large enough to allow the rapid decay rate of the kernel involved to take its effect in the integration.

With the assumed periodicity,

$$f(x,t) = f(x+2n\pi,t) \qquad (n = \pm 1, \pm 2, \pm 3, \cdots), \tag{4.30}$$

for $f = \zeta, u_s, u_n$, the integrals in (4.7) can be summed up to give a single integral over the primary period. In fact,

$$\begin{aligned}
\int_{-\infty}^{\infty} \frac{f(\xi)}{\hat{z}(x)-\hat{z}(\xi)} d\xi &= \int_{-\pi}^{\pi} \sum_{n=-\infty}^{\infty} \frac{f(\xi+2n\pi)}{\hat{z}(x)-\hat{z}(\xi+2n\pi)} d\xi \\
&= \sum_{n=-\infty}^{\infty} \int_{-\pi}^{\pi} \frac{f(\xi)}{(\hat{z}(x)-\hat{z}(\xi))-2n\pi} d\xi \\
&= \int_{-\pi}^{\pi} \frac{f(\xi)}{2} \cot\left[\frac{\hat{z}(x)-\hat{z}(\xi)}{2}\right] d\xi.
\end{aligned} \tag{4.31}$$

Similarly, the other integrals in (4.7) can also be so summed up. Thus, equation (4.7) becomes

$$\begin{aligned}
2\pi u_n(x) &= \Re \int_{-\pi}^{\pi} \hat{z_x}(x) \cot\left[\frac{(\hat{z}(x)-\hat{z}(\xi))}{2}\right] (u_s(\xi) - i\, u_n(\xi)) d\xi \\
&- \Re \int_{-\pi}^{\pi} \hat{z_x}(x) \cot\left[\frac{(\hat{z}(x)-\hat{z^*}(\xi)+2\,i)}{2}\right] (u_s(\xi) + i\, u_n(\xi)) d\xi.
\end{aligned} \tag{4.32}$$

Therefore, with the assumed periodicity, the basic model equations are now consisted of (4.5), (4.6) and (4.32).

For discretization of the integral equation (4.32), we again use the alternating trapezoidal rule for the singular integral, and the trapezoidal rule for the regular integral as before and we finally have the discrete basic equations as follows:

$$(\zeta_i)_t = u_{ni}, \tag{4.33}$$

$$\frac{d\,u_{si}}{d\,t} = -D_h \left[\zeta_i + \frac{u_{si}^2 - u_{ni}^2 - 2u_{si}\, u_{ni}\, D_h\zeta_i}{2(1+(D_h\zeta_i)^2)}\right]_i, \tag{4.34}$$

$$2\pi u_{ni} = \sum_{j=-N+1}^{N,\,(j-i)\ odd} \Re\left[D_h\hat{z}_i \cot\left(\frac{\hat{z}_i^p - \hat{z}_j^p}{2}\right)(u_{sj} - i(u_n)_j)\right] 2h - \sum_{j=-N+1}^{j=N} \Re\left[D_h\hat{z}_i \cot\left(\frac{\hat{z}_i^p - \hat{z}_j^{p*} + 2i}{2}\right)(u_{sj} + i(u_n)_j)\right] h, \tag{4.35}$$

for computing nonlinear solitary waves with periodic expansion.

4.1.3 Consistency and linear stability at the discrete level

Consistency

We now examine the degree of how accurate the discretized equations can approximate their continuous counterpart, equations (4.5), (4.6) and (4.7). It is well know that the trapezoidal rule has the spectral accuracy for periodic function $f(x) \in C^m[-\pi, \pi]$ (Isaacson & Keller, 1966), namely,

$$\int_{-\pi}^{\pi} f(x)dx - \sum_{j=-N+1}^{N} f(x_j)h = O(h^m), \tag{4.36}$$

and is accurate to order $O(h^2)$ for non-periodic functions(Isaacson & Keller, 1966), $g(x)$ say,

$$\int_{-\pi}^{\pi} g(x)dx - \sum_{j=-N+1}^{N} g(x_j)h = O(h^2). \tag{4.37}$$

The alternating trapezoidal rule gives the spectral accuracy for the Cauchy-type singular integral of periodic functions,

$$\sum_{j=-N+1}^{N,(i-j)\ odd} f(x_j)2h = 2\sum_{j=-N+1}^{N} f(x_j)h - \sum_{j=-N+1}^{N,(i-j)\ even} f(x_{2j})(2h) = \int_{-\pi}^{\pi} f(x)dx + O(h^m), \tag{4.38}$$

but only a second-order accuracy for the singular integral of non-periodic functions.

For the derivative operators, we note that if D_h is an rth-order approximation of D_x, then

$$|D_h\zeta_j - \zeta_x(x_j)| = O(h^r). \tag{4.39}$$

Similarly, the error due to smoothing in regard to free-surface position is

$$|\zeta_j^p - \zeta(x_j)| = O(h^r). \tag{4.40}$$

If we select the spectral derivative operator and set $P(kh) \equiv 1$, then $r = m$ for periodic functions. Put the above relations together, and we can conclude that the present scheme is consistent and accurate to $O(h^m)$ under periodic boundary conditions and to $O(h^2)$ for non-periodic flows.

Linear stability

Stability analysis of the numerical method for evaluating exact solution to our basic equations, involving nonlinear singular integrals with the Cauchy kernel, is difficult, partly due to the high frequency errors that would naturally result from the nonlinearity of the problem. However, the linear stability analysis should still be of great significance since its resulting criteria for the equilibrium state could help identify sources of instability and cast light on how best to resolve such numerical instability problems.

From (4.26)-(4.28) we readily obtain the linearized discrete equations as follows:

$$(\zeta_m)_t = u_{nm}, \tag{4.41}$$

$$(u_{sm})_t = -D_h(\zeta_m), \tag{4.42}$$

$$\begin{aligned} \pi u_{nm} = & \sum_{(m-j)odd} \frac{u_{sj}}{x_m - x_j}\, 2h - \sum_j \frac{u_{sj}(x_m - x_j)}{(x_m - x_j)^2 + 4} h \\ & - \sum_j \frac{2u_{nj}}{(x_m - x_j)^2 + 4} h. \end{aligned} \tag{4.43}$$

The last equation involves three kernels:

$$K_1(x_j) = \frac{2}{x_j}, \qquad K_2(x_j) = \frac{x_j}{(x_j^2 + 4)}, \qquad K_3(x_j) = \frac{2}{(x_j^2 + 4)}. \tag{4.44}$$

Defining the discrete convolution of f_j and g_j as

$$(g * f)_j = \sum_m g_{j-m}\, f_m\, h, \tag{4.45}$$

we see that equation (4.43) is a sum of convolutions of the velocity components with the above kernels and its Fourier transform is found as

$$\pi\ \tilde{u}_{nk} = \tilde{K}_{1k}\tilde{u}_{sk} - \tilde{K}_{2k}\tilde{u}_{sk} - \tilde{K}_{3k}\tilde{u}_{nk}. \tag{4.46}$$

Following Beale et al.(1996), we find that the Fourier transform $\tilde{K}_{1k}$ has the sum:

$$\tilde{K}_{1k} = h \sum_{m=-\infty}^{\infty,odd} \frac{2}{m\,h} e^{-i\,k\,m\,h} = 2 \sum_{n=-\infty}^{\infty} \frac{1}{2n+1} e^{-i\,k\,(2n+1)\,h} = -i\,\pi\,\mathrm{sgn}(k\,h), \quad (|kh| < \pi). \tag{4.47}$$

For K_2, we have

$$\begin{aligned} \tilde{K}_{2k} &= \sum_{n=-\infty}^{\infty} \frac{nh}{(nh)^2+4}\, h\, e^{i\ k\ n\ h} \\ &= \left(\sum_{n=-\infty}^{\infty} \frac{n}{(n)^2+4/,h^2} e^{i\ k\ n\ h} + err \right) - err \end{aligned} \tag{4.48}$$

where the singled-out error term is

$$err = e^{-2\pi/h} \left(\sum_{n=-\infty}^{\infty,\,n,\,odd} - \sum_{n=-\infty}^{\infty,\,n,\,even} \right) \frac{n}{(n)^2+(-2/h)^2} e^{i\ k\ n\ h}, \tag{4.49}$$

which decays exponentially as h approaches zero and we use $O(h^m)$ to denote its order. Making use of the following relation,

$$\begin{aligned} \pi\ \mathrm{sgn}(x) e^{a|x|} &= \sum_{n=-\infty}^{\infty} \frac{-n\,i}{n^2+a^2}(1-(-1)^n e^{a\,\pi}) e^{i\,n\,x} \\ &= \left[\sum_{n=-\infty}^{\infty} + e^{a\pi} \left(\sum_{n=-\infty}^{\infty,odd} - \sum_{n=-\infty}^{\infty,even} \right) \right] \frac{-ni}{(n^2+a^2)} e^{i\,n\,x},\ a<0, \end{aligned} \tag{4.50}$$

we have

$$\tilde{K}_{2k} = -\pi\, i\, \mathrm{sgn}(k)\, e^{-2|k|} + O(\exp(-2\pi/h)). \tag{4.51}$$

Similarly, for K_3, we obtain

$$\tilde{K}_{3k} = -\pi\, e^{-2|k|} + O(\exp(-2\pi/h)), \tag{4.52}$$

for which we have made use of the following relation

$$\begin{aligned} \pi\, e^{a|x|} &= \sum_{n=-\infty}^{\infty} -\frac{a}{n^2+a^2}(1-(-1)^n e^{a\pi})e^{i\,n\,x} \\ &= \left[\sum_{n=-\infty}^{\infty} + e^{a\pi}\Big(\sum_{n=-\infty}^{\infty,odd} - \sum_{n=-\infty}^{\infty,even}\Big)\right] \frac{-a}{n^2+a^2} e^{i\,n\,x},\ a<0. \end{aligned} \tag{4.53}$$

$$\tag{4.54}$$

Applying discrete Fourier transform to equations (4.41)-(4.43) and using the above relations, we finally attain the linearized basic equations in spectral form as

$$\tilde{\zeta}_{kt} = \tilde{u}_{nk}, \tag{4.55}$$

$$\tilde{u}_{skt} = ik\,\rho(kh)\tilde{\zeta}_k, \tag{4.56}$$

$$\tilde{u}_{nk} = i\mathrm{sgn}(k)\tilde{u}_{sk} - i\mathrm{sgn}(k)e^{-2|k|}\tilde{u}_{sk} - e^{-2|k|}\tilde{u}_{nk}. \tag{4.57}$$

It readily follows that this discrete version of equations has the dispersion relation

$$\lambda^2 = -\rho(kh)\, k\, \tanh(k) \tag{4.58}$$

for the numerical scheme. The scheme is stable but not as accurate for high wave-number modes as compared with the dispersion relation at the continuous level. However, we can use the spectral difference operator (with $\rho(kh) = 1$) in our scheme to conserve the same dispersion relation as that of the continuous level to get a spectrally accurate scheme.

4.1.4 Other aspects of the numerical scheme

The time-marching method

To compute the ordinary differential equations which we have obtained in the previous section, we may use any stable ordinary-differential-equation solver as long as we keep the time step within the stable domain of the method. In our scheme, in particular, we use the 4th-order Adams multi-step method to perform the time marching except that we start the initial steps with the 4th-order Runge-Kutta method. In each step, we use the Gauss-Seidel method iteratively to solve the Cauchy integral. The iteration is stopped when the difference between two successive steps becomes less than a threshold value. In our computation, this threshold value is set to be 10^{-10}. The initial guess of data for starting the iteration plays an important role on the efficiency of the scheme; we use the extrapolation formula,

$$f_n = 4f_{n-1} - 6f_{n-2} + 4f_{n-3} - f_{n-4}, \tag{4.59}$$

to compute the initial data based on the solutions obtained from calculation of the preceding four steps. In most cases, only four to five iterations were needed to reach our threshold value at each time step.

Resolution, aliasing error and roundoff error

An important aspect of numerical computation is the resolution. With a given number of nodal points, $2N$ say, we can only represent the wave profile within a range of wave-number less than N. However, waves with amplitudes greater than a certain threshold have a wider spectrum, then to have more points in such cases will be needed for representing such large waves with a required accuracy. We can not describe a wave with a large amplitude with insufficient number of nodal points. That is, the mesh size will have to be further reduced to provide the resolution necessary for portraying it. When waves approach the highest amplitude, the profile becomes very sharp at the crest like a singular point such as a cornered vertex with an internal angel of $2\pi/3$ for gravity waves. In such cases, we will need many modes in the spectral space to

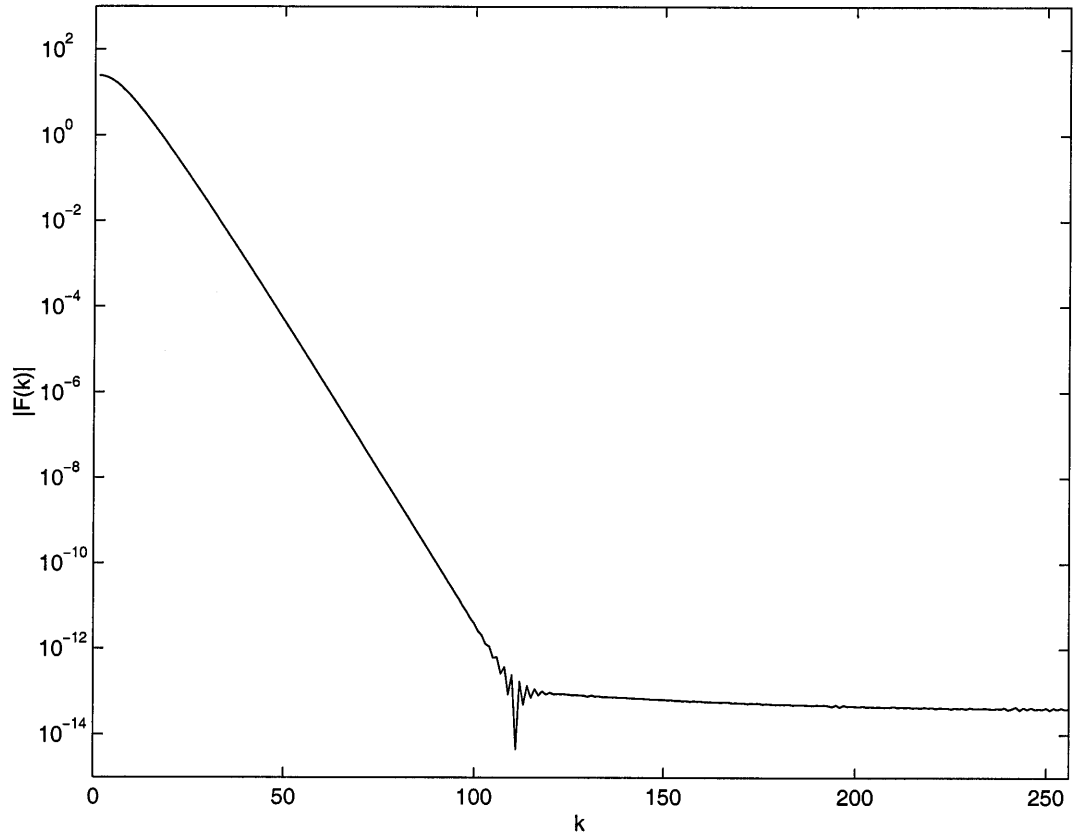

Figure 4.1: The spectrum of a solitary wave of amplitude $\alpha = 0.7$. A number of nodal points $2N > 240$ will be sufficient for describing this wave. $|F(k)|$: modular of the component at wave number k of the Fourier transformation of the free surface elevation ζ.

describe it. If we choose the number of nodal points $2N$ less than this number, we would lose the capability of describing it with a reasonable accuracy.

In our computation, we choose a number $2N$ for making the set of nodal points large enough to start computation so that the modulus of the components in the spectrum of a wave of a given amplitude would fall off to a low flattened level at wave-numbers around N in spectrum. If this criterion is met, this chosen number for $2N$ should then provide the sufficient resolution for describing that particular wave. In Figure 4.1 we show the spectrum of a solitary wave of amplitude $\alpha = 0.7$ in which the modulus of the components with wave number larger than 120 fall off to a flattened level around 10^{-13}. For this particular case, choosing a number of

nodal points $2N \geq 240$ will provide sufficient resolution for describing the wave with a satisfied accuracy. However, the components with wave-numbers higher than N, whose modulus may be very small compared with the components of lower wave-number, could still cause aliasing errors on the components with wave-numbers less than N. Further, these errors can be amplified by a differential operator and thereby cause numerical instability. For this reason, a dealiasing filter is used to remove these errors. In our scheme, a 25th-order Fourier smoothing filter, given by

$$p(kh) = \exp\left(-10(2|k|/N)^{25}\right), \text{ for } |k| \leq N, \tag{4.60}$$

is applied to smoothen surface variables in each time step.

Appropriate choices of a large number of nodal points $2N$, which provides the resolution needed, and a dealiasing filter, which removes the aliasing error, are two important factors in computation of high amplitude waves. In our experience, the choice of a large $2N$ is even more important. Otherwise, the computation may well crash in just a few time steps, no mater how the dealiasing filter is employed. In such cases, the primary cause of instability is due to the choice of a $2N$ being too small for the computation. However, the computation could run a long time before it crashes if we would pick a large enough $2N$ and turn off the dealiasing filter.

In this manner, the discretized integrals are computed by iteration until the numerical variation between two consecutive steps is less than a specified threshold value ϵ. The components in the spectrum with energy less than this ϵ are due to numerical round-off, which are physically meaningless. To keep this kind of error from polluting the solution and generating instability, a nonlinear filter:

$$\mathcal{F}_k = \begin{cases} \mathcal{F}_k : & |\mathcal{F}_k| \geq \epsilon \\ 0 & : \text{otherwise} \end{cases} \tag{4.61}$$

is applied to computing of u_n in every time step.

4.2 The Point-vortex method

4.2.1 Mathematical model

The governing equations

As an alternative, we now introduce *the point-vortex method* to investigate evolution of fully nonlinear gravity waves on a uniform layer of incompressible and irrotational fluid of unit rest depth. We parameterize the free water surface with a complex position variable $z(\alpha)$ at time t, with the x and y coordinates as its real and imaginary parts, i.e., $z(\alpha,t) = x(\alpha) + i\,y(\alpha,t)$. The parameter α is the Lagrangian coordinate variable which identifies the initial position of a particle on the free surface. Following Beale, Hou and Lowengrub (1996), we express the complex velocity potential $\Phi(\alpha,t)$ in the flow domain in terms of a distribution of dipole of strength $\mu(\alpha,t)$ so that

$$\Phi(\alpha,t) = \frac{1}{2\,\pi\,i}\int_{\partial\mathcal{D}} \frac{1}{z(\alpha,t) - z(\alpha',t)}\;\mu(\alpha',t)\;dz(\alpha'), \tag{4.62}$$

where $z(\alpha,t)$ and $z(\alpha',t)$ are two points on the flow boundary $\partial\mathcal{D}$ and the integral assumes the Cauchy principal value. In (4.62), time t is merely a parameter and may be omitted for brevity. In the flow domain $\mathcal{D}$, Φ has the velocity potential $\phi(x,y,t)$ and stream function $\psi(x,y,t)$ as its real and imaginary components, respectively,

$$\Phi(z,t) = \phi(x,y,t) + i\,\psi(x,y,t) \qquad (z = x + i\,y \in \mathcal{D} + \partial\mathcal{D}). \tag{4.63}$$

The velocity potential in the interior is given by

$$\phi(x,y) = \Re\,\Phi = \oint_{\partial\mathcal{D}} \frac{\partial}{\partial\,n} G(z(\alpha) - z(\alpha'))\;\mu(\alpha')\;ds(\alpha'), \tag{4.64}$$

where $G(z) = (2\,\pi)^{-1}\log\,|z|$, and n is the unit normal vector at $z(\alpha',t) \in \partial\mathcal{D}$ outward from the flow domain. The value of ϕ on the free surface can be determined by applying the Plemelj formula of complex variables to integral representation (4.64)

for ϕ to yield

$$\phi(\alpha) = \frac{1}{2}\mu(\alpha) + \Re\,\frac{1}{2\,\pi\,i}\int \frac{1}{z(\alpha) - z(\alpha')}\;\mu(\alpha')\;dz(\alpha'), \tag{4.65}$$

or

$$\phi(\alpha) = \frac{1}{2}\mu(\alpha) + \oint_{\partial\mathcal{D}} \frac{\partial}{\partial\,n} G(z(\alpha) - z(\alpha'))\;\mu(\alpha')\;ds(\alpha'), \tag{4.66}$$

where the integration is carried counterclockwise along $\partial\mathcal{D}$, the boundary of the domain $\mathcal{D}$. For the special case with a horizontal bottom, by the symmetry of the problem due to $v(-1,t) = 0$, the domain $\mathcal{D}$ can be analytically continued to its extended domain $\mathcal{D}_e$: $(-2-\zeta < y < \zeta,\ -\infty < x < \infty)$. Accordingly, we may place a surface dipole strength on the image of the free surface by reflection into the flat bottom, i.e., let $\mu(z^* - 2i) = \mu(z)$ for z on the free surface, $z^* - 2i$ being its image and the $*$ denoting the complex conjugate. We may of course revise the original boundary $\partial\mathcal{D}$ into $\partial\mathcal{D}_e$, the boundary of $\mathcal{D}_e$, thus curtailing the need of calculating velocity $\underline{u}(x) = u(x,-1)$ on the horizontal bottom. The contributions from the two vertical paths cancel by virtue of the fluid being at rest at infinity. The remaining line integrals along the free surface and its image may be written, on account of the symmetry, as

$$\begin{aligned}\phi(\alpha) \;=\; & \frac{1}{2}\mu(\alpha) + \int_{-\infty}^{\infty} \frac{\partial}{\partial\,n} G(z(\alpha) - z(\alpha'))\;\mu(\alpha')\;ds(\alpha') \\ & - \int_{-\infty}^{\infty} \frac{\partial}{\partial\,n} G(z(\alpha) - z^*(\alpha') + 2i)\;\mu(\alpha')\;ds(\alpha').\end{aligned} \tag{4.67}$$

Differentiating both sides of this equation with respect to α and integrating by parts, we obtain

$$\phi_\alpha(\alpha) = \frac{1}{2}\gamma(\alpha) + \Re\left[\frac{z_\alpha(\alpha)}{2\,\pi\,i}\left(\int_{-\infty}^{\infty} \frac{\gamma(\alpha')}{z(\alpha) - z(\alpha')}\;d\alpha' - \int_{-\infty}^{\infty} \frac{\gamma(\alpha')}{z(\alpha) - z^*(\alpha') + 2i}\;d\alpha'\right)\right], \tag{4.68}$$

where $\gamma = \mu_\alpha = \partial\;\mu/\partial\;\alpha$ is vortex sheet strength. Differentiating the complex potential with respect to z, we obtain the complex velocity $w = u - i\,v = d\Phi/dz$

which has the integral representation

$$w(z,t) = \frac{1}{2\pi i}\left[\int_{-\infty}^{\infty} \frac{\gamma(\alpha')}{z - z(\alpha')}\, d\alpha' - \int_{-\infty}^{\infty} \frac{\gamma(\alpha')}{z - z^*(\alpha') + 2i}\, d\alpha'\right]. \tag{4.69}$$

Using the Plemelj formula, we obtain the velocity on the free surface,

$$w(\alpha) = \frac{1}{2\pi i}\left[\int_{-\infty}^{\infty} \frac{\gamma(\alpha')}{z(\alpha) - z(\alpha')}\, d\alpha' - \int_{-\infty}^{\infty} \frac{\gamma(\alpha')}{z(\alpha) - z^*(\alpha') + 2i}\, d\alpha'\right] + \frac{\gamma(\alpha)}{2z_\alpha(\alpha)}, \tag{4.70}$$

for which we have taken the limit of z approaching the free surface from the fluid side.

The evolution of the free surface elevation and velocity potential are governed by the kinematic and dynamical conditions, namely,

$$z_t(\alpha,t) = w^*(\alpha,t) \tag{4.71}$$

and

$$\phi_t(\alpha,t) - \frac{1}{2}|w|^2 + \zeta = 0, \tag{4.72}$$

where the ambient pressure is gauged to zero and the time is scaled by $(h/g)^{1/2}$. Here, it is important to note that $\phi_t(\alpha,t)$ in (4.72) is the material rate of variation in ϕ, it is related to the Eulerian variation $\phi_t(x,y,t)$ by

$$\phi_t(\alpha,t) = \phi_t(x,y,t) + (u^2 + v^2). \tag{4.73}$$

In summary, we have for computing shallow water waves based on the point-vortex method the governing equations as follows:

$$\begin{aligned} z_t^*(\alpha,t) &= w(\alpha,t) \\ &= \frac{1}{2\pi i}\left[\int_{-\infty}^{\infty} \frac{\gamma(\alpha')}{z(\alpha) - z(\alpha')}\, d\alpha' - \int_{-\infty}^{\infty} \frac{\gamma(\alpha')}{z(\alpha) - z^*(\alpha') + 2i}\, d\alpha'\right] \\ &\quad + \frac{\gamma(\alpha)}{2z_\alpha(\alpha)}, \end{aligned} \tag{4.74}$$

$$\phi_t(\alpha,t) = \frac{1}{2}(u^2 + v^2) - \zeta, \tag{4.75}$$

$$\gamma(\alpha) = \Re\left[\frac{z_\alpha(\alpha)}{\pi i}\left(\int_{-\infty}^{\infty}\frac{\gamma(\alpha')}{z(\alpha)-z^*(\alpha')+2i}\,d\alpha' - \int_{-\infty}^{\infty}\frac{\gamma(\alpha')}{z(\alpha)-z(\alpha')}\,d\alpha'\right)\right] + 2\phi_\alpha(\alpha). \tag{4.76}$$

We shall call this method the Point-vortex method.

The dispersive relation

We proceed to find the dispersion relation of the linearized system of (4.74)-(4.76) by perturbing the nonlinear system from its equilibrium state. We assume

$$z(\alpha) = \alpha + x' + i\,y', \quad \gamma = \gamma', \quad \phi = \phi', \tag{4.77}$$

where $(x', y', \gamma', \phi') = O(\epsilon) << 1$. Linearizing equations (4.74) to (4.76) and omitting the primes, we have,

$$(\phi_\alpha)_t = -y_\alpha, \tag{4.78}$$

$$x_t = \frac{1}{2\pi}\int_{-\infty}^{\infty}\frac{2\gamma(\alpha')}{(\alpha-\alpha')^2+4}d\alpha' + \frac{\gamma(\alpha)}{2}, \tag{4.79}$$

$$y_t = \frac{1}{2\pi}\int_{-\infty}^{\infty}\frac{\gamma(\alpha')}{\alpha-\alpha'}d\alpha' - \frac{1}{2\pi}\int_{-\infty}^{\infty}\frac{(\alpha-\alpha')\,\gamma(\alpha')}{(\alpha-\alpha')^2+4}d\alpha', \tag{4.80}$$

$$\gamma(\alpha) = \int_{-\infty}^{\infty}\frac{-2\gamma(\alpha')}{(\alpha-\alpha')^2+4}d\alpha' + 2\phi_\alpha. \tag{4.81}$$

Applying the Fourier transform with respect to the variable α, to the above equations and using the relations in table 4.1, we obtain

$$\mathcal{X}_t = \frac{1}{2}(1+e^{-2|k|})\Gamma, \tag{4.82}$$

$$\mathcal{Y}_t = \frac{-i}{2}\mathrm{sgn}(k)(1-e^{-2|k|})\Gamma, \tag{4.83}$$

$$\Phi_{\alpha t} = -ik\mathcal{Y}, \tag{4.84}$$

$$\Gamma = 2\Phi_\alpha/(1+e^{-2|k|}), \tag{4.85}$$

or in matrix form,

$$\begin{pmatrix} \mathcal{X} \\ \mathcal{Y} \\ \Phi_\alpha \end{pmatrix}_t = \begin{pmatrix} 0 & 0 & 1 \\ 0 & 0 & i\mathrm{sgn}(k)\ \tanh(k) \\ 0 & ik & 0 \end{pmatrix} \begin{pmatrix} \mathcal{X} \\ \mathcal{Y} \\ \Phi_\alpha \end{pmatrix}. \tag{4.86}$$

The eigenvalues of the above linearized system are $\lambda_0 = 0$, ${\lambda_{1,2}}^2 = -k\ tanh(k)$. This result agrees with the dispersive relation for waves by linear theory.

4.2.2 Numerical scheme

Beale, Hou and Lowengrub(1996) have proved that the present scheme for the case of gravity waves in deep water is convergent. The bottom effect term added to this model for shallow water waves will not change the convergence of the scheme since the integral along the bottom is regular in nature.

Similar to the way we used in developing the FNFD method, we select a derivative operator (which can be chosen among the 2nd-order center, 4th-order center and a spectral differential operator) jointly a filter, for smoothening the free surface elevation, and quadrature rules, for calculating the integrations, so as to provide a stable and accurate numerical method. Here we follow Beale et al. (1996) to discretize equations (4.74)-(4.76). The integration involving the free surface variables is performed by the alternating trapezoidal rule and the integration along the mirror image of the free surface, by the trapezoidal rule.

The Lagrange markers are first uniformly distributed over the computation region $-\pi \leq x \leq \pi$ and allowed to evolve with time according to equations (4.74)- (4.76). The computation region can be mapped onto the physical region, $-L \leq x' \leq L$, with a scaling factor L/π. L is taken to be large enough as we argued in section 4.1. The numerical algorithm for calculation of (4.74)-(4.76) can thus be represented as follows:

$$\phi_{kt} = \frac{1}{2}(u_k^2 + v_k^2) - y_k, \tag{4.87}$$

$$\tilde{z}_{kt} = \frac{\gamma_k}{2(D_h z)_k} + \frac{1}{2\pi i} \sum_{j=-N+1}^{N,(j-k)\,odd} \frac{\gamma_j\, 2h}{z_k^p - z_j^p} - \frac{1}{2\pi i} \sum_{j=-N+1}^{N} \frac{\gamma_j\, h}{z_k^p - \overline{z^p}_j + 2i}, \tag{4.88}$$

$$\gamma_k = 2(D_h\phi)_k - \Re\left(\frac{(D_h z)_k}{\pi i} \sum_{j=-N+1}^{N,(j-k)\,odd} \frac{\gamma_j\, 2h}{z_k^p - z_j^p}\right) + \Re\left(\frac{(D_h z)_k}{\pi i} \sum_{j=-N+1}^{N} \frac{\gamma_j\, h}{z_k^p - \overline{z^p}_j + 2i}\right). \tag{4.89}$$

The time-marching computation can be executed by employing an ordinary-differential-equation solver, for which task we use the Adams solver in our scheme. In each time step, z and ϕ are updated first and γ is solved from the integral equation by iteration. Dealiasing filter (4.60) is applied to smoothen the free surface elevation at each time step in order to remove any possible aliasing error. The nonlinear filter (4.61) is then used to remove the round-off error.

Chapter 5 Analysis of the numerical results

The two numerical methods developed in the preceding chapters are applied to compute fully nonlinear shallow water waves of large amplitude. The excess mass and excess surface energy that must be conserved are computed to check the accuracy of the methods. In particular, solitary waves of large amplitude are computed using both methods and the results are compared with the exact solution for permanent solitary waves computed by Wu & Kao (2000).

5.1 Accuracy of the numerical schemes

In the present computation of asymptotically evolving solitary-like waves propagating on shallow water of uniform depth, the accuracy of the two numerical methods employed here will be measured by examining the variation in the excess mass,

$$M = \sum_{k=1}^{N} \zeta_i h, \tag{5.1}$$

and the excess surface energy

$$E = \sum_{k=1}^{N} (\frac{u_i^2 + v_i^2}{2} + \zeta_i) h, \tag{5.2}$$

both of which should be conserved. We start computation with an initial wave profile and wave speed c of a solitary wave furnished by the exact solution for a permanent solitary wave of equal amplitude obtained by the method of Wu & Kao (2000). At each nondimensional time unit, the total mass and the total energy are computed based on the free surface elevation and velocity at the free surface. The variations of the total mass and total energy from their initial values during the first 100 nondimensional

α_0	$\overline{\alpha}$	$2L$	$2N$	ΔM	ΔE	$c/\sqrt{g\,h}$	$c_s/\sqrt{g\,h}$
0.1000	0.09992	40	128	1.20e-11	2.78e-6	1.0491	1.0485
0.1000	0.09997	40	256	6.87e-12	2.78e-6	1.0489	1.0485
0.1000	0.09998	40	512	2.43e-12	2.78e-6	1.0488	1.0485
0.2867	0.2860	40	128	2.77e-10	1.69e-5	1.1320	1.1319
0.2867	0.2865	40	256	3.36e-11	1.40e-5	1.1320	1.1319
0.2867	0.2866	40	512	7.32e-12	5.01e-6	1.1320	1.1319
0.5252	0.5233	40	128	6.92e-10	1.01e-5	1.2245	1.2248
0.5252	0.5247	40	256	4.23e-10	9.02e-6	1.2247	1.2248
0.5252	0.5251	40	512	1.39e-11	5.30e-6	1.2248	1.2248
0.6970	0.6908	32	128	2.68e-07	1.36e-4	1.2779	1.2781
0.6970	0.6958	32	256	5.32e-10	5.25e-5	1.2779	1.2781
0.6970	0.6967	32	512	1.71e-10	2.03e-6	1.2781	1.2781
0.8001	0.8000	32	1024	4.01e-12	1.61e-5	1.2942	1.2942

Table 5.1: Numerical results of wave amplitude, wave speed, variation of excess mass and excess surface energy during the first 100 nondimensional time units for various wave amplitudes computed by using the FNFD scheme. α_0: the amplitude of initial wave; $\overline{\alpha} = \sum_{i=1}^{100} \alpha_i$; $2L$: length of the computation region; $2N$: number of computation points; $\Delta M = \sqrt{(\sum_{i=1}^{n}(M_i - \overline{M})^2)/n}$; $\Delta E = \sqrt{(\sum_{i=1}^{n}(E_i - \overline{E})^2)/n}$; c: wave speed computed by the FNFD method; c_s: wave speed computed by the method of Wu & Kao.

time units performed by using the two unsteady methods are shown in table (5.1) and table (5.2). The results given in the two tables clearly show improved rates of convergence of both methods with increasing number of nodal points. Both the FNFD and Point-vortex methods provide excellent conservations on the mass and energy. The FNFD method is more accurate on conserving total mass with the smallest error less than 10^{-10} in all the cases.

The Point-vortex method based on the Lagrange markers provides auto-adaptive meshes which is efficient and accurate to compute waves of low to moderately high amplitude. It can also be used to compute the roll-over of waves. However, the Lagrange markers tend to move toward to the crest from both sides and finally cluster together so densely in computation of the almost highest solitary waves as to make it difficult to continue on the work. In such circumstances, the computation has to be stopped and the markers be rearranged by interpolation to proceed with further computation. The clustering of the Lagrange markers also put a restriction on the size

α_0	$\overline{\alpha}$	$2L$	$2N$	ΔM	ΔE	$c/\sqrt{g\,h}$	$c_s/\sqrt{g\,h}$
0.1000	0.09993	40	128	1.55e-5	1.84e-5	1.0493	1.0485
0.1000	0.09997	40	256	3.88e-6	6.36e-6	1.0488	1.0485
0.1000	0.09998	40	512	9.69e-7	3.57e-6	1.0487	1.0485
0.2867	0.2863	40	128	1.62e-4	1.90e-4	1.1319	1.1319
0.2867	0.2866	40	256	4.06e-5	5.40e-5	1.1321	1.1319
0.5252	0.5245	40	128	8.11e-4	1.08e-3	1.2248	1.2248
0.5252	0.5250	40	256	2.04e-4	2.73e-4	1.2247	1.2248
0.6970	0.6961	32	128	1.86e-3	2.78e-3	1.2792	1.2781
0.6970	0.6968	32	256	4.68e-4	6.80e-4	1.2782	1.2781
0.6970	0.6969	32	512	9.15e-5	1.15e-4	1.2779	1.2781

Table 5.2: Numerical results of wave amplitude, wave speed, variation of excess mass and excess surface energy during the first 100 nondimensional time units for various wave amplitudes computed by using the Point-vortex scheme. α_0: The amplitude of initial wave; $\overline{\alpha} = \sum_{i=1}^{100} \alpha_i$; $2L$: length of the computation region; $2N$: number of computation points; $\Delta M = \sqrt{(\sum_{i=1}^{n}(M_i - \overline{M})^2)/n}$; $\Delta E = \sqrt{(\sum_{i=1}^{n}(E_i - \overline{E})^2)/n}$; c: wave speed computed by the Point-vortex method; c_s: wave speed computed by the method of Wu & Kao.

of time steps. In our numerical experiment, the highest wave amplitude of solitary wave that can be computed by the Point-vortex method is $\alpha = 0.75$. The FNFD method is better for computing the almost highest waves since in this method we use the Euler meshes which avoid the problem of clustering. With this advantage, we are able to compute solitary waves up to the amplitude $\alpha = 0.8219$ using the FNFD method, as shown in Figure 5.1.

We note that for waves of rather small amplitudes, the FNFD method with different but uniform sizes of meshes is found to provide results with almost the same accuracy. However, the accuracy apparently improves with decreasing mesh size when we use the FNFD method to compute waves of moderate to large amplitudes. These results illustrate the importance of choosing an appropriate number of nodal points to have it large enough to provide the resolution needed for describing solitary waves of high amplitudes. Figure 5.2 shows the spectrum of the water surface elevation of a solitary wave of amplitude $\alpha = 0.1$, the moduli of the components in the spectrum with wave numbers greater than $k \approx 20$ are around 10^{-5}. With $2N = 128$ as the number of computation points, the wave is well described and increasing the number

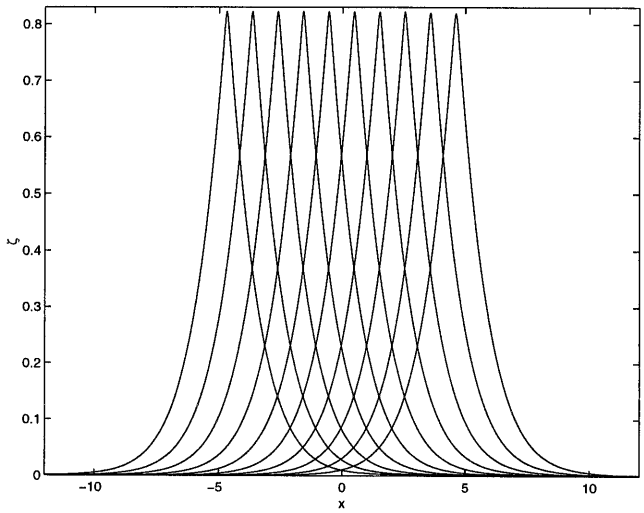

Figure 5.1: Propagation of a solitary wave of large -time asymptotic amplitude $\alpha = 0.8219$.

of nodal points does not improve the accuracy. Figure 5.3 shows the spectrum of surface elevation of a solitary wave of amplitude $\alpha = 0.8$, the modulus drops to around 10^{-5} for components with wave-number as high as $k \approx 300$ and greater. In this case, the computation with a number of nodal points $2N = 128$ is found to be not stable due to the high aliasing error and we must choose a higher number of nordal point, for example $2N = 1024$ to provide the necessary resolution.

5.2 Comparison with the permanent form

The numerical methods developed in the last two chapters, namely, the FNFD method using the Euler meshes and the Point-vortex method using the Lagrange markers have been used to compute solitary waves of large amplitudes. The results so obtained will now be compared with the results obtained by Wu & Kao (2000) using the exact theory for steady solitary waves permanent in form. They developed a method to compute the permanent wave forms of fully nonlinear steady shallow water waves by using conformal mapping method. The singular behavior of the solution at infinity of the physical plan is found to bear a global effect on the analysis and construction method of the exact solution. When this effect is well handled to achieve an optimum

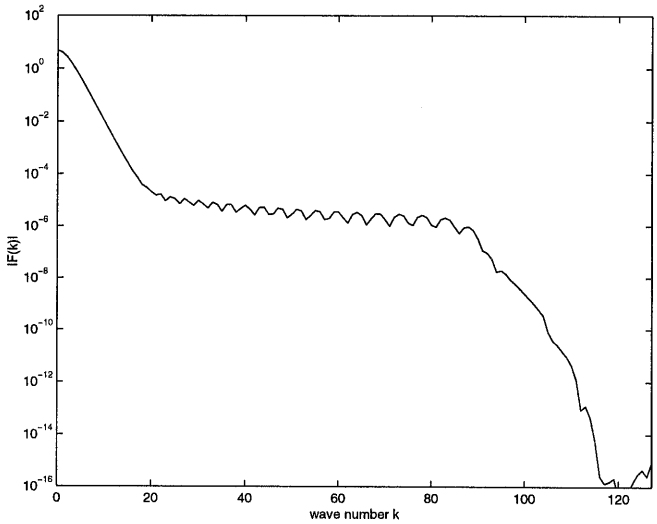

Figure 5.2: The spectrum of a solitary wave of amplitude $\alpha = 0.1$.

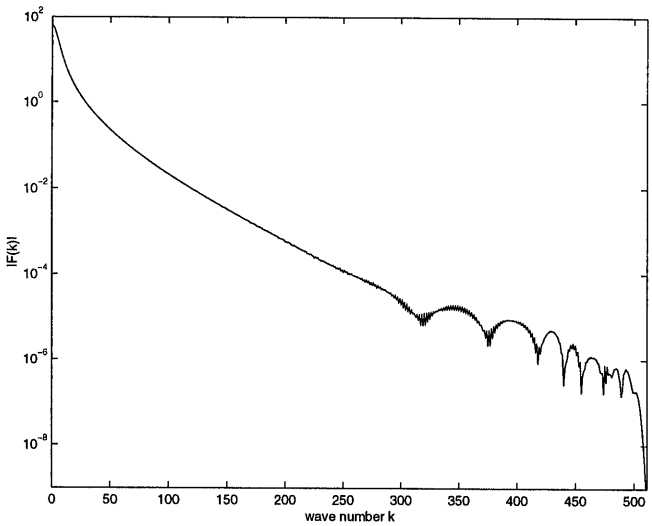

Figure 5.3: The spectrum of a solitary wave of amplitude $\alpha = 0.8$.

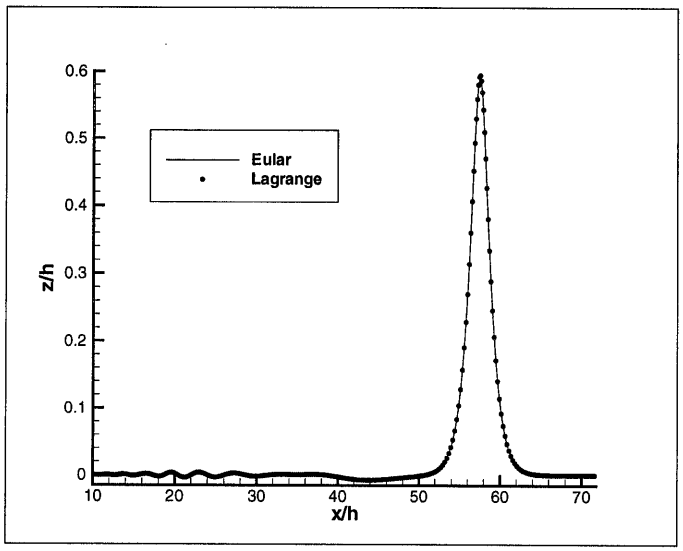

Figure 5.4: Wave profiles computed by the FNFD and Point-vortex methods with the initial wave profile at $t = 0$ given by the first-order solution of KdV Model with $\alpha = 0.6$, the profiles being shown at $t = 46$.

overall balance, solution can be obtained to very high accuracy with a relative error less than 10^{-10}, up to the highest solitary wave (with a cornered vertex of interior angle 120° and amplitude $\alpha_{max} = 0.8331990\cdots$ and wave velocity $c = 1.2908904\cdots$). The accuracy of the two unsteady schemes are assessed by comparison of their results with the corresponding ones by the permanent wave method.

We first compute the time evolution of a right-going solitary wave with a moderately large amplitude, starting with the initial profile and wave speed given by the solution of the Korteweg-de Vries (KdV) equation as a first order solitary wave, followed by the time-marching computation of the two fully nonlinear methods till the profile reaches in each case its own asymptotic state whose terminal amplitude is different, by a certain slight degree, from the initial input. The asymptotic solution of the unsteady-wave computation is then used for feed back to the steady-wave method as a determined parameter to compute the profile of the final steady wave for comparison, now based on equal amplitude. Starting from the same initial condition, the free surface variations are computed by both the FNFD and the Point-vortex methods and shown in Figure 5.4. The wave profiles given by both schemes are found in good agreement with each other. In more details, as indicated in Figure 5.6, a

train of left-going waves of very small amplitude is separated at the first moment from the right-going wave train which is led by the primary wave. Then the dominant solitary wave out runs the packet of small right-going wave train, finally leaving the right-going wave train behind it. Eventually, the main solitary wave reaches its asymptotic state, i.e., the wave profile shifts a distance c per-unit-time and keeps its form unchanged within a specific error limit. The final amplitude and phase speed are then numerically measured and fed back as parameters to start the steady -wave computation. In Figure 5.7 the profiles given by the three methods are compared.

We then start the unsteady-wave computations of the asymptotic wave by feeding the permanent wave solution obtained from the steady-wave method as the initial condition. Fully nonlinear shallow water waves with different asymptotic amplitudes are computed and checked by comparison with the initial data. The computation region is selected large enough for the free surface elevation to remain less than 10^{-5} at the two ends of the region. In all the cases we have succeeded in obtaining the permanent right-going solitary waves within the threshold error limit. The wave speeds are determined numerically from the wave profiles obtained at each time step and compared with the corresponding wave speeds given by the steady-wave method in table 5.1 and table 5.2. In Figure 5.5 we present the results relating the wave amplitude and wave speed determined by the three methods. All the comparisons show that the two numerical schemes developed for calculation of fully nonlinear unsteady waves on shallow water are accurate and stable, with a relative error less than 10^{-4} up to the amplitude as large as $\alpha = 0.822$.

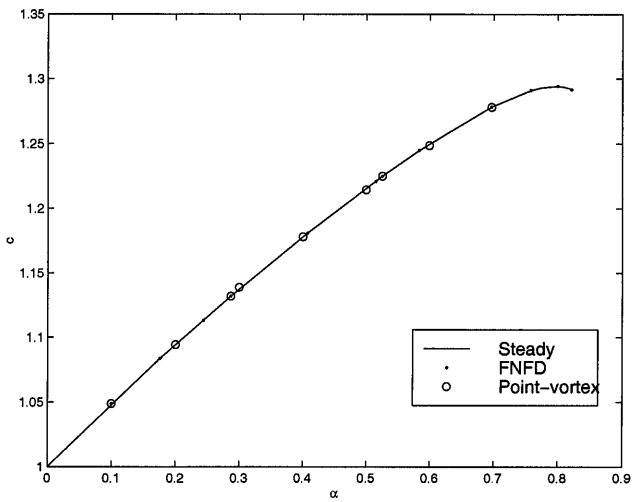

Figure 5.5: Wave speed versus wave amplitude computed by the three methods: the steady-wave theory method, the FNFD and the Point-vortex method.

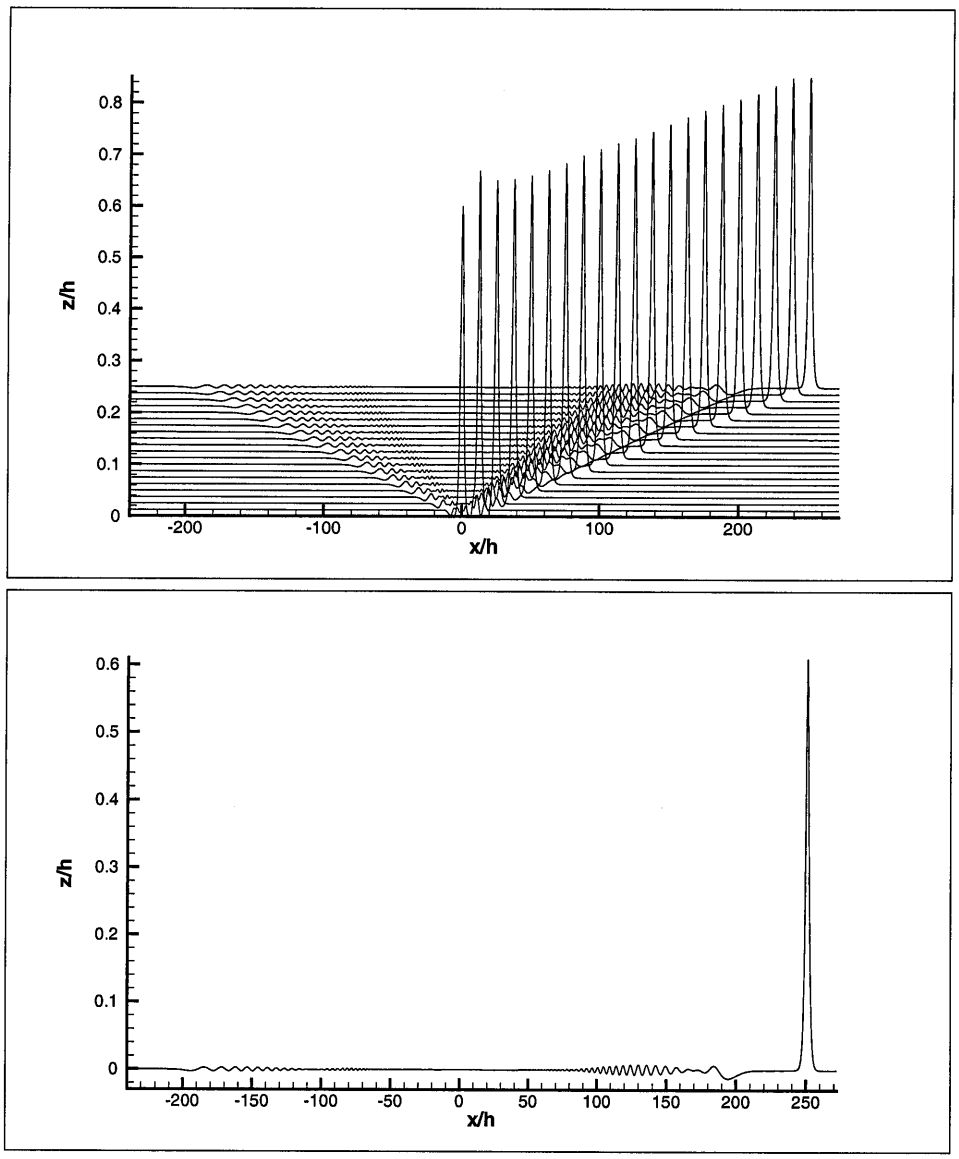

Figure 5.6: Evolution of a solitary wave started initially from the first-order solution of the KdV model equation for a solitary wave of amplitude $\alpha = 0.6$. Top: A time sequence snapshot of the free surface elevations given by the FNFD calculation at different time intervals $\Delta t = 10$. Bottom: The free surface elevation at t=200.

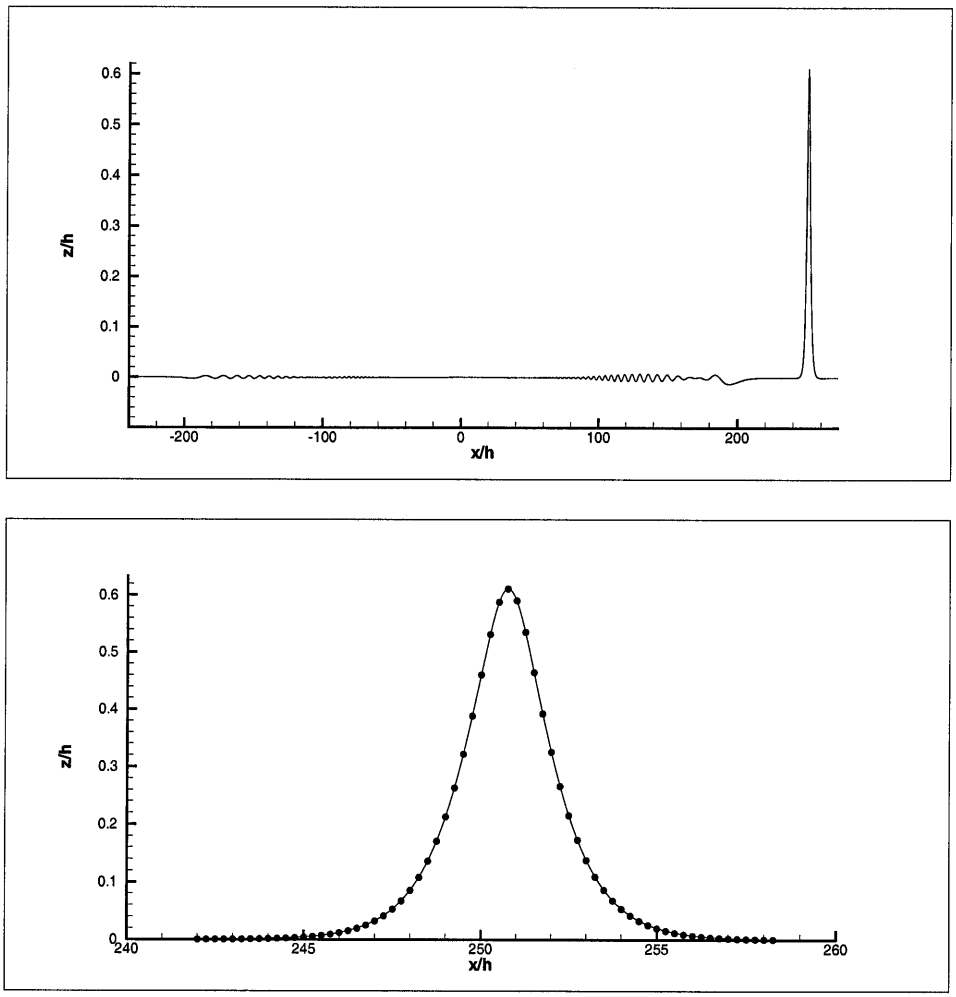

Figure 5.7: Comparison of the asymptotic wave profile with the steady wave profile. Top: The free surface elevation at t=200 started form the first order solution with $\alpha = 0.6$. Bottom: Enlarged view for comparison between the steady wave profile,—, and the asymptotic wave profile $\cdots$, given at top.

Chapter 6 Numerical studies of interactions between solitary waves

6.1 Introduction

Nonlinear wave interactions are of great importance not only in basic science but also in technological development and applications to many disciplines. A simple class of problems is concerned with two solitary waves propagating in opposite directions along a straight channel of uniform rectangular cross-sectional shape and engaging in binary encounters, or collisions. The salient features of nonlinear wave-wave interactions, such as wave modulations in shape, amplitude and phase, are quite well exhibited in the Boussinesq class of binary wave collisions. Zabusky and Kruskal (1965) show that the KdV equation possesses a number of remarkable properties including the phenomenon of reappearance of initial flow configurations assigned to a spatially periodic motion, giving rise to a temporally periodic response, on which phenomenon (and additional wave-wave interaction behaviors) the term of *soliton* is coined. The KdV equation has since furnished a rich field in which an enormous amount of intensive research has blossomed into what may be called a distinguished colorful modern history of applied and pure mathematics, physics, biology, and engineering and applied science. Close collaborations between various disciplines also emerged as a distinct mark of the time as similar phenomena are found commonplace in nonlinear systems.

For the class of head-on collisions of solitons, the special case of total reflection of a soliton by an inviscid vertical wall has been investigated by Chan and Street (1970) using the SUMMAC integration of the Navier-Stokes equations, by Byatt-Smith (1971) using a conformal mapped integral equation, by Maxworthy (1976) and Weidman & Maxworthy (1978) experimentally, by Power and Chwang (1984) using

perturbation methods for a comparative study, and by Yih and Wu (1995) from a different approach. For end-wall reflection, the theory has been extended to higher orders by Su & Mirie (1980). In another direction, the theory has been generalized by Wu (1995) for bidirectional interactions between multiple solitons of the Boussinesq class and by Cooker et al. (1997) for the Euler equations.

For the overtaking interactions between two solitary waves, the two solitary waves either pass through or remain separated throughout the encounter depending on the ratio between the amplitudes of the two solitary waves. The critical criterion separating the single-peak and double-peak regimes for overtaking soliton encounters was first noted by Zabusky (1967), proved for its existence and numerically analyzed by Lax (1968), experimentally measured by Weidman & Maxworthy (1978), and analytically determined by Wu (1995).

In this chapter, we study head-on collisions between two fully nonlinear solitary waves by using the unsteady wave motion methods developed in chapter 4.

6.2 Head-on collision between solitary waves

6.2.1 Binary head-on collision between two identical solitary waves

We conduct a numerical study on the physical process of reflection of a solitary wave by a vertical wall, or, equivalently, the head on collision of two identical solitary waves propagating in opposite directions on a layer of inviscid fluid of uniform rest depth.

Two identical solitary waves propagating in opposite directions are placed far enough away from the center (where the wall is situated at $x = 0$) such that the free surface elevation at the center is less than 10^{-5} at $t = 0$ to begin with. The initial solitary profile and speed used for time-marching computation are given from the permanent wave computation using the method of Wu & Kao (2000). In Figure 6.1 we show a head-on collision of two identical solitary waves of amplitude $\alpha = 0.6$. The two waves propagate toward each other with a constant speed till the crests reach

a distance about three times the water depth from the center where the waves have their crests asymptotically accelerating to reach the center at a time called the time of attachment, t_a, with an amplitude of attachment, ζ_a, remaining at the wall (for a finite period called the phase-locking period) with the amplitude at wall first increasing, as the trailing tail continues coming inward and converting kinetic energy to potential energy, to reach a maximum amplitude ζ_0 at the time of maximum run-up, $t = t_0$, and then reverse in procedure to drop down and leave the wall at a time called the time of detachment, t_d, with an amplitude of detachment, ζ_d. It has been found that at the lowest-order nonlinear-and-dispersive (i.e., the Boussinesq level) theory, the procedure has a time-reversal symmetry, namely, $\zeta(x, -t) = \zeta(-x, t)$ where $t = 0$ is the instant the wave crest reaches its maximum at the center. However, this symmetry is modified in higher-order theories, such as given by Su & Mirie (1982) for the third-order theory and by Cooker (1990) for the Euler model. It is shown here that, in addition to a modulation of the symmetry, the reflected dominant wave propagates away from the center with a dispersive wave train trailing behind it. After the wave train having traveled away form the center, the free surface at the center calms down and finally returns to its initial value ($\zeta \approx 0$).

In Figures 6.2-6.7, we show the trajectories of the wave crests and the free surface elevation at the wall during the head-on interaction between solitary waves of small to modulate amplitudes.

In table 6.1 we present the results on the time of attachment, t_a, the amplitude of attachment, ζ_a, the maximum run-up time, t_0, with the maximum amplitude ζ_0, the time of detachment, t_d, the amplitude of detachment, ζ_d, and the incoming and outgoing wave speed c_i and c_r of the initial incoming and the terminal reflected solitary waves (of different amplitudes) for this binary encounter. These results are compared and shown in Figures 6.8-6.10 with those of Sue & Mierie which are accurate to order of α^3. The third-order weakly nonlinear asymptotic theory agrees quite well with the fully nonlinear results for the amplitude of attachment and maximum run-up. For the detaching amplitude, weakly nonlinear theory can provide a good prediction for waves with amplitude less than 0.4. However, the detaching amplitude given by the

α	α_∞	ζ_a	ζ_0	ζ_d	$t_0 - t_a$	$t_d - t_0$	t_r	c_i	c_r
0.1000	0.0996	0.1359	0.2062	0.1329	2.44	2.48	4.92	1.0522	1.0520
0.2000	0.1997	0.2738	0.4269	0.2579	1.79	1.87	3.67	1.1056	1.0939
0.3000	0.2967	0.4104	0.6604	0.3587	1.54	1.69	3.22	1.1360	1.1361
0.3999	0.3947	0.5521	0.9239	0.4451	1.41	1.59	3.00	1.1784	1.1734
0.4500	0.4433	0.6194	1.0721	0.4832	1.39	1.55	2.94	1.2000	1.1969
0.4998	0.4906	0.6888	1.2387	0.5171	1.38	1.52	2.90	1.2140	1.2123
0.5500	0.5360	0.7578	1.4328	0.5247	1.42	1.51	2.92	1.2231	1.2286
0.5995	0.5785	0.8254	1.6680	0.4814	1.50	1.49	2.99	1.2513	1.2454
0.6109	0.5835	0.8450	1.7264	0.4801	1.52	1.48	3.00	1.2544	1.2480
0.6492	—	0.8999	1.9551	0.4777	1.59	1.47	3.07	1.2672	—
0.7000	—	0.9680	2.3267	—	1.71	—	—	1.2793	—

Table 6.1: Some numerical results for head-on collisions between solitary waves of initial amplitude α. ζ_∞: asymptotic amplitude of the reflected wave. ζ_a: amplitude when crest merges with wall at time t_a; ζ_0: maximum amplitude of wave at wall at time t_0; ζ_d: amplitude when crest detaches from wall at time t_d; $t_r = t_d - t_a$: phase-locking time, c_i: wave speed of incoming wave; c_r: asymptotic wave speed of reflected wave.

fully nonlinear numerical computation at $\alpha = 0.55$ or higher is noticeably different from the result computed from Sue & Mierie. Figure 6.11 shows the profiles before and after the detachment during a head-on collision of solitary waves of amplitude $\alpha = 0.6$, the water at the wall is pushed so high by the collision that it still has a rise when the crests of the dominant reflected waves already emerge to leave the wall. At this moment, there are three local maximum points on the free surface as shown in Figure 6.11.

As for the phase-locking time, $t_r = t_d - t_a$, the fully nonlinear results are found to be always longer than that of the weakly nonlinear asymptotic theory. The ratio of $(t_0 - t_a)/t_r$ is quite close to 0.5 for all the waves in the comprehensive range covered, which means that the maximum runup is always nearly at the center of the phase-locking time period, regardless of wave amplitude.

6.2.2 Asymmetrical head-on collisions

During asymmetrical head-on collisions between two solitary waves of different amplitudes, the crests of the two incoming solitons do not actually merge, but with the

smaller one evanescing at time t_a, with $\zeta_x = \zeta_{xx} = 0$ at $x = x_a$ and reaching an amplitude $\zeta = \zeta_a$, with the taller wave gaining in height to a maximum height ζ_0 at $t = t_0$, at $x = x_0$, and reversing in procedure with time, and with the smaller soliton reappearing to depart at time $t = t_d$, $x = x_d$, with amplitude ζ_d, at which $\zeta_x = \zeta_{xx} = 0$. It is known that at the lowest-order nonlinear theory this process has a time-reversal symmetry and the two terminal solitons have their profile unchanged from their initial form once they are totally separated (Whitham 1974). In cases when fully nonlinear waves are considered, this time-reversal symmetry will be modified and two trains of dispersive waves are induced to trail the reflected solitons after the crests have separated from each other during the collision. Figures 6.14-6.16 show an example of the head-on collision between two solitary waves of amplitude $\alpha = 0.6$ and $\alpha = 0.4$. Figure 6.17 shows the trajectory of the crests during the head-on collision.

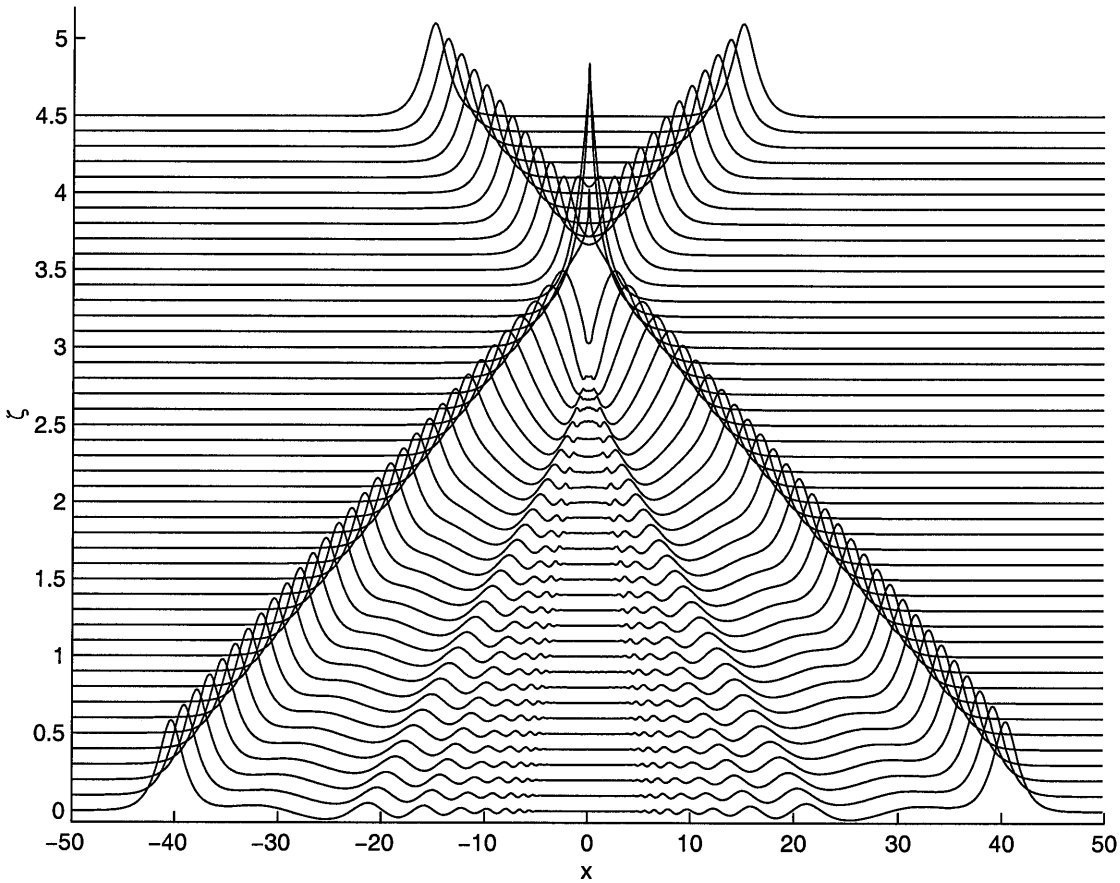

Figure 6.1: Head-on collision between two identical solitary waves of amplitude $\alpha = 0.6$.

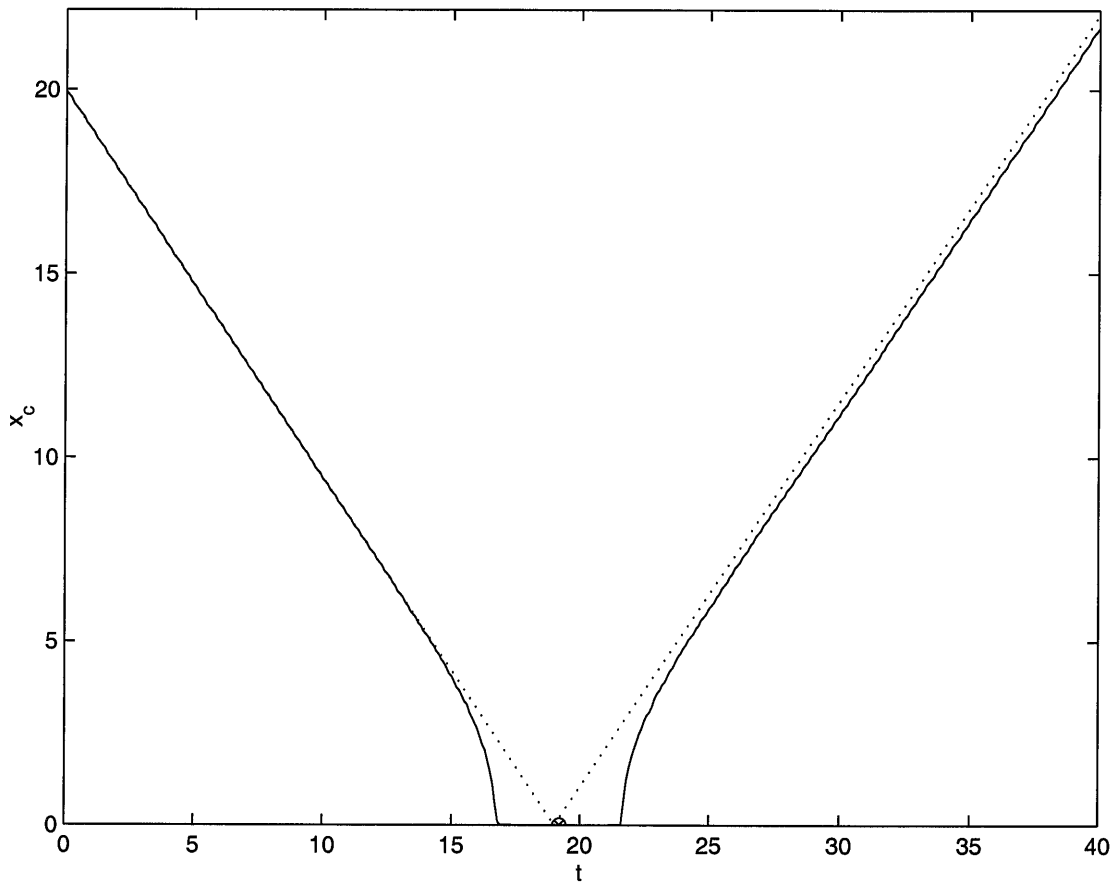

Figure 6.2: The trajectory of the wave crest during a head-on collision between two solitary waves of amplitude $\alpha = 0.1$. $\otimes$: the time at maximum run-up.

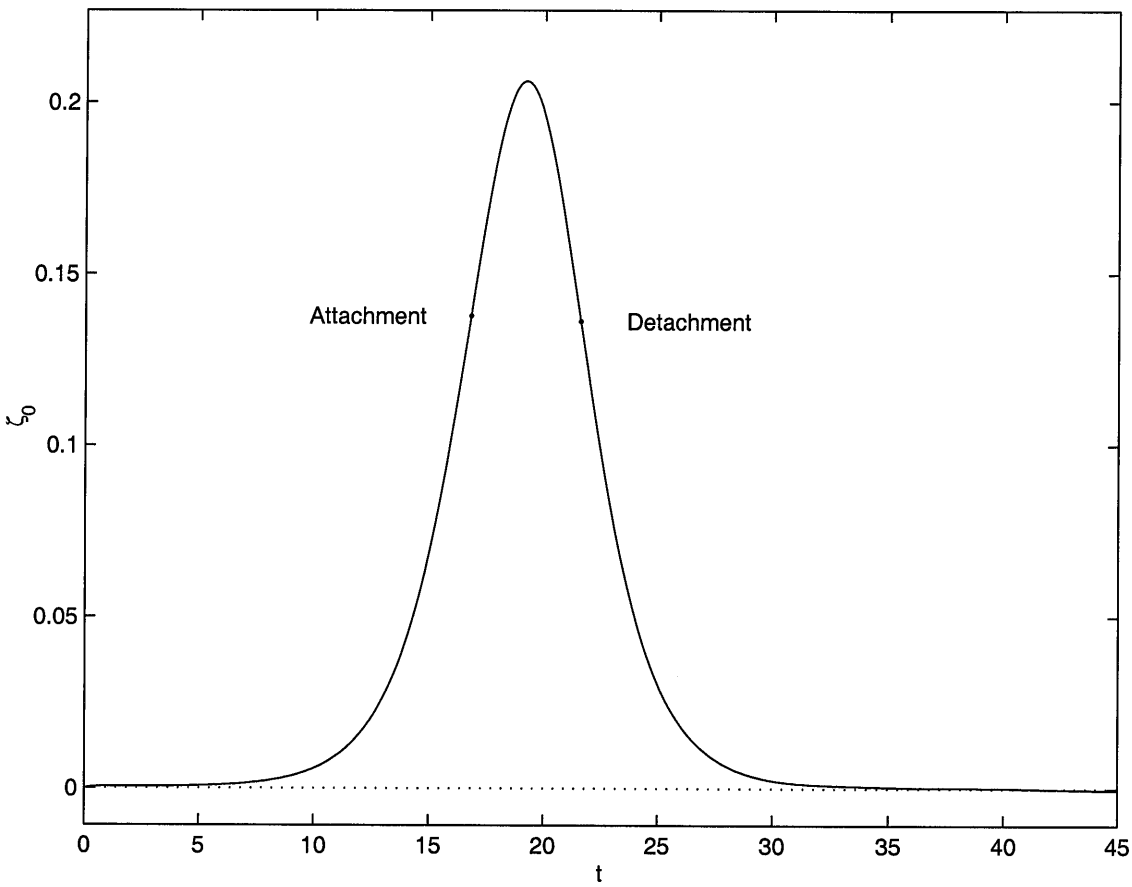

Figure 6.3: Variations of the water height at the wall with time t throughout a head-on collision between two solitary waves of amplitude $\alpha = 0.1$. (It is not symmetric about t_0, i.e., $\zeta(0, t - t_0) \neq \zeta(0, t_0 - t)$, as is obvious in Figure 6.5.)

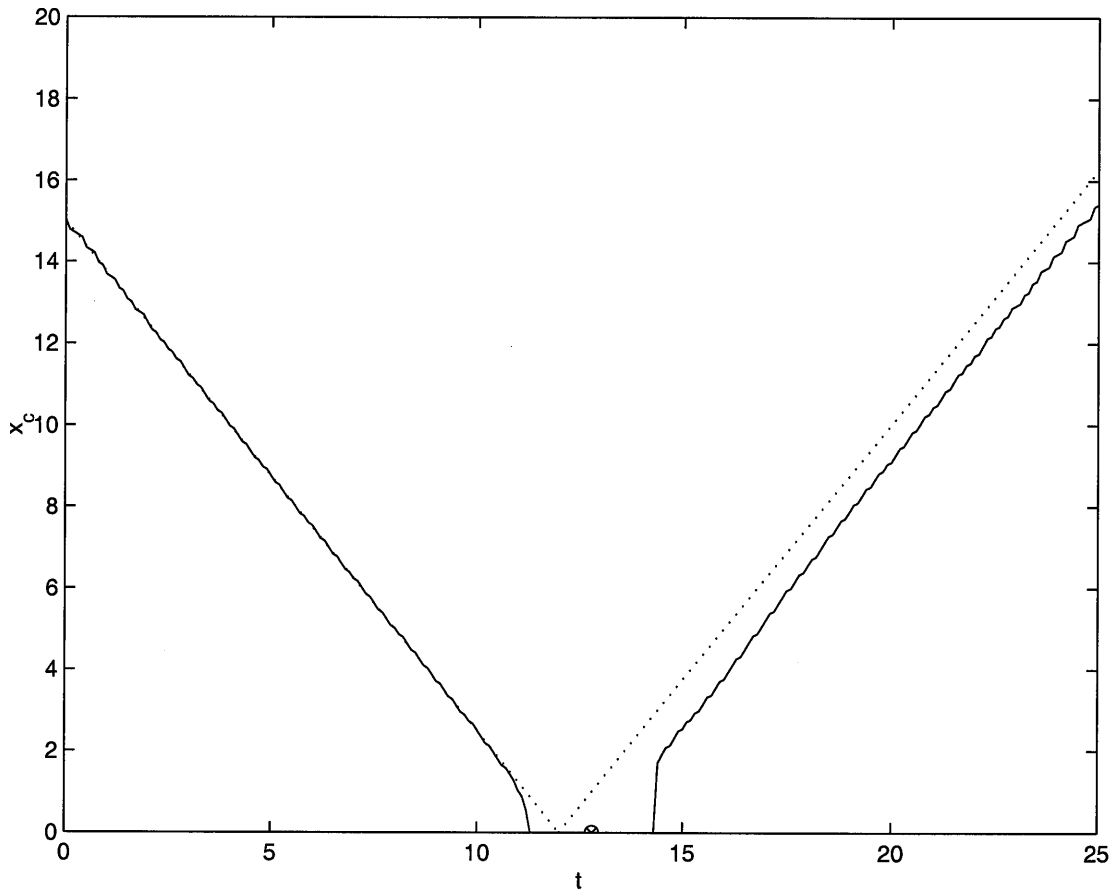

Figure 6.4: Trajectory of the wave crest during a head-on collision between two solitary waves of amplitude $\alpha = 0.6$. $\otimes$: the time at maximum run-up.

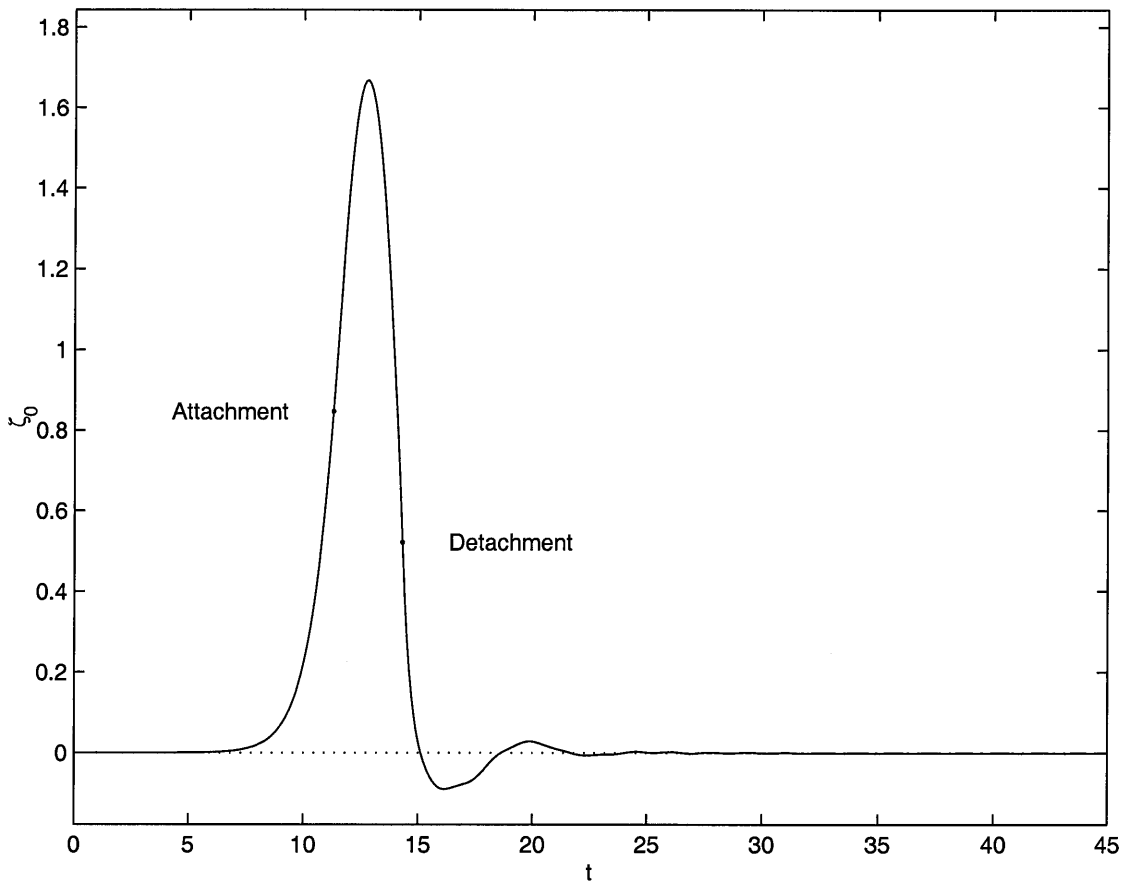

Figure 6.5: Variations of the water height at the wall with time t throughout a head-on collision between two solitary waves of amplitude $\alpha = 0.6$.

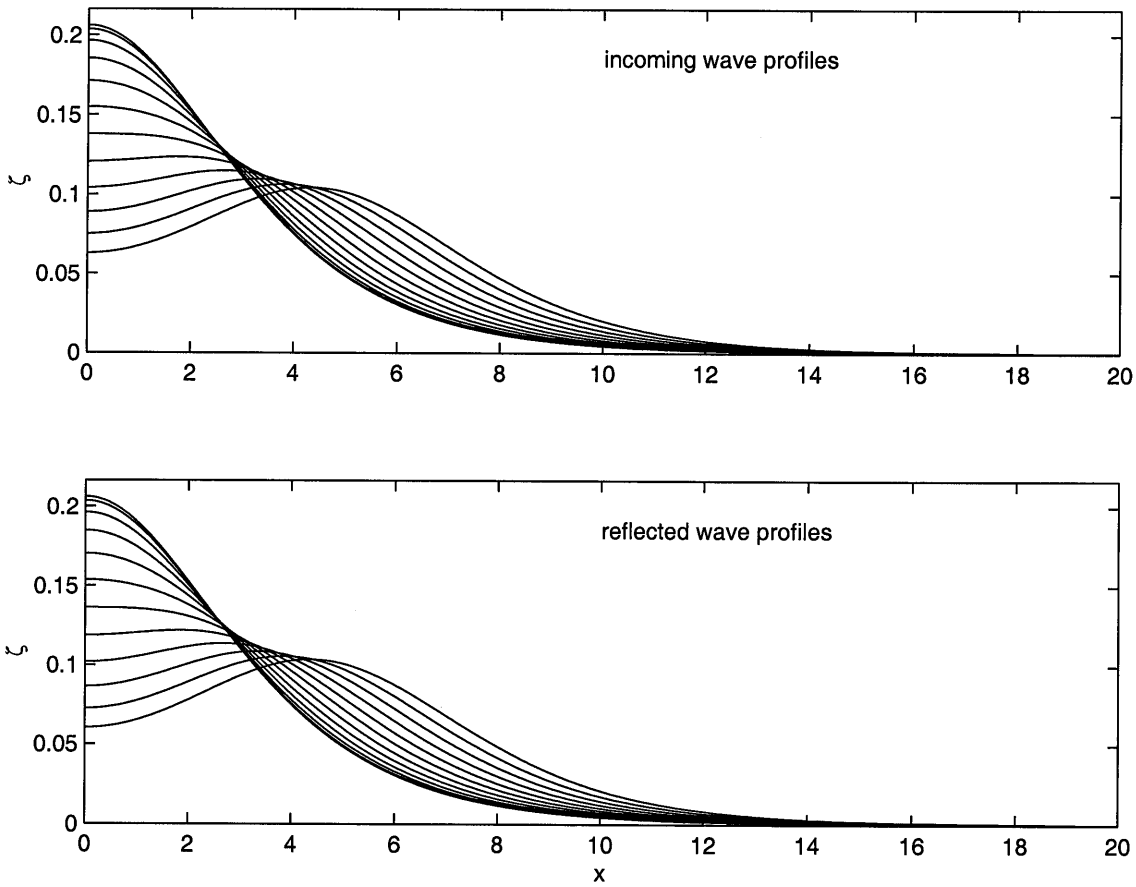

Figure 6.6: The wave profiles before and after the maximum run-up during a head-on collision between two solitary waves of amplitude $\alpha = 0.1$.

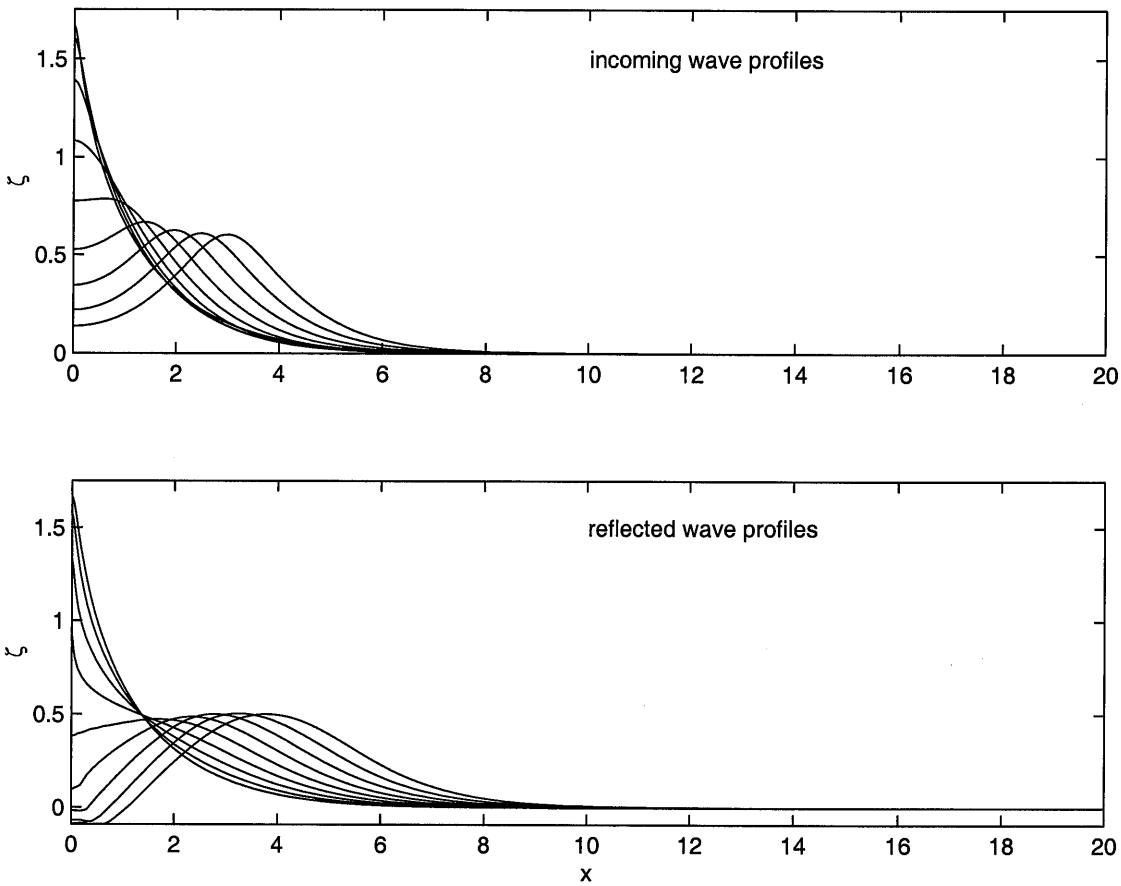

Figure 6.7: The wave profiles before and after maximum run-up during a head-on collision between two solitary waves of amplitude $\alpha = 0.6$.

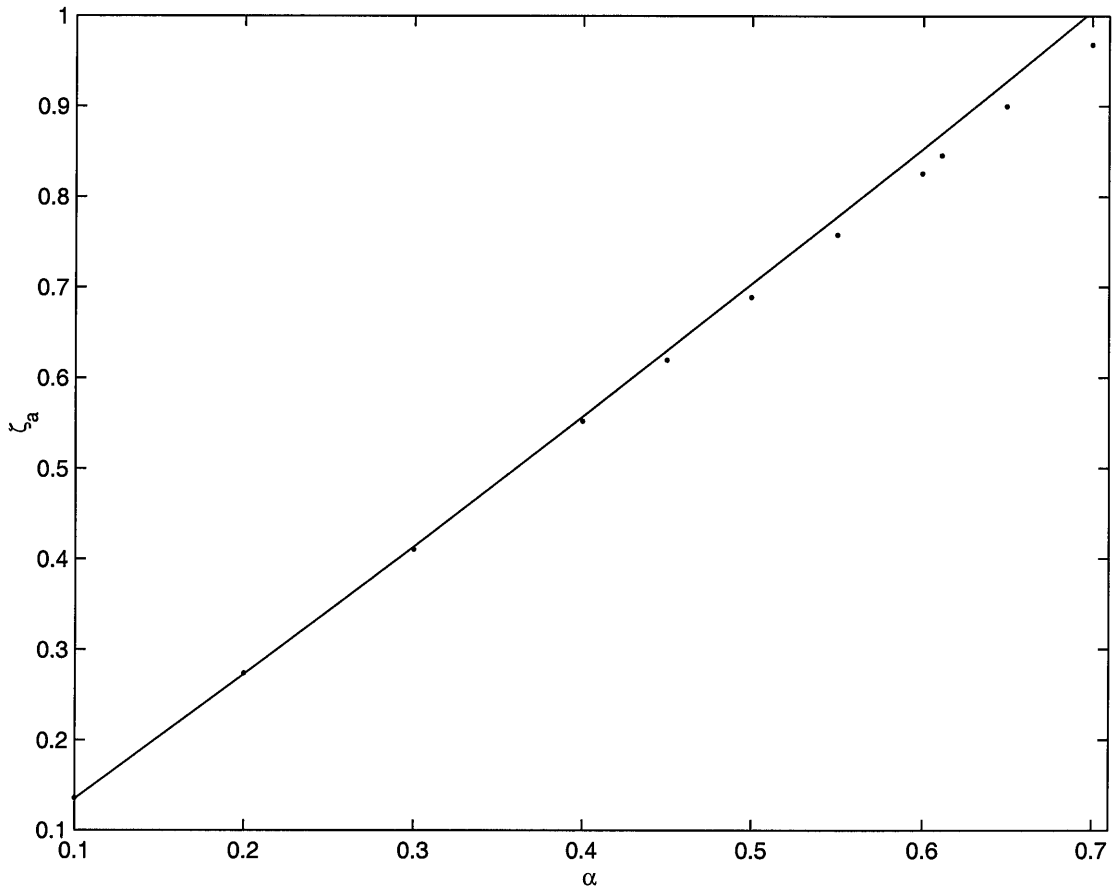

Figure 6.8: Comparison between the amplitude of attachment given by the present FNFD numerical result (in dots) and that by the third order asymptotic theory of Sue & Mierie (in solid line): $\zeta_a = 4\alpha/3 + (\sqrt{3}(2+\kappa) - 1)\alpha^2/9, \quad \kappa = \tanh^{-1}(1/\sqrt{3})$.

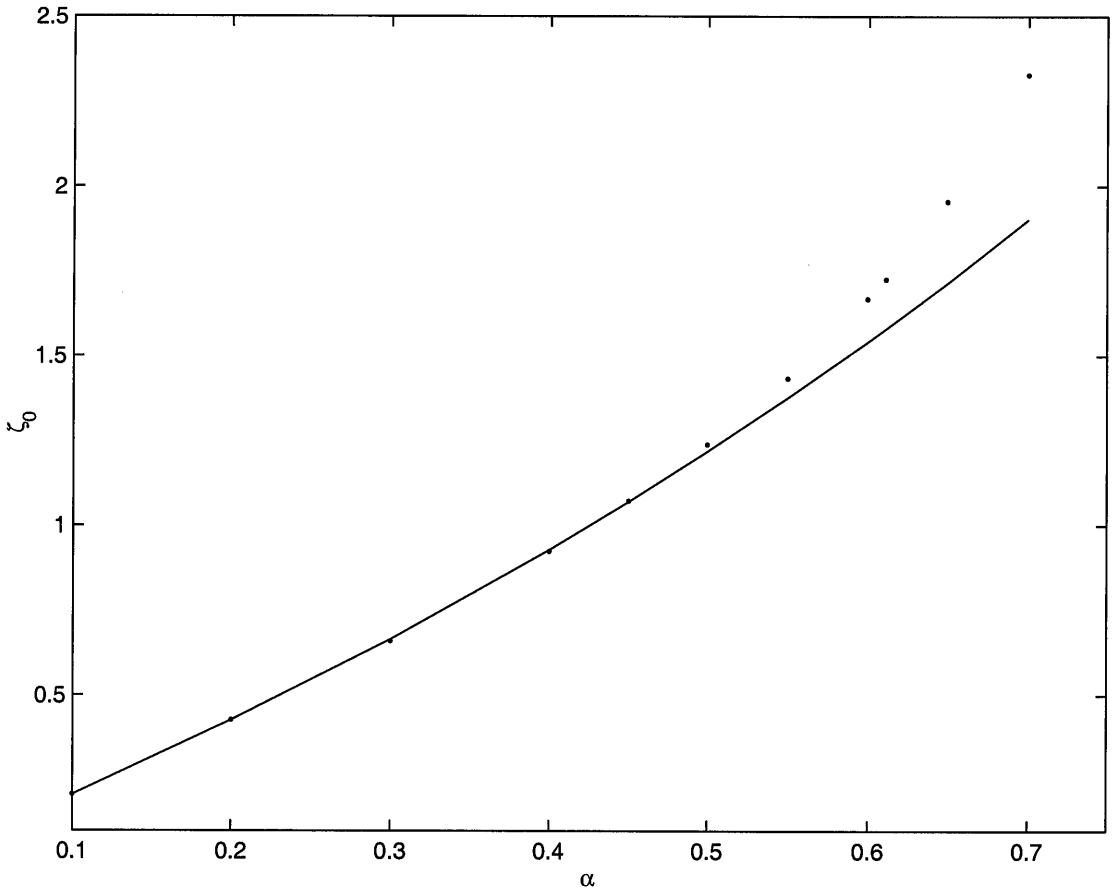

Figure 6.9: Comparison between the maximum run-up given by the present FNFD numerical result (in dots) and that by the third order asymptotic theory of Sue & Mierie (in solid line): $\zeta_0 = 2\alpha + \alpha^2/2 + 3\alpha^3/4$.

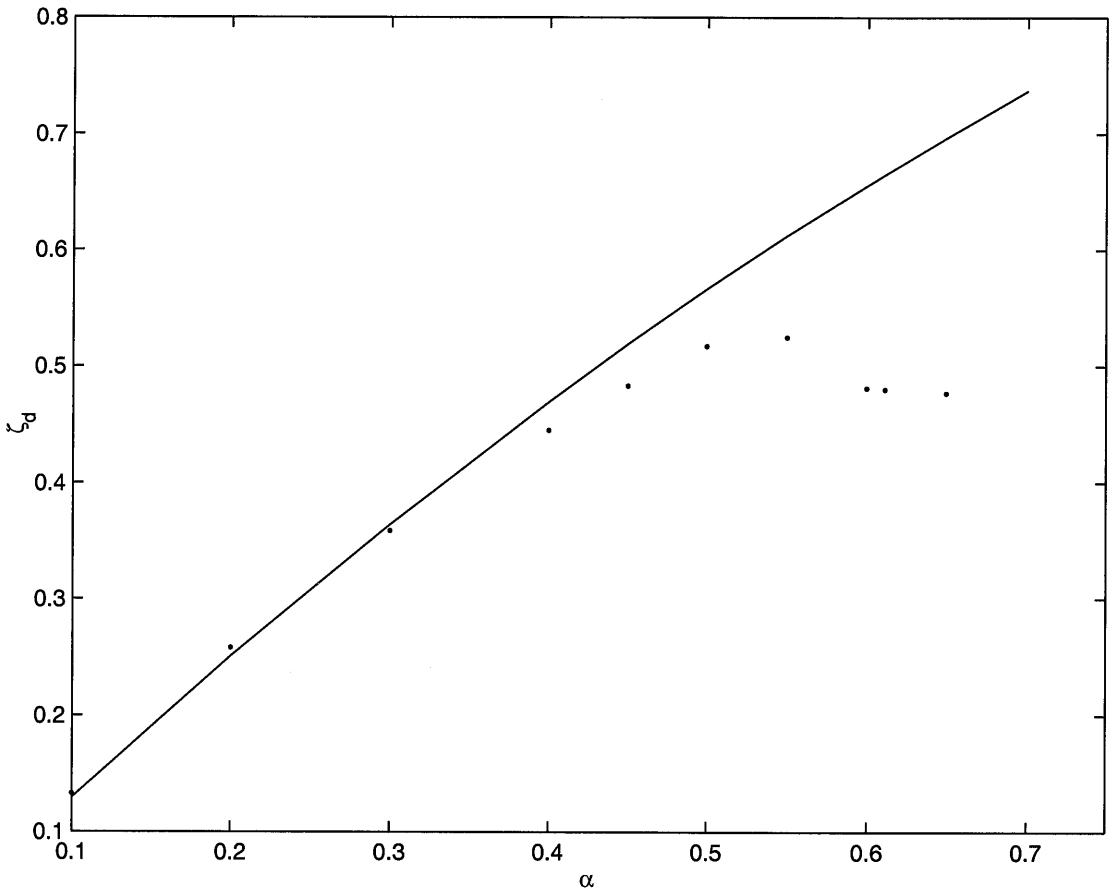

Figure 6.10: Comparison between the amplitude of detachment given by the present FNFD numerical result (in dots) and that of the third order asymptotic theory of Sue & Mierie (in solid line): $\zeta_d = 4\alpha/3 - (\sqrt{3}(2+\kappa) - 1)\alpha^2/9, \qquad \kappa = \tanh^{-1}(1/\sqrt{3})$.

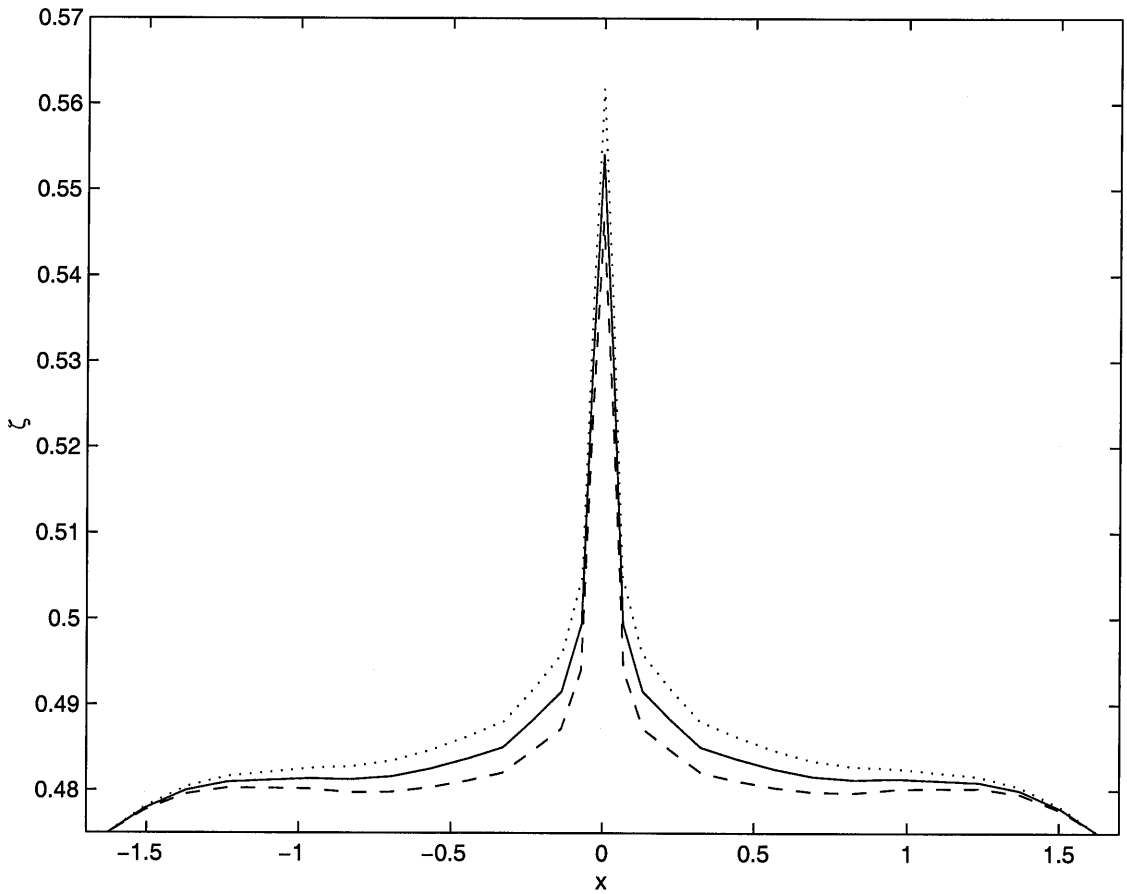

Figure 6.11: Magnified view of the wave profiles shortly before, at, and shortly after the detachment during a head-on collision between two solitary waves of amplitude $\alpha = 0.6$. Dot: wave profile at $t = t_d - 0.005$, solid: wave profile at $t = t_d$, dashed: wave profile at $t = t_d + 0.005$.

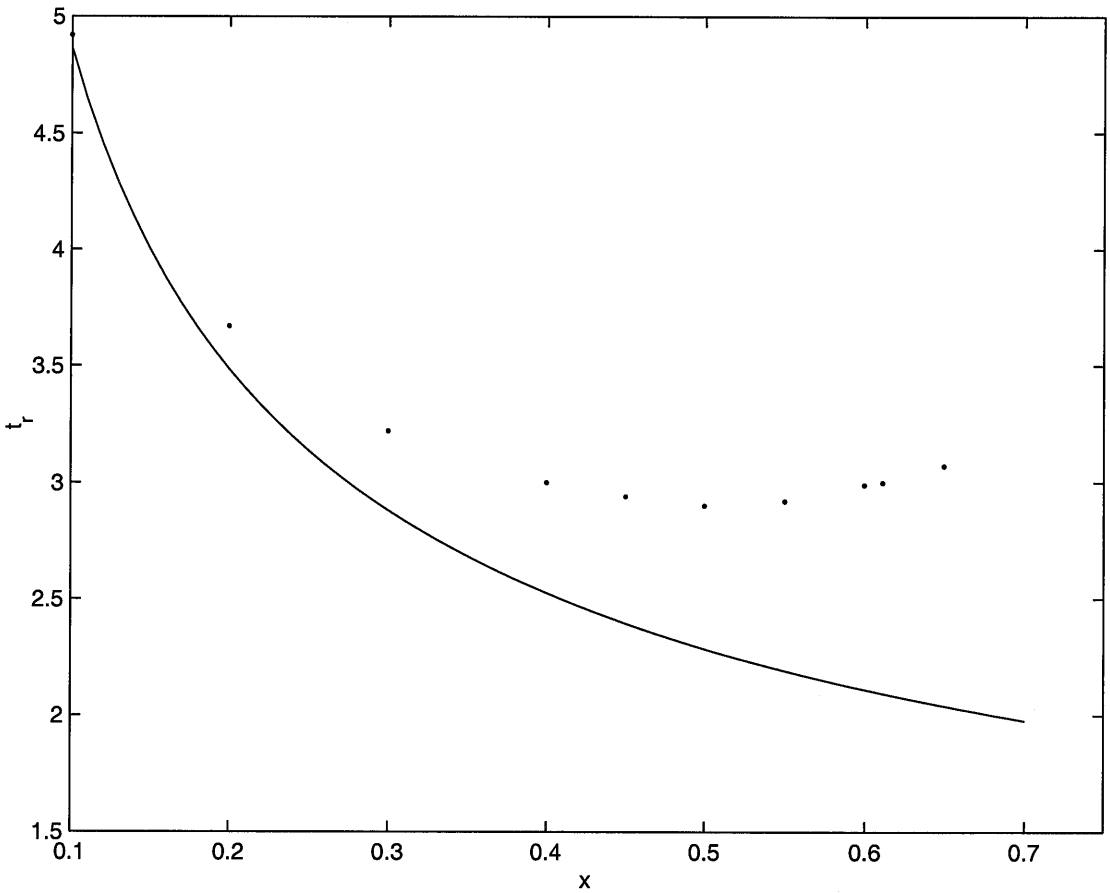

Figure 6.12: Comparison between the phase-locking time period given by the present FNFD numerical method (in dots) and that of the third order asymptotic theory of Sue & Mierie (in solid line) $t_r = t_d - t_a$ with: $t_a = 2(-\kappa\alpha^{-1/2} + (2-\kappa)\alpha^{1/2}/8)/\sqrt{3}$, and $t_d = 2(\kappa\alpha^{-1/2} + (2+\kappa)\alpha^{1/2}/8)/\sqrt{3}, \quad \kappa = \tanh^{-1}(1/\sqrt{3})$.

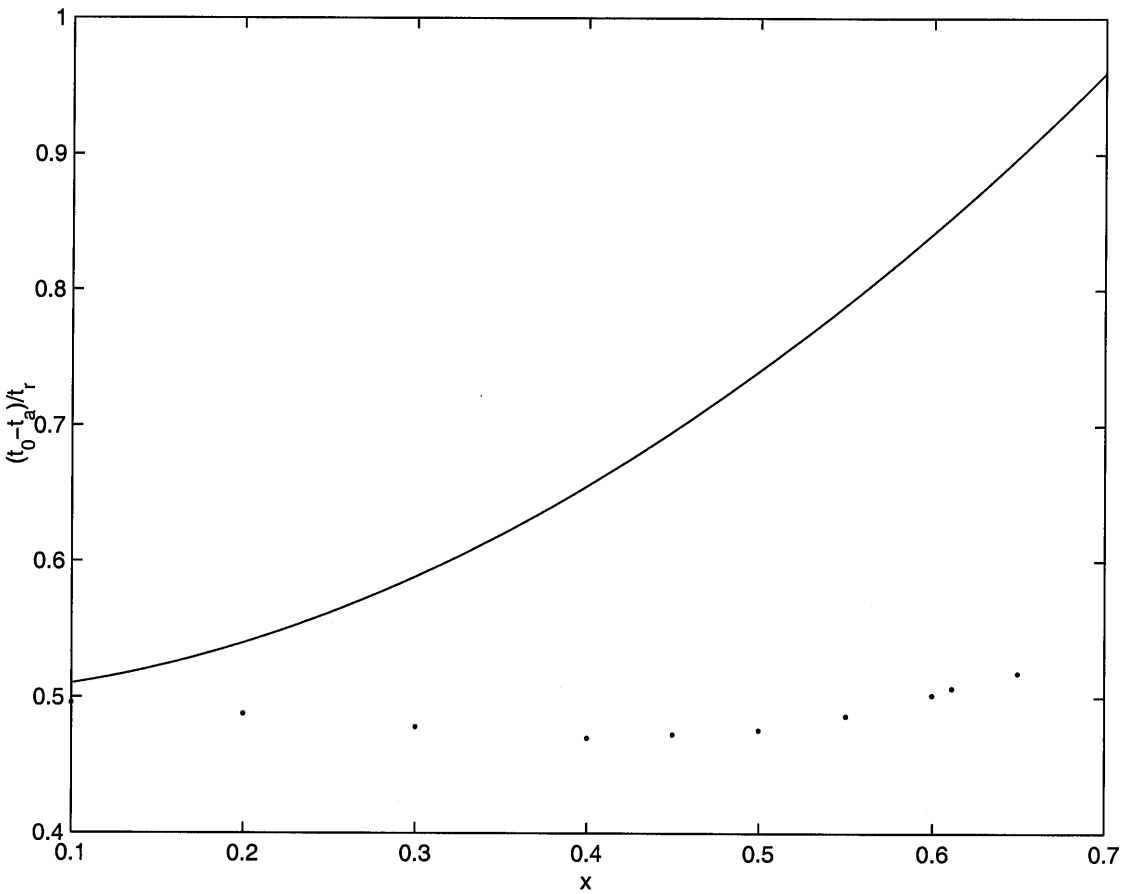

Figure 6.13: Comparison between the $(t_0 - t_a)/t_r$ given by the present FNFD numerical method (in dots) and that by Sue & Mierie (in solid line). The t_0 computed by Sue & Mierie is given by: $t_0 = (\alpha^{1/2} + 43\alpha^{3/2}/8)/(2\sqrt{3})$.

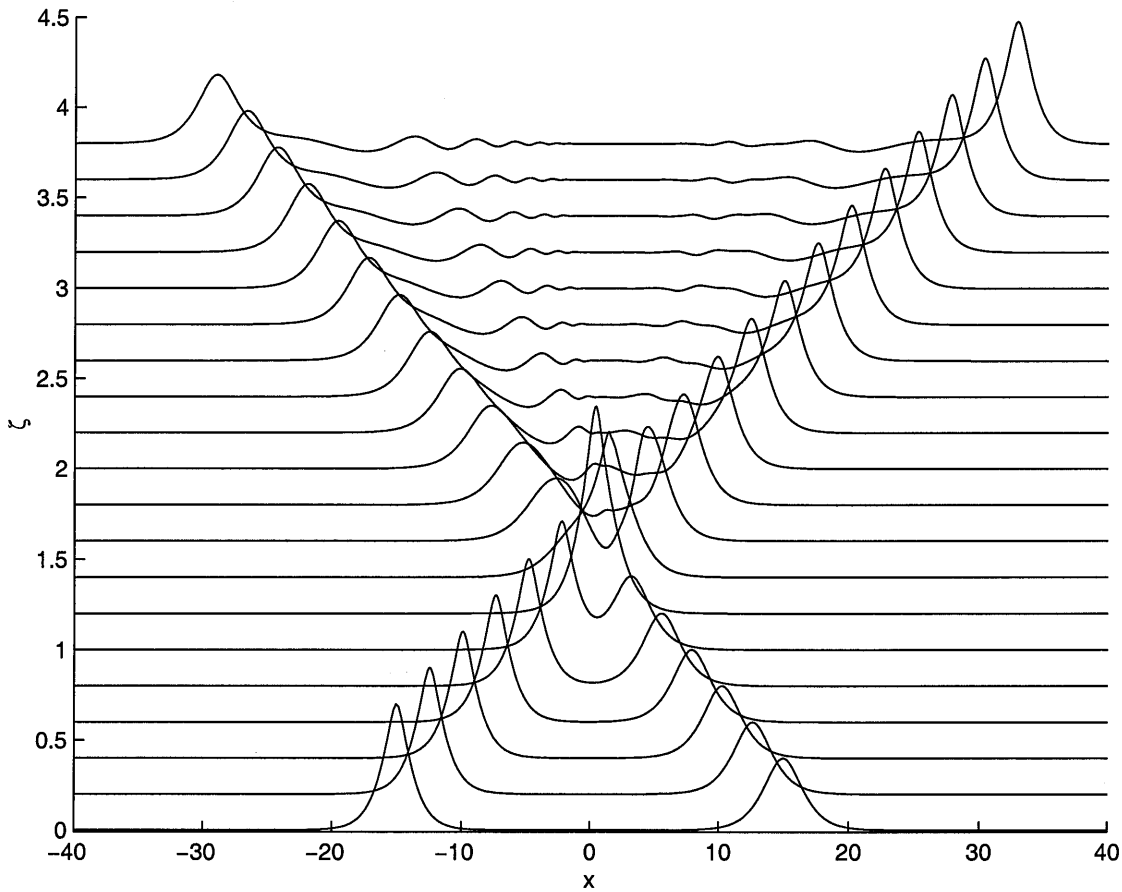

Figure 6.14: The asymptotic head-on collision between solitary waves of amplitude $\alpha = 0.6$ and $\alpha = 0.4$; The wave profiles are given with time intervals $\Delta t = 20$ apart, advancing upward.

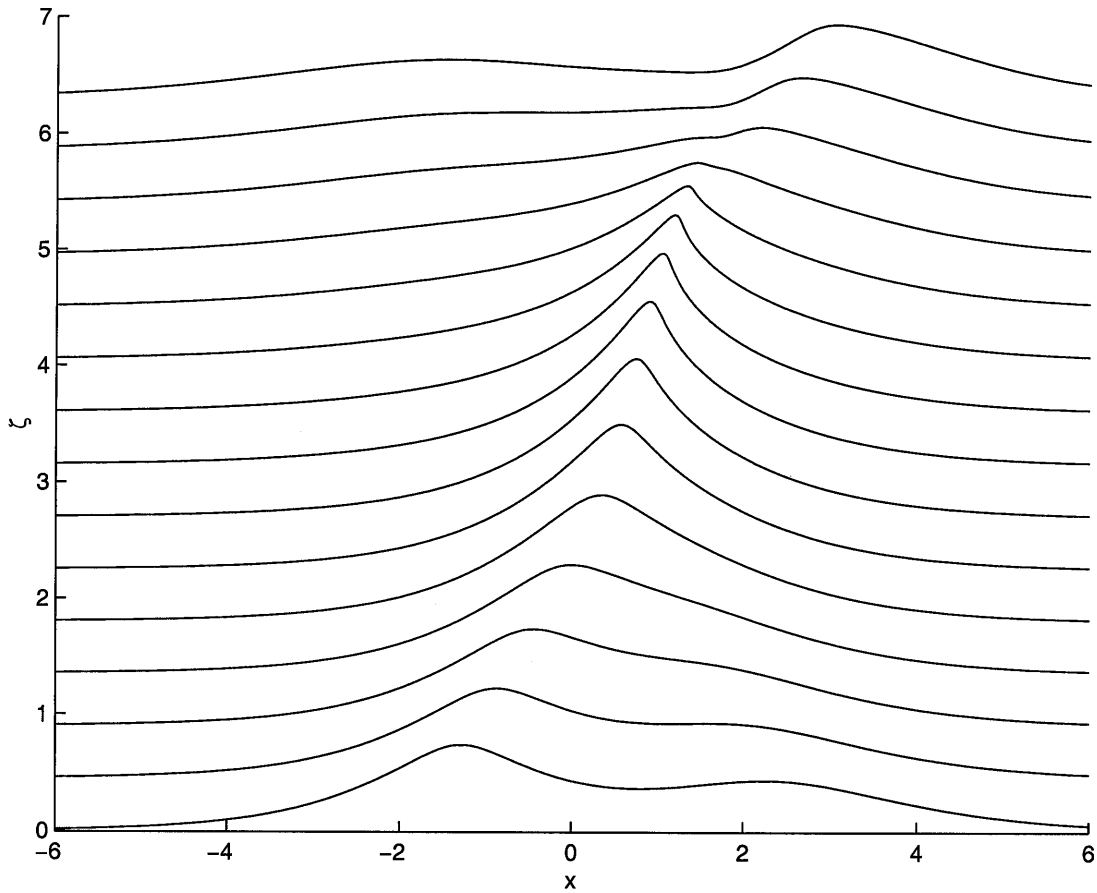

Figure 6.15: A more detailed view of the wave profiles in Figure 6.14 over the time period of phase-locking. The wave profiles are given with time intervals $\Delta t = 3$ apart, advancing upward.

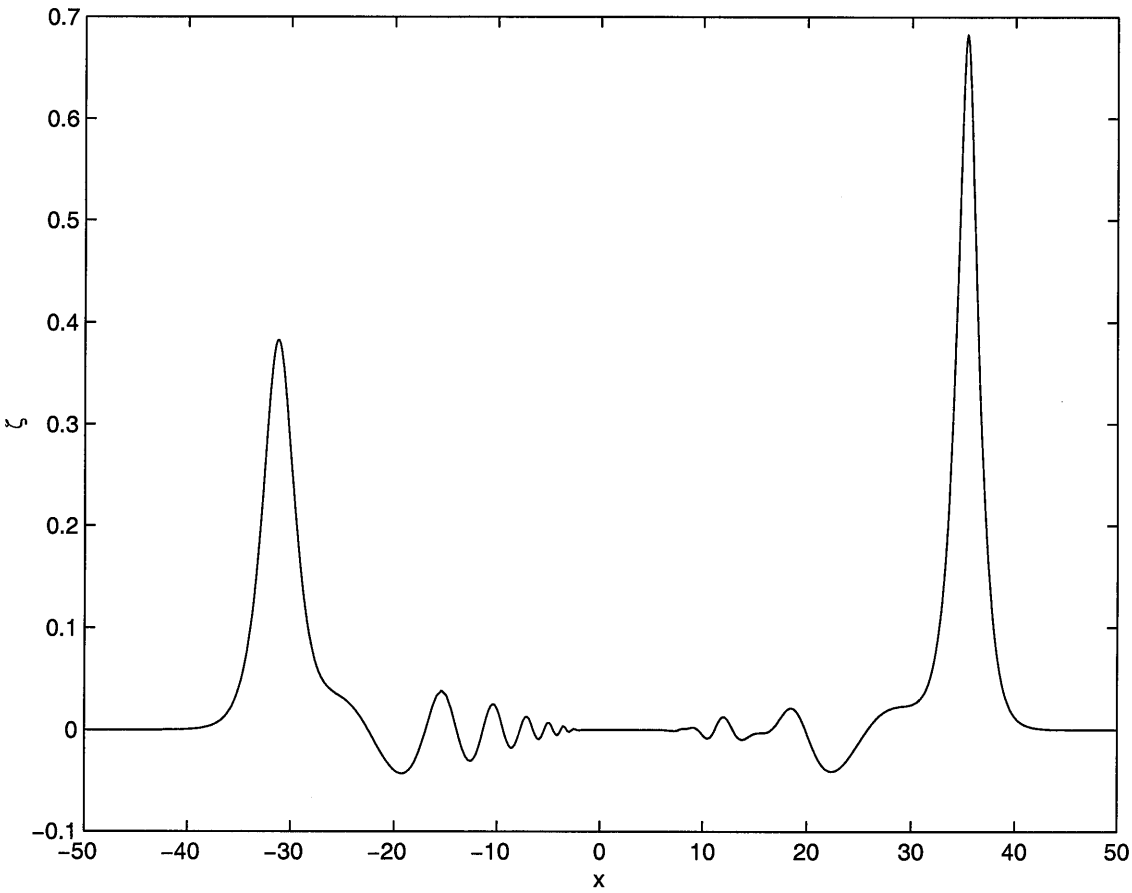

Figure 6.16: Magnified view of the free surface elevation during a head-on collision between two solitary waves of amplitude $\alpha = 0.6$ and $\alpha = 0.4$ after separating of the wave crests.

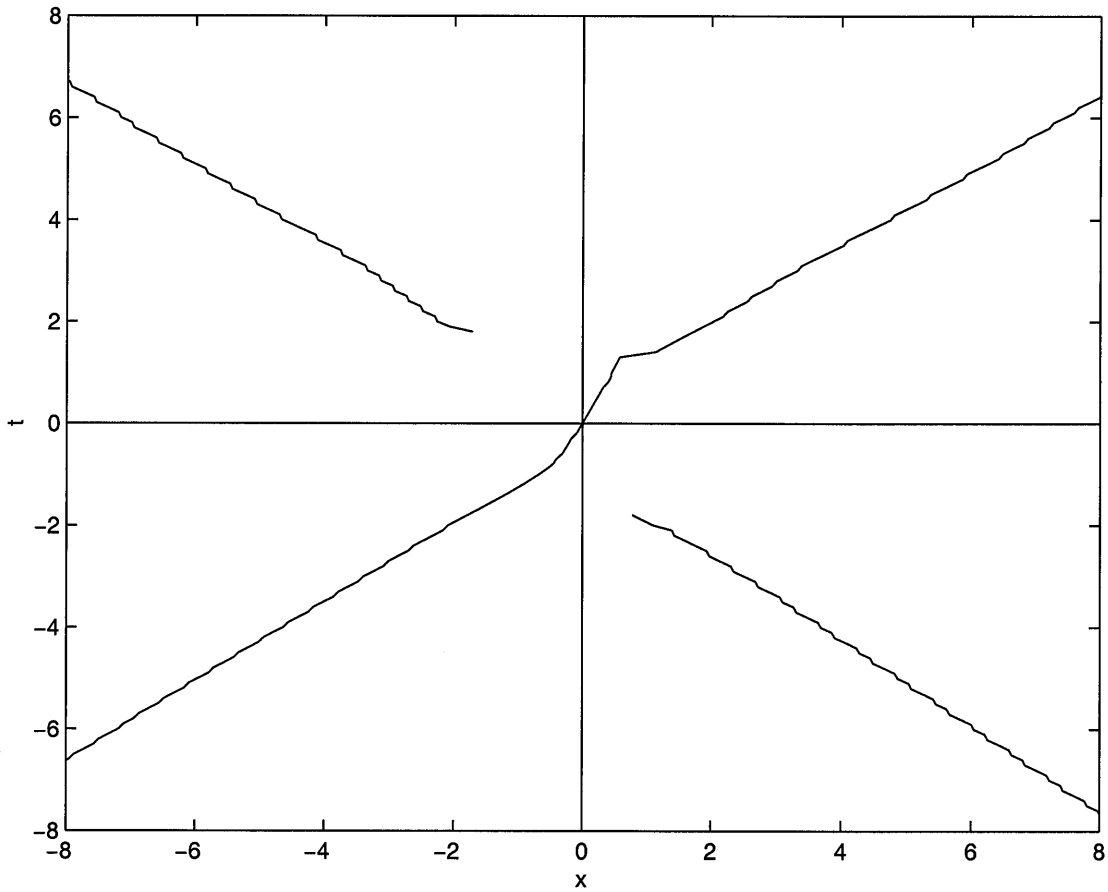

Figure 6.17: The trajectories of the wave crests during a head-on collision between two solitary waves of amplitude $\alpha = 0.6$ and $\alpha = 0.4$.

Chapter 7 Capillary-gravity solitary waves

In this chapter, we will study the joint effects of gravity and surface tension on nonlinear long waves by modifying the model equations developed in chapter 2 to include a uniform surface tension. The model equations closed in the differential form is applied, with using perturbation method, to develop an asymptotic theory with accuracy up to 4th-order for capillary-gravity solitary waves. Our results are qualitatively in agree with the results of previous contributions such as the works of Sun (1991), Sun & Shen (1993) and Vanden-Broeck (1991) but with higher accuracy never achieved before. The FNFD numerical method developed in chapter 4 is adapted for computing nonlinear long waves under the joint effects of gravity and surface tension. Comparison between the higher-order asymptotic solutions for capillary-gravity waves and the corresponding fully nonlinear numerical results are presented later in this chapter.

7.1 Higher-order asymptotic solutions

7.1.1 The governing equations

In the presence of the capillary effect, the dynamic condition (2.5) at the free surface of two dimensional flow is found to become

$$\hat{p} = p_a - T\,\frac{\zeta_{xx}}{(1+\zeta_x^2)^{3/2}} \qquad (\text{at } \; y = \zeta(x,t)), \tag{7.1}$$

where T is the constant surface tension. Consequently, the projected momentum equation (2.12) at the free surface combines with (7.1) to give

$$\hat{u}_t + \hat{u}\ \hat{u}_x + [g + \hat{D}^2\zeta]\ \zeta_x = (\frac{T\,\zeta_{xx}}{\rho\,(1+\zeta_x^2)^{3/2}})_x. \tag{7.2}$$

while the kinematic equation and the Laplace equation for the velocity potential remain the same,

$$\hat{v} = \hat{D}\zeta = \zeta_t + \hat{u}\ \zeta_x, \tag{7.3}$$

$$\phi_{xx} + \phi_{yy} = 0. \tag{7.4}$$

The two exact equations (7.2) and (7.3) can be closed either in differential form by a series expansion of the velocity potential or in integral form by adopting the boundary integral of Cauchy's theory.

First, we shall use a reductive perturbation method to find the first few leading-order approximations. We write equations (7.2), (7.3) and (7.4) in dimensionless form, using the scales in (2.16) and $\rho g h^2$ for T, as follows:

$$\phi_{yy} + \epsilon^2\phi_{xx} = 0, \tag{7.5}$$

$$\hat{u}_t + \hat{u}\hat{u}_x + [1 + \epsilon^2\hat{D}^2\zeta]\zeta_x = \epsilon^2\ \tau(\frac{\zeta_{xx}}{\sqrt{1+\epsilon^2\zeta_x^2}})_x, \tag{7.6}$$

$$\hat{v} = \hat{D}\zeta = \zeta_t\ +\ \hat{u}\,\zeta_x. \tag{7.7}$$

where

$$\tau = \frac{T}{\rho g h^2} \tag{7.8}$$

is Bond number.

The boundary conditions at the bottom is

$$\underline{v} = 0, \quad \text{at } y = -1. \tag{7.9}$$

We seek a series solution of (7.5) in the following form,

$$\phi(x,y,t;\epsilon) = \sum_{n=0}^{\infty} \phi_n(x,y,t)\ \epsilon^{2n} \tag{7.10}$$

which under condition (7.9) becomes, as before in (2.23),

$$\phi(x,y,t;\epsilon) = \sum_{n=0}^{\infty} (-1)^n\ \epsilon^{2n} \frac{(y+1)^{2n}}{(2n)!} \frac{d^{2n}}{dx^{2n}} \phi_0(x,t). \tag{7.11}$$

From this series expansion for ϕ, we have the velocity at bottom,

$$\underline{u}(x,t) = \frac{d}{dx}\phi|_{y=-1} = \frac{d}{dx}\phi_0(x,t), \tag{7.12}$$

and the velocity components at the free surface,

$$\hat{u}(x,t) = \frac{d}{dx}\phi|_{y=\zeta} = \sum_{n=0}^{\infty} (-1)^n\ \epsilon^{2n} \frac{(\zeta+1)^{2n}}{(2n)!} \frac{d^{2n}}{dx^{2n}} \underline{u}(x,t), \tag{7.13}$$

$$\hat{v}(x,t) = \frac{1}{\epsilon^2}\frac{d}{dy}\phi|_{y=\zeta} = \sum_{n=1}^{\infty} (-1)^n\ \epsilon^{2n-2} \frac{(\zeta+1)^{2n-1}}{(2n-1)!} \frac{d^{2n-1}}{dx^{2n-1}} \underline{u}(x,t). \tag{7.14}$$

We now seek the solitary wave solution of equations (7.2), (7.3) (7.13) and (7.14) in wave frame as we did in chapter 3 so that all the variables can be written in term of phase function $\theta = k\,(x - ct)$, such that $f(x,t) = f(\theta)$ for flow variables. In this wave frame, and under the assumption of $\alpha = \epsilon^2$, we have the governing equations as follows:

$$\zeta + \frac{\hat{u}^2}{2} - c\,\hat{u} + \alpha\ k^2\ \frac{(\hat{u}-c)^2}{2}\ (\zeta')^2 = \alpha\,\tau\,\zeta''/(1+\zeta'^2)^{3/2}, \tag{7.15}$$

$$\hat{v} - k\ (\hat{u}-c)\,\zeta' = 0, \tag{7.16}$$

$$\hat{u} = \sum_{n=0}^{\infty} (-1)^n\ \alpha^n\ \frac{(\zeta+1)^{2n}}{(2n)!}\ k^{2n}\ \underline{u}^{(2n)}, \tag{7.17}$$

$$\hat{v} = \sum_{n=1}^{\infty} (-1)^n\ \alpha^{n-1}\ \frac{(\zeta+1)^{2n-1}}{(2n-1)!}\ k^{2n-1}\ \underline{u}^{(2n-1)}, \tag{7.18}$$

with the prime denotes the operator $d/d\theta$. This system of equations is an extension of (3.21)-(3.24) with the surface tension term added to equation (3.22). The method

to solve equations (7.15)-(7.18) is exactly the same as for (3.21)-(3.24) in chapter 3 and we will just present the results here.

7.1.2 Higher-order capillary-gravity solitary waves

The first order equations are the same as (3.25) and (3.26), hence again

$$c_0 = 1, \tag{7.19}$$

$$u_1 = \zeta_1, \tag{7.20}$$

for the right-going wave and ζ_1 is determined by considering the second order equations.

The second-order equations are found to be the same as (3.35)-(3.37) except with the coefficient $(-1/2)$ of the term $k_0^2\zeta_1''$ in (3.37) replaced by $-(1/2+\tau)$. Consequently, the solvability condition for the second-order equations requires, in analogy to (3.39), that

$$-c_1\ \zeta_1^2 + \frac{1}{2}\ \zeta_1^3 + \frac{1}{6}(1-3\tau)\ k_0^2\ (\zeta_1')^2 = 0. \tag{7.21}$$

Here, $\tau = 1/3$ is a critical value at which equation (7.21) becomes singular and does not have solitary wave solutions as found earliear by Benjamin (1982) and Vanden-Broeck & Shen (1983). Depending on the value of τ, we invoke the following boundary condition

$$\zeta_1(0) = \begin{cases} 1 & 0 \le \tau < 1/3, \\ -1 & \tau > 1/3, \end{cases} \tag{7.22}$$

to let ζ fall off exponentially toward infinity. Under this premise, we have found few leading-order solutions by using the Mathematica code in appendix A and present the results below.

Denoting

$$\mathcal{N} = \begin{cases} 1, & 0 \le \tau < 1/3 \\ -1, & \tau > 1/3 \end{cases}, \tag{7.23}$$

and

$$\mathcal{S} = \mathrm{sech}^2(\theta), \tag{7.24}$$

we have the leading 4th-order solution for the free surface elevation and the bottom velocity as

$$\zeta = \sum_{n=1}^{4} \alpha^n \zeta_n + O(\alpha^5), \tag{7.25}$$

$$\underline{u} = \sum_{n=1}^{4} \alpha^n u_n + O(\alpha^5), \tag{7.26}$$

in which,

$$\begin{aligned}
\zeta_1 &= \mathcal{N}\,\mathcal{S}, \\
\zeta_2 &= \frac{3\,(-1-4\tau+12\tau^2)}{4\,(1-3\tau)^2}(\mathcal{S}-\mathcal{S}^2), \\
\zeta_3 &= \mathcal{N}\,[(5+60\tau-246\tau^2+72\tau^3+216\tau^4)\,\mathcal{S} \\
&\quad +(-151-1020\tau+2832\tau^2+5040\tau^3-10800\tau^4)\,\mathcal{S}^2 \\
&\quad +(101+420\tau-372\tau^2-5760\tau^3+8640\tau^4)\,\mathcal{S}^3]/(80\,(1-3\tau)^4), \\
\zeta_4 &= [4(-8209-38325\tau+182808\tau^2+427680\tau^3-1828980\tau^4 \\
&\quad +1117800\tau^5+291600\tau^6)\,\mathcal{S} \\
&\quad +4(23282+204675\tau-481284\tau^2-2592540\tau^3+6345540\tau^4 \\
&\quad +170100\tau^5-5248800\tau^6)\,\mathcal{S}^2 \\
&\quad +(-112393-1237800\tau+2534616\tau^2+9322560\tau^3-9570960\tau^4 \\
&\quad -43934400\tau^5+55987200\tau^6)\,\mathcal{S}^3 \\
&\quad -9(-5789-63600\tau+148968\tau^2+73680\tau^3+943920\tau^4 \\
&\quad -4309200\tau^5+4017600\tau^6)\,\mathcal{S}^4]/(24000\,(1-3\tau)^6),
\end{aligned} \tag{7.27}$$

and

$$\begin{aligned}
u_1 &= \mathcal{N}\,\mathcal{S}, \\
u_2 &= [(1-30\tau+54\tau^2)\mathcal{S}+(-4+45\tau-72\tau^2)\mathcal{S}^2]/(4\,(1-3\tau)^2), \\
u_3 &= \mathcal{N}\,[2(-19+384\tau-591\tau^2-1530\tau^3+2295\tau^4)\mathcal{S} \\
&\quad +(-16+540\tau-10713\tau^2+34470\tau^3-30240\tau^4)\mathcal{S}^2
\end{aligned}$$

$$
\begin{aligned}
&+3(32-600\tau+4631\tau^2-11640\tau^3+9360\tau^4)\mathcal{S}^3]/(80\,(1-3\tau)^4),\\
u_4 \;=\;& [2(-30176-154275\tau-3424338\tau^2+22967820\tau^3-38745945\tau^4\\
&+10120950\tau^5+10461150\tau^6)\mathcal{S}\\
&+7(28628-449625\tau+6168339\tau^2-12484260\tau^3-31273290\tau^4\\
&+108511650\tau^5-77857200\tau^6)\mathcal{S}^2\\
&+7(4832-330600\tau+4630041\tau^2-62030340\tau^3+255481290\tau^4\\
&-416696400\tau^5+239695200\tau^6)\mathcal{S}^3\\
&+21(-12608+343200\tau-3743004\tau^2+24343785\tau^3-74468160\tau^4\\
&+105591600\tau^5-56764800\tau^6)\mathcal{S}^4]/(168000\,(1-3\tau)^6). \qquad (7.28)
\end{aligned}
$$

For the wave speed and the corresponding wave number, we obtain

$$
\begin{aligned}
c \;=\;& 1+\mathcal{N}\,\frac{1}{2}\,\alpha-\frac{5+1/(1-3\tau)^2}{40}\,\alpha^2\\
&+\mathcal{N}\,\frac{30-426\tau+1827\tau^2-3780\tau^3+2835\tau^4}{560\,(1-3\tau)^4}\,\alpha^3\\
&-\frac{3\,(412-5448\tau+40140\tau^2-152820\tau^3+352485\tau^4-425250\tau^5+212625\tau^6)}{22400\,(1-3\tau)^6}\,\alpha^4,
\end{aligned}
\qquad (7.29)
$$

and

$$
k=\begin{cases}\sqrt{3}/(2\sqrt{1-3\tau})\;K, & 0\le\tau<1/3\\ \sqrt{3}/(2\sqrt{3\tau-1})\;K, & \tau>1/3\end{cases}, \qquad (7.30)
$$

where

$$
\begin{aligned}
K \;=\;& 1-\mathcal{N}\,\frac{(5-12\tau)}{8\,(1-3\tau)^2}\,\alpha+\frac{355+72\tau(20\tau-21)}{640\,(1-3\tau)^4}\alpha^2\\
&+\mathcal{N}\,\frac{-100627+530460\tau-817056\tau^2+138240\tau^3}{179200\,(1-3\tau)^6}\,\alpha^3. \qquad (7.31)
\end{aligned}
$$

Capillary-gravity solitary waves are elevation (or depression) polarized waves which move faster (or slower) than linear gravity waves for $0\le\tau<1/3$ (or $\tau>1/3$). Figures 7.1-7.4 show the free surface elevations computed by the leading four-order theories

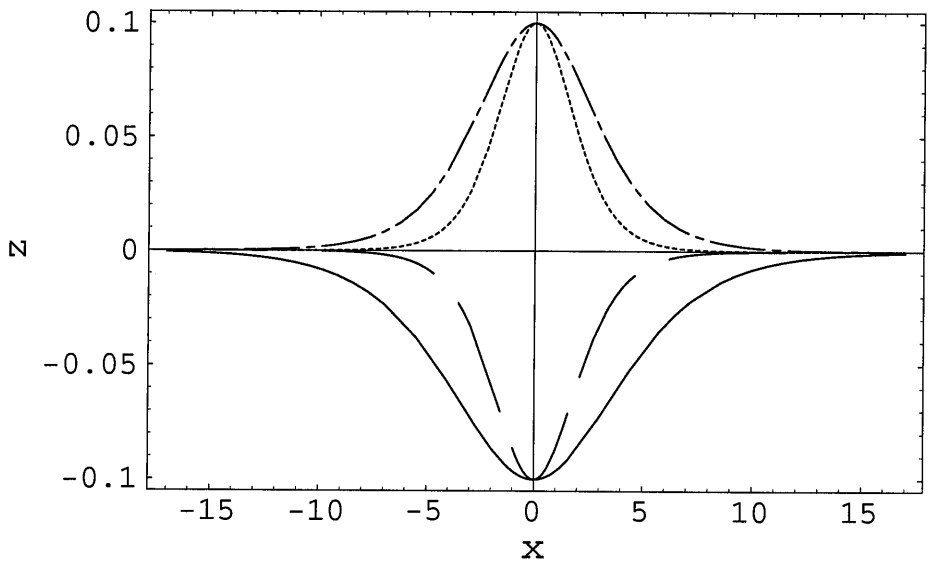

Figure 7.1: Wave profiles of capillary-gravity solitary waves of amplitude $\alpha = 0.1$ given by the first order asymptotic theory with various values of τ. Dashdotted: $\tau = 0$, dotted: $\tau = 1/5$, dashed: $\tau = 1/2$, solid: $\tau = 1$.

for capillary-gravity solitary wave of amplitude $\alpha = 0.1$ with various values of τ. We compare the wave form computed by the first four order asymptotic theories in Figure 7.5 for a given τ. The difference among solutions of the second, third and fourth for both elevation and depression waves is very little. This indicates rapid convergent rate of the higher-order asymptotic theories for waves of small amplitude.

The curvature at the crest of waves with small and moderately large amplitude computed by different order approximations are plotted in Figure 7.6 and 7.7. The free surface at the crest becomes more curved as the surface tension increase.

7.2 Numerical scheme for computing fully nonlinear capillary-gravity waves

For numerical computation of fully nonlinear gravity-capillary waves, it is more convenient to use, instead of the differential closure form of velocity potential ϕ, the Cauchy contour integral representation (2.30) of ϕ to close the system of model equations jointly with (7.3) and (7.2). A boundary integral method based on the

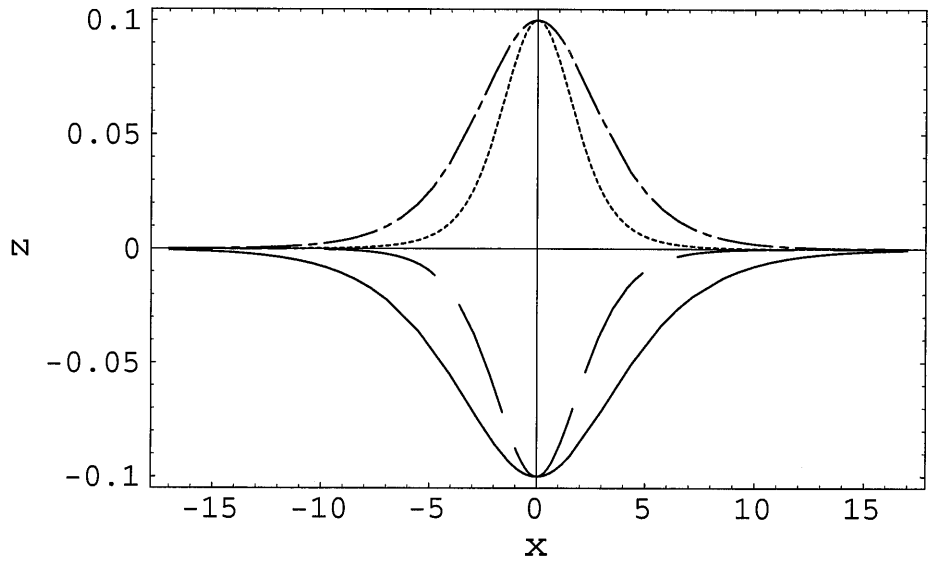

Figure 7.2: Wave profiles of capillary-gravity solitary wave of amplitude $\alpha = 0.1$ given by the second order asymptotic theory with various values of τ. Dashdotted: $\tau = 0$, dotted: $\tau = 1/5$, dashed: $\tau = 1/2$, solid: $\tau = 1$.

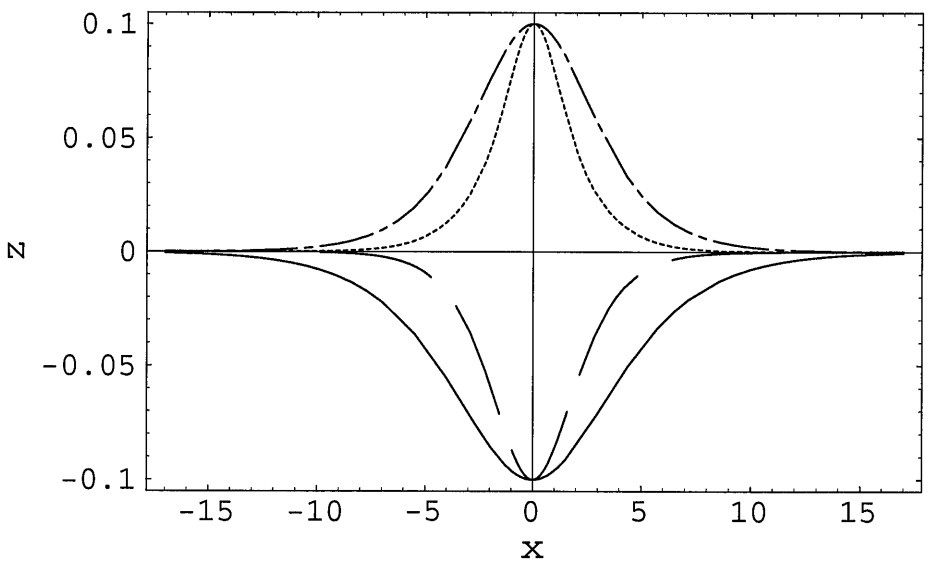

Figure 7.3: Wave profiles of capillary-gravity solitary wave of amplitude $\alpha = 0.1$ given by the third order asymptotic theory with various values of τ. Dashdotted: $\tau = 0$, dotted: $\tau = 1/5$, dashed: $\tau = 1/2$, solid: $\tau = 1$.

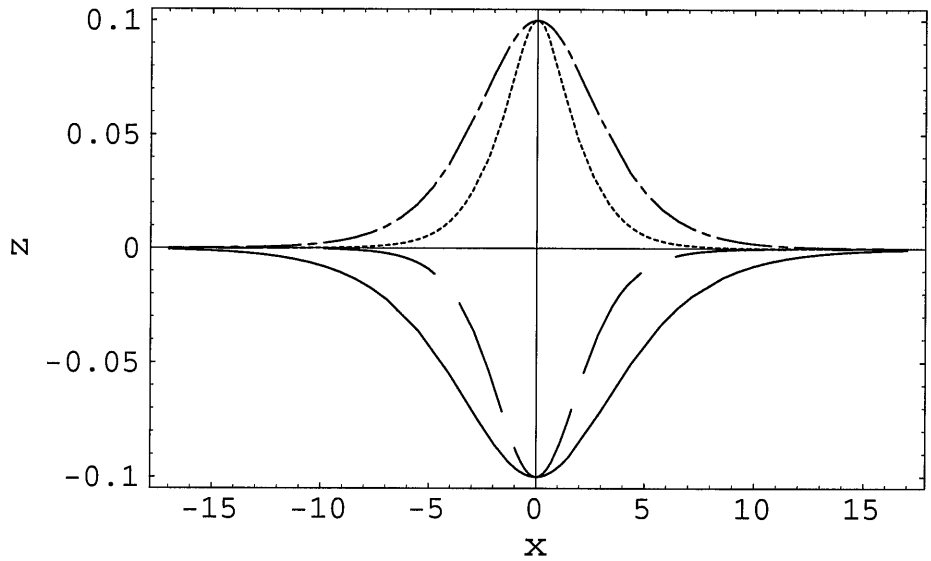

Figure 7.4: Wave profiles of capillary-gravity solitary wave of amplitude $\alpha = 0.1$ given by the fourth order asymptotic theory with various values of τ. Dashdotted: $\tau = 0$, dotted: $\tau = 1/5$, dashed: $\tau = 1/2$, solid: $\tau = 1$.

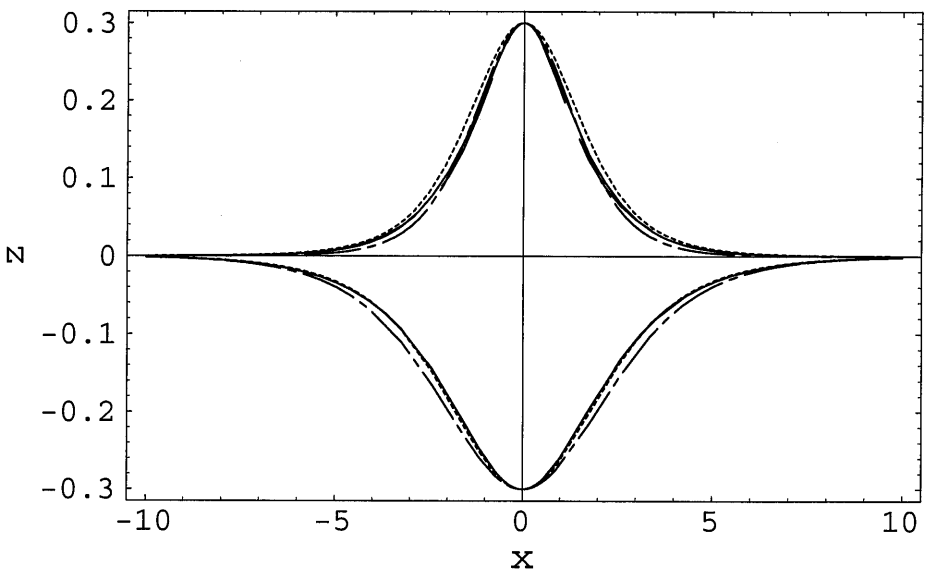

Figure 7.5: Wave profiles of the capillary-gravity solitary wave of amplitude $\alpha = 0.3$ given by the leading four orders of asymptotic theory with $\tau = 1/10$ for elevation wave and with $\tau = 1$ for depression wave. Dashdotted: 1st-order theory, dotted: 2nd-order theory, dashed: 3rd-order theory, solid: 4th-order theory.

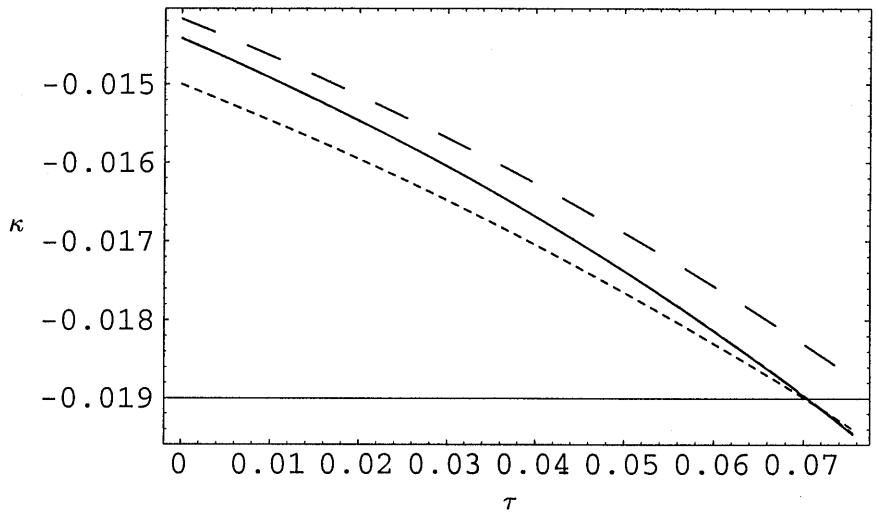

Figure 7.6: The curvature at the crest of solitary wave of amplitude $\alpha = 0.1$. Dotted: 1st order, Dashed: 2nd order, DashDotted: 3rd order, Solid: 4th order.

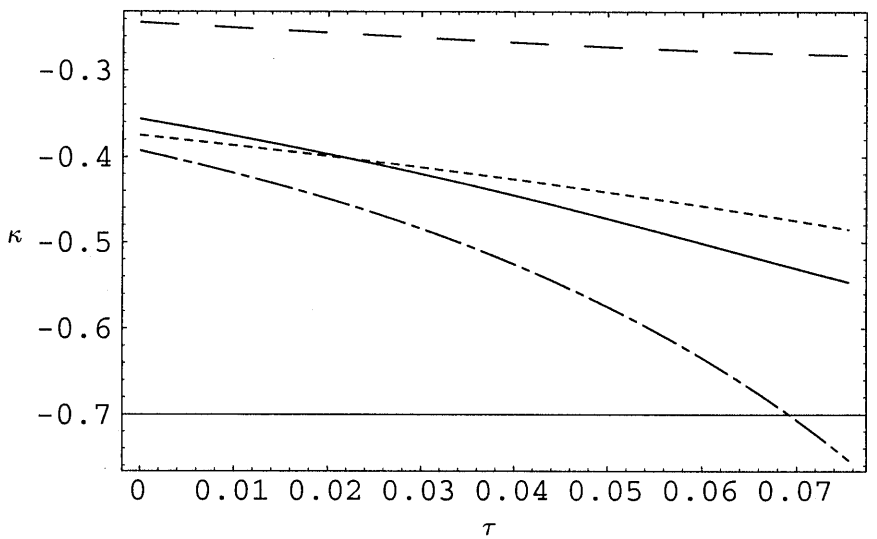

Figure 7.7: The curvature at the crest of solitary wave of amplitude $\alpha = 0.5$. Dotted: 1st order, Dashed: 2nd order, DashDotted: 3rd order, Solid: 4th order.

integral closure equation similar to that in chapter 4 is developed here for the time-dependent, two-dimensional shallow water capillary-gravity waves. With the basic equations written in terms of (ζ, u_s, u_n) defined in (4.1), equations (7.3), (7.2) and (2.30) can be rearranged to produce a set of exact model equations for modeling nonlinear capillary-gravity waves as follows:

$$\zeta_t = u_n, \tag{7.32}$$

$$(u_s)_t = -\left[\zeta + \frac{1}{2R^2}\left(u_s^2 - u_n^2 - 2u_s u_n \zeta_x\right) - \tau \frac{\zeta_{xx}}{\sqrt{1+\zeta_x^2}^3}\right]_x, \tag{7.33}$$

$$\begin{aligned} \pi u_n(x,t) = {} & \Re \int_{-\infty}^{\infty} \left[\frac{\hat{z}_x(x)}{\hat{z}(x) - \hat{z}(x')}\right] [u_s(x') - i\, u_n(x')] dx' \\ & -\Re \int_{-\infty}^{\infty} \left[\frac{\hat{z}_x(x)}{\hat{z}(x) - \hat{z}^*(x') + 2i}\right] [u_s(x') + i u_n(x')] dx'. \end{aligned} \tag{7.34}$$

The linearized version of the above equations reads as,

$$\zeta_t = u_n, \tag{7.35}$$

$$(u_s)_t = -\zeta_x + \tau\, \zeta_{xxx}, \tag{7.36}$$

$$\begin{aligned} \pi u_n(x) = {} & \int_{-\infty}^{\infty} \left[\frac{1}{x - x'} dx' - \frac{(x - x')}{(x - x')^2 + 4}\right] u_s(x') dx' \\ & - \int_{-\infty}^{\infty} \frac{2u_n(x')}{(x - x')^2 + 4} dx'. \end{aligned} \tag{7.37}$$

We again apply the Fourier transformation to the above linearized equations and use the relations in table 4.1 to obtain following equations in Fourier form

$$\mathcal{Z}_t = \mathcal{U}_n, \tag{7.38}$$

$$(\mathcal{U}_s)_t = -i\,(k\,\mathcal{Z} + \tau\, k^3 \mathcal{Z}), \tag{7.39}$$

$$\mathcal{U}_n = -i\,\mathcal{U}_s\, \mathrm{sgn}(k) \tanh(|k|). \tag{7.40}$$

This set of linear equations for capillary-gravity waves in shallow water is found to have the following dispersion relation:

$$\lambda^2 = -k(1 + \tau\, k^2)\ \tanh(k). \tag{7.41}$$

This result agrees with the linear water wave theory.

The discretization of (7.32)-(7.34) is similar to that given in chapter (4) to ensure that the balance of terms at continuous level is preserved at the discrete level. The surface tension term put a stricter restriction on the size of time step due to the higher derivative terms arising from the surface tension effect.

The numerical method is used to study the evolution of free surface flow under the joint effects of gravity and surface tension. We start computation with the initial wave profile and wave speed given by the 4th-order asymptotic perturbation theory. Figures 7.8 and 7.9 show the results for elevation- and depression-polarized capillary-gravity solitary waves of amplitude $\alpha = 0.2$ with $\tau = 74/980$, and $\alpha = 0.2$ with $\tau = 2/3$, respectively (the former is for water laboratory premise). Both examples show that the results of the asymptotic theory of $O(\alpha^3)$ are in excellent agreement with the fully nonlinear numerical results for waves of small amplitudes. For waves of higher amplitudes, the numerical results exhibit the following characteristics in more detail. For a right-going primary wave, a train of left-going dispersive waves of small amplitudes separates at the initial moment from the right-going main wave, and then a train of right-going waves of very small amplitude is cast to trail behind the leading dominant elevation-polarized solitary wave. In sharp contrast, for depression-polarized main waves, interestingly, the right-going dispersive wave train propagates ahead to lead the dominant solitary wave. Figures 7.10 and 7.11 show two examples of capillary-gravity solitary wave of amplitude $\alpha = 0.5$ with $\tau = 74/980$, and $\alpha = 0.5$ and $\tau = 2/3$, respectively; the numerical results are obtained with the initial condition given by the solution of the fourth-order asymptotic theory.

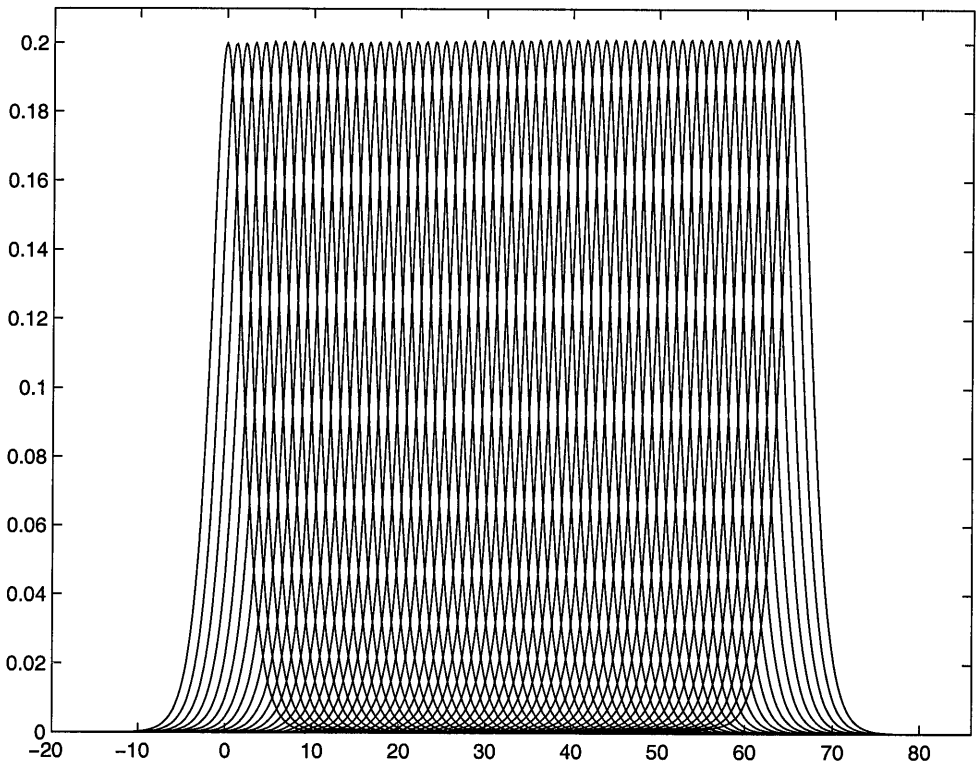

Figure 7.8: Evolution of a terminal capillary-gravity solitary wave of amplitude $\alpha = 0.2$ with $\tau = 74/980$, with the initial condition provided by the fourth-order asymptotic theory.

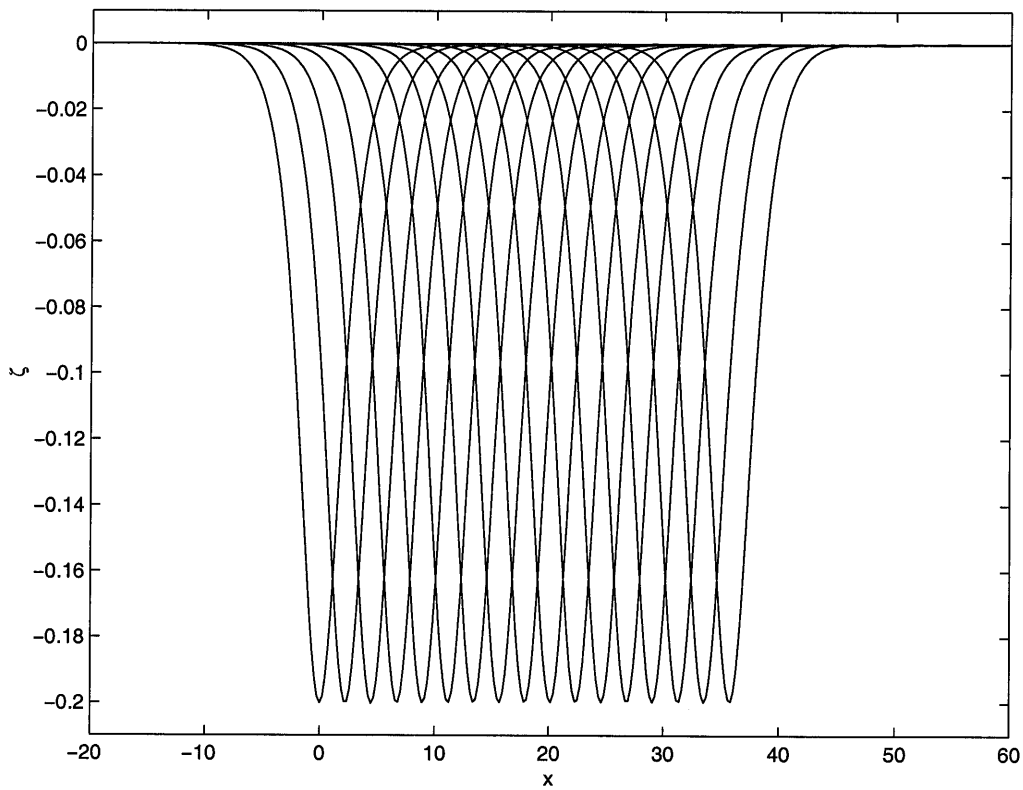

Figure 7.9: Evolution of a terminal capillary-gravity solitary wave of amplitude $\alpha = 0.2$ with $\tau = 2/3$, with the initial condition provided by the fourth-order asymptotic theory.

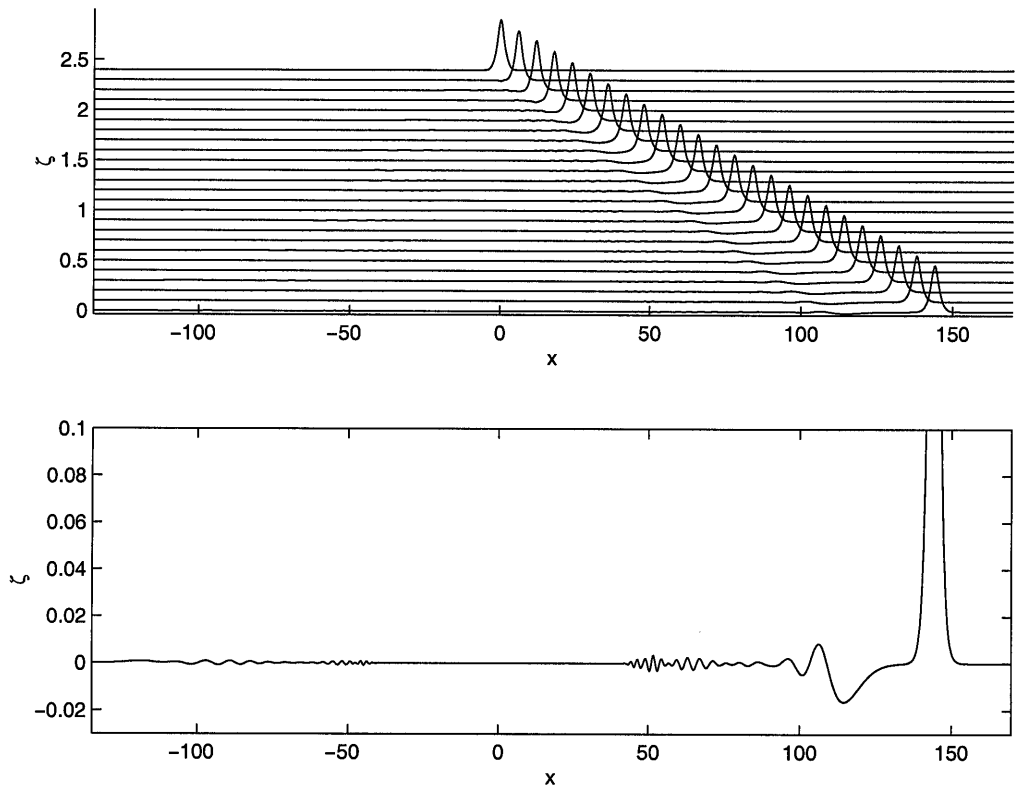

Figure 7.10: Top: Evolution of a capillary-gravity solitary wave of amplitude $\alpha = 0.5$ with $\tau = 74/980$, with the initial condition provided by the solution of the fourth-order asymptotic theory. Bottom: Magnified view of the wave profile at t=120.

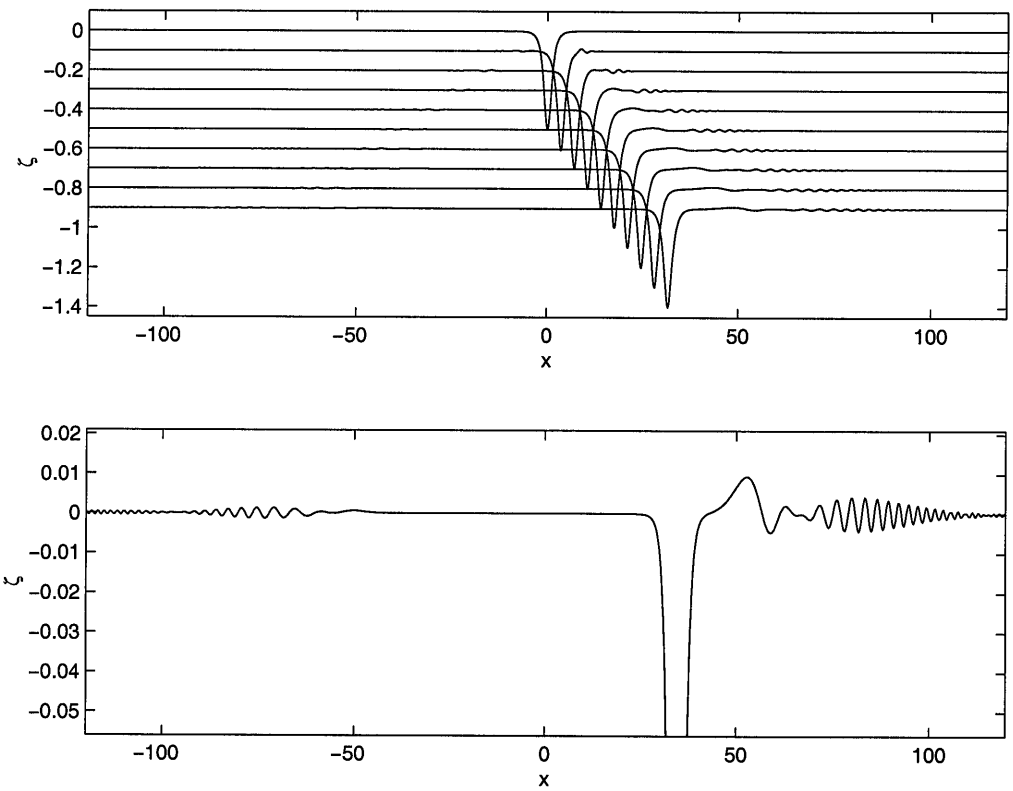

Figure 7.11: Top: Evolution of a capillary-gravity solitary wave of amplitude $\alpha = 0.5$ with $\tau = 2/3$, with the initial condition provided by the solution of the fourth-order asymptotic theory. Bottom: Magnified view of the wave profile at t=50.

Chapter 8 Fully nonlinear internal long-wave model for two-fluid system

8.1 Introduction

Internal waves was first observed by Fridtjov Nansen in 1896, who called it the *dead water* problem. Following that, active research has been stimulated to gain better understanding of flows involving internal waves. Many important engineering problems, such as oil exploration in deep water and mixing processes in the interior of the ocean, are related to the dynamics of internal waves. Internal waves in the ocean and lakes can have very large amplitudes due to the small difference in water density commonly observed. Such large amplitudes are usually beyond the range of validity held for weakly nonlinear theory.

Keulegan (1953) and Long (1956) investigated interfacial solitary waves with the weakly nonlinear Boussinesq equations and the KdV equation. Benjamin (1967) studied the general case of continuous stratification and obtained solitary wave of algebraic profile as a special case. Ono (1975) generalized the work of Benjamin and derived the so called Benjamin-Ono equation. Joseph (1977) and Kubota, Ko & Dobbs (1978) derived a theory for solitary interfacial waves in stratified fluids with finite to large depth. Zhu, Wu & Yates (1987) studied the transcritical two-layer flow over an uneven bottom topography. Evans & Ford (1997) computed stationary interfacial solitary waves of large to maximum amplitude using an exact potential-flow integral equation. Grue et al. (1997) studied the unsteady interfacial waves of large amplitude using a scheme of the pseudo-Lagrange particles. Wu (1996) developed an exact fully nonlinear model for unsteady internal waves for a two-fluid system.

In this chapter, we study the properties of interfacial waves in a two-fluid system based on Wu's model. Section 8.2 discusses the governing equations. The discretiza-

tion of the equations are similar to that described in detail in chapter 4. We present some numerical examples and compare them with the steady solutions of Evans & Ford's (1997) in section 8.4.

8.2 Mathematic formulations

We study two-dimensional inviscid long wave motions under the action of gravity on a two-layer fluid of uniform rest depths h_1 and h_2 and constant densities ρ_1 and ρ_2, respectively, with indices 1 and 2 referring to the lower and upper layers, and with $\rho_2 < \rho_1$ for ensuring the static stability. For simplicity, we consider here the interfacial waves in two-layered fluids bounded top and bottom by two horizontal flat plates of infinite extent. The theoretical results subjected to this confinement are generally useful to provide accurate simulations of the analogous motion in two-layered fluid systems that have the top surface also free to move, as pointed out theoretically and experimently by Zhu et al. (1986, 1987) except for the special case in which the top fluid layer is exceedingly thin compared to the wavelength and for $(1 - \rho_2/\rho_1)$ not very small. A coordinate system is introduced, with the x-axis sitting along the interface at rest and the y-axis pointing upwards as indicated in Figure 8.1. The fluid moves with velocity (u, w) in the flow field bounded below and above by rigid walls at $y = -h_1$ and $y = h_2$, respectively. The interface is represented by $y = \zeta(x, t)$, which is measured from its rest position at $y = 0$ as a function of the horizontal position x and time t. Assuming the fluid incompressible and inviscid, we have the same Euler equations of continuity and momentum as (2.1)-(2.3) for both layers of the fluid, i.e., for $j = 1, 2$,

$$u_{jx} + v_{jy} = 0, \tag{8.1}$$

$$\frac{d\,u_j}{d\,t} = u_{jt} + u_j\,u_{jx} + v_j\,u_{jy} = -\frac{1}{\rho_j}\,p_{jx}, \tag{8.2}$$

$$\frac{d\,v_j}{d\,t} = v_{jt} + u_j\,v_{jx} + v_j\,v_{jy} = -\frac{1}{\rho_j}\,p_{jz} - g \tag{8.3}$$

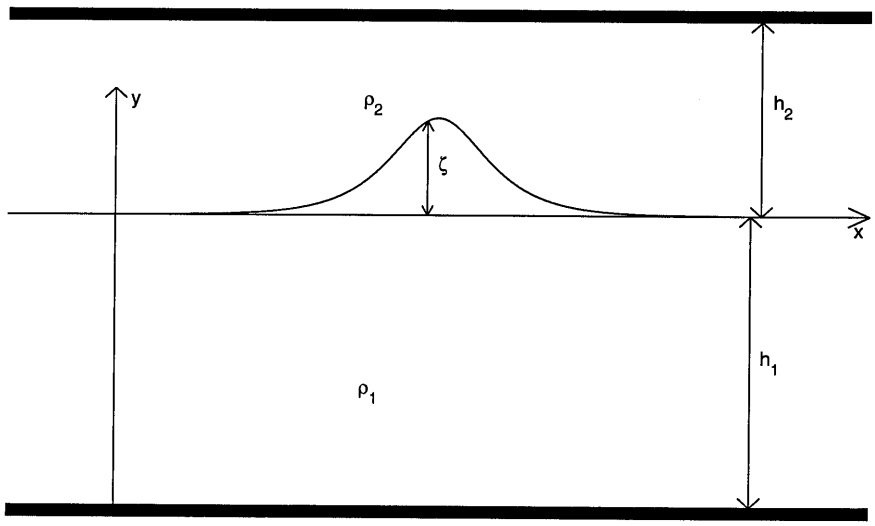

Figure 8.1: Sketch of a two-fluid system.

where p is the pressure, and g the gravitational acceleration. Here, the subscripts denote partial differentiation.

The kinematic boundary conditions at the interface, top and bottom are given by

$$\tilde{v}_j = \zeta_t + \tilde{u}_j\, \zeta_x, \quad (\text{ on } y = \zeta(x,t)), \tag{8.4}$$

$$\underline{v}_1 = 0, \quad (\text{ on } y = -h_1), \tag{8.5}$$

$$\overline{v}_2 = 0, \quad (\text{ on } y = h_2), \tag{8.6}$$

where the underline, overline and tilde represent the variables at the bottom, top and interface, respectively.

The dynamic boundary condition at the interface is

$$\tilde{p}_1(x,t) = \tilde{p}_2(x,t) \qquad (y = \zeta(x,t)) \tag{8.7}$$

where $\tilde{p}_j(x,t)$ is the pressure at the interface and the subindicies $j = 1,\ 2$ refer to the lower and upper layers of fluid, respectively.

The momentum equations can be projected onto the interface, in a way similar to

that illustrated in chapter 2, to obtain an equation for $(\tilde{u}_1, \tilde{u}_2, \zeta)$ as

$$\tilde{u}_{1t} + \tilde{u}_1\tilde{u}_{1x} + [g + \tilde{D_1}^2\zeta]\zeta_x = \sigma\left(\tilde{u}_{2t} + \tilde{u}_2\tilde{u}_{2x} + [g + \tilde{D_2}^2\zeta]\zeta_x\right) \tag{8.8}$$

where

$$\sigma = \frac{\rho_2}{\rho_1}, \quad \tilde{D_j} = \partial_t + \tilde{u}_j\ \tilde{u}_{jx} \qquad (j = 1, 2). \tag{8.9}$$

This equation, though involving only $(\tilde{u_1}, \tilde{u_2}, \zeta)$, has incorporated the vertical momentum equation as well as conditions (8.4) and (8.7)at the interface to yield this equation of an overall equilibrium, as pointed out by Wu (1999b). The interfacial kinematic condition remains intact,

$$\tilde{v_j} \ = \ \tilde{D_j}\zeta \ = \ \zeta_t + \tilde{u_j}\ \zeta_x. \qquad (j = 1, 2) \tag{8.10}$$

The three equations (8.8) and (8.10) involving five variables $(\tilde{v_1}, \tilde{v_2}, \tilde{u_1}, \tilde{u_2}, \zeta)$ are exact. Closure of the system requires finding additional two equations that relate the five variables. For the irrotational motions considered here, the velocity potentials, $\phi_j(x, y, t)$, $(j = 1, 2)$, satisfy, by (8.1), the Laplace equation,

$$\phi_{jxx} + \phi_{jyy} = 0 \qquad (j = 1, 2), \tag{8.11}$$

in there flow domain, respectively. Closure of the system can be accomplished in integral form by adopting two boundary integral equations pertaining to (8.11).

An exact solution of the Laplace equation in integral form may be obtained by Cauchy's integral theorem. Adopting complex analysis, we introduce the complex variable $z_j = x_j + i\, y_j$ and complex velocities $w_j(z) = u_j - i\, v_j$, where $i = \sqrt{-1}$. Since the w_j's are analytic functions of z, we have Cauchy's integral theorem,

$$i\Omega(z)w_j(z_j, t) = \oint_{\partial\mathcal{D}_j} \frac{w_j(z_j', t)}{z_j' - z_j} dz_j', \qquad (j = 1, 2), \tag{8.12}$$

where the contour is counterclockwise along the boundaries $\partial\mathcal{D}$ of the flow domain $\mathcal{D}_j$, $(j = 1, 2)$. Ω is defined in the same way as that in (2.27) and the integrals assume

their Cauchy principal value with $z \in \partial\mathcal{D}_j$.

The rigid-wall conditions (8.5) and (8.6) make it possible to apply Schwarz's principle of symmetry, namely

$$w_1(z^* - 2\,h_1\,i, t) = w_1^*(z), \quad w_2(z^* + 2\,h_2\,i) = w_2^*(z), \tag{8.13}$$

and thereby to avoid the need for calculating the horizontal velocities on the rigid walls. With the original flow domain $\mathcal{D}_j$ extended to $\mathcal{D}_{ej}$ including the mirror images of $\mathcal{D}_j$ (into $y = (-1)^j\,h_j,\ j = 1, 2$), and with $\partial\mathcal{D}_j$ extended to $\partial\mathcal{D}_{ej}$, the boundary of $\mathcal{D}_ej$, we obtain the velocities on the two sides of the interface in terms of the integral equations as follows,

$$\pi i w_1(\tilde{z}) = \int_{-\infty}^{\infty} \frac{w_1(\tilde{z}')}{\tilde{z} - \tilde{z}'} d\tilde{z}' + \int_{-\infty}^{\infty} \frac{w_1^*(\tilde{z}')}{\tilde{z}'^* - 2ih_1 - \tilde{z}} d\tilde{z}'^*, \tag{8.14}$$

$$-\pi i w_2(\tilde{z}) = \int_{-\infty}^{\infty} \frac{w_2(\tilde{z}')}{\tilde{z} - \tilde{z}'} d\tilde{z}' + \int_{-\infty}^{\infty} \frac{w_2^*(\tilde{z}')}{\tilde{z}'^* + 2ih_2 - \tilde{z}} d\tilde{z}'^*, \tag{8.15}$$

in which the contributions from the vertical paths at the two end of the computation region are zero due to the fact that the fluids at infinity are at rest. These two equations provide a closure to equations (8.8) and (8.10) in constituting the set of exact modal equations for FNFD internal waves in this two-layer fluid system.

For the purpose of computation, we adopt two pairs of tangential-like and normal-like velocity components on both sides of the interface,

$$u_{sj} = \tilde{u_j} + \tilde{v_j}\ \zeta_x, \qquad u_{nj} = \tilde{v_j} - \tilde{u_j}\ \zeta_x \quad (j = 1, 2), \tag{8.16}$$

similar to what we did in chapter 4. According to condition (8.10), we have

$$u_{n1} = u_{n2} = u_n. \tag{8.17}$$

In terms of the new unknowns $(\zeta, u_{s1}, u_{s2}, u_n)$, (8.10), (8.8), (8.14) and (8.15) can

be rearranged to produce a new set of exact model equations as

$$\zeta_t = u_n, \tag{8.18}$$

$$(u_{s1} - \sigma u_{s2})_t = -\left[\left((u_{s1}^2 - \sigma u_{s2}^2) - u_n^2(1-\sigma) - 2\, u_n\, \zeta_x(u_{s1} - \sigma u_{s2})\right)/(2R^2)\right]_x - [\zeta(1-\sigma)]_x, \tag{8.19}$$

$$\pi\, i\, (u_{s1}(x) - i u_n(x)) = \int_{-\infty}^{\infty} \left(\frac{z_x(x)}{z(x) - z(x')}\right) (u_{s1}(x') - i\, u_n(x'))\, dx' + \int_{-\infty}^{\infty} \frac{z_x(x)}{z^*(x') - 2\,i\,h_1 - z(x)}\, (u_{s1}(x') + i\, u_n(x'))dx', \tag{8.20}$$

$$-\pi\, i\, (u_{s2}(x) - i u_n(x)) = \int_{-\infty}^{\infty} \left(\frac{z_x(x)}{z(x) - z(x')}\right) (u_{s1}(x') - i\, u_n(x'))\, dx' + \int_{-\infty}^{\infty} \frac{z_x(x)}{z^*(x') + 2\,i\,h_2 - z(x)}\, (u_{s1}(x') + i\, u_n(x'))dx', \tag{8.21}$$

Following Grue et al. (1997), we note that (8.19) suggests us to adopt two new variables, $P = u_{s1} - \sigma\, u_{s_2}$ and $Q = u_{s1} + u_{s2}$, in terms of which (8.19) becomes

$$P_t = -[\frac{p^2(1-\sigma) + \sigma Q^2(\sigma - 1) + 4\sigma PQ}{2(1+\sigma)^2|R|^2} - \frac{u_n\zeta_x}{|R|^2}P + (\zeta - \frac{u_n^2}{2|R|^2})(1-\sigma)]_x. \tag{8.22}$$

In addition, taking the imaginary part of the difference between the (8.20) and (8.21), we have the following equation,

$$\begin{aligned}
\pi Q(x) \;=\; & \frac{2}{1+\sigma} \int_{-\infty}^{\infty} \Im\left(\frac{z_x(x)}{z(x) - z(x')}\right) P(x')dx' \\
& + \frac{\sigma - 1}{\sigma + 1} \int_{-\infty}^{\infty} \Im\left(\frac{z_x(x)}{z(x) - z(x')}\right) Q(x')\, dx' \\
& + \int_{-\infty}^{\infty} \Re\left(\frac{z_x(x')}{z^*(x') - 2\,i\,h_1 - z(x)} - \frac{z_x(x)}{z^*(x') + 2\,i\,h_2 - z(x)}\right) u_n(x')\, dx' \\
& + \int_{-\infty}^{\infty} \Im\left(\frac{z_x(x)}{z^*(x') - 2\,i\,h_1 - z(x)} + \frac{z_x(x)}{z^*(x') + 2\,i\,h_2 - z(x)}\right) \frac{P(x')}{1+\sigma}\, dx' \\
& + \int_{-\infty}^{\infty} \Im\left(\frac{z_x(x)\,\sigma}{z^*(x') - 2\,i\,h_1 - z(x)} - \frac{z_x(x)}{z^*(x') + 2\,i\,h_2 - z(x)}\right) \frac{Q(x')}{1+\sigma}\, dx'.
\end{aligned}$$

(8.23)

Next, taking the sum of (8.20) and the product of σ with (8.21), we have

$$\begin{aligned}
\pi u_n(x) &= \frac{1}{1+\sigma}\int_{-\infty}^{\infty} \Re\left(\frac{z_x(x)}{z(x)-z(x')}\right)P(x')dx' \\
&+ \frac{1-\sigma}{1+\sigma}\int_{-\infty}^{\infty} \Im\left(\frac{z_x(x)}{z(x)-z(x')}\right)u_n(x')dx' \\
&+ \int_{-\infty}^{\infty} \Re\left(\frac{z_x(x)}{z^*(x')-2ih_1-z(x)}+\frac{z_x(x)\ \sigma}{z^*(x')+2ih_2-z(x)}\right)\frac{P(x')}{(1+\sigma)^2}dx' \\
&+ \int_{-\infty}^{\infty} \Re\left(\frac{z_x(x)}{z^*(x')-2ih_1-z(x)}-\frac{z_x(x)}{z^*(x')+2ih_2-z(x)}\right)\frac{Q(x')\ \sigma}{(1+\sigma)^2}dx' \\
&- \int_{-\infty}^{\infty} \Im\left(\frac{z_x(x)}{z^*(x')-2ih_1-z(x)}-\frac{z_x(x)\ \sigma}{z^*(x')+2ih_2-z(x)}\right)\frac{u_n(x')}{1+\sigma}dx'.
\end{aligned} \tag{8.24}$$

Therefore, we have the governing equations (8.18), (8.22), (8.23) and (8.24) for the four unknowns P, Q, u_n and ζ.

In this system, (8.18) and (8.22) provide the time evolution of ζ and P. Given an initial condition, these two equations can update ζ and P to new values. Equations (8.24) and (8.23) close the system by providing u_n and Q with the updated ζ and P. Equations (8.23) and (8.24) are Fredholm integral equations of the second kind, which is well know for its convergence and efficiency in numerical computation for solution. The system (8.18), (8.22), (8.23) and (8.24) will be taken as the model equations for our numerical studies on large-time asymptotic behavior of solitary-like internal waves.

8.3 Stability analysis of the linearized system; the dispersion relationship

We next perform a linear stability analysis of the basic model equations. Assuming (ζ, P, Q, u_n) to be sufficiently smooth and small in magnitude, all of order $O(\epsilon) \ll 1$, we find the linearized version of system (8.18), and (8.22)- (8.24) as

$$\zeta_t = u_n, \tag{8.25}$$

$$P_t = -(1-\sigma)\,\zeta_x, \tag{8.26}$$

$$\begin{aligned}
\pi u_n(x) = & -\int_{-\infty}^{\infty}\left(\frac{x-x'}{(x-x')^2+4h_1^2}+\frac{\sigma\,(x-x')}{(x-x')^2+4h_2^2}\right)P(x')dx' \\
& -\int_{-\infty}^{\infty}\left(\frac{x-x'}{(x-x')^2+4h_1^2}-\frac{x-x'}{(x-x')^2+4h_2^2}\right)\frac{Q(x')\,\sigma}{1+\sigma}dx' \\
& -\int_{-\infty}^{\infty}\left(\frac{2\,h_1}{(x-x')^2+4h_1^2}+\frac{2\,h_2\,\sigma}{(x-x')^2+4h_2^2}\right)u_n(x')dx' \\
& +\int_{-\infty}^{\infty}\frac{P(x')}{x-x'}dx',
\end{aligned} \tag{8.27}$$

$$\begin{aligned}
\pi Q(x) = & -\int_{-\infty}^{\infty}\left(\frac{x-x'}{(x-x')^2+4h_1^2}+\frac{x-x'}{(x-x')^2+4h_2^2}\right)u_n(x')dx' \\
& +\int_{-\infty}^{\infty}\left(\frac{2\,h_1}{(x-x')^2+4h_1^2}-\frac{2\,h_2}{(x-x')^2+4h_2^2}\right)\frac{P(x')}{1+\sigma}dx' \\
& +\int_{-\infty}^{\infty}\left(\frac{2\,h_1\,\sigma}{(x-x')^2+4h_1^2}+\frac{2\,h_2}{(x-x')^2+4h_2^2}\right)\frac{Q(x')}{1+\sigma}dx'.
\end{aligned} \tag{8.28}$$

Applying the Fourier transformation as defined by (4.1) to equations (8.25)-(8.28) and using the relations in table 4.1, we have

$$\mathcal{Z}_t = \mathcal{U}_n, \tag{8.29}$$

$$(\mathcal{P})_t = -i\,k\,(1-\sigma)\,\mathcal{Z}, \tag{8.30}$$

$$\mathcal{U}_n = -i\,\frac{\left(1-e^{-2\,k\,h_1}+\sigma-\sigma\,e^{-2\,k\,h_2}\right)}{(1+\sigma)\,(1+e^{-2\,k\,h_1}+\sigma+\sigma\,e^{-2\,k\,h_2})}\,\mathcal{P}$$

$$+i\ \mathrm{sgn}(k)\ \frac{\sigma}{(1+\sigma)\ (1+e^{-2\,k\,h_1}+\sigma+\sigma\ e^{-2\,k\,h_2})}\ \mathcal{Q}, \tag{8.31}$$

$$\mathcal{Q} = \frac{e^{-2\,k\,h_1}-e^{-2\,k\,h_2}}{1-e^{-2\,k\,h_2}+\sigma-\sigma\ e^{-2\,k\,h_1}}\ \mathcal{P} + i\ \mathrm{sgn}(k)\ (1+\sigma)\ \frac{e^{-2\,k\,h_1}-e^{-2\,k\,h_2}}{1-e^{-2\,k\,h_2}+\sigma-\sigma\ e^{-2\,k\,h_1}}\ \mathcal{U}_n. \tag{8.32}$$

Substituting (8.32) into (8.31) we find, after some regrouping,

$$\mathcal{U}_n = -i\ \mathrm{sgn}(k)\ \frac{1}{1+\sigma}\ \mathcal{P}. \tag{8.33}$$

The solution to the eigenvalue problem for the simplified equations

$$\mathcal{Z}_t = -i\ \mathrm{sgn}(k)\ \frac{1}{1+\sigma}\ \mathcal{P}, \tag{8.34}$$

$$(\mathcal{P})_t = -i\ k\ \mathrm{sgn}(k)\ (1-\sigma)\ \mathcal{Z}, \tag{8.35}$$

$$\tag{8.36}$$

provides, for both $\mathcal{Z}$ and $\mathcal{P}$ bearing a time factor $\exp(i\,\omega\,t)$, the dispersion relation

$$\omega^2 = k\ \frac{1-\sigma}{1+\sigma}, \tag{8.37}$$

which is in agreement with the linearized theory of internal waves.

8.4 Numerical results

We use (8.18), (8.22), (8.24) and (8.23) as the governing equations for computing interfacial solitary waves between two-layer fluids. The Numerical aspects of this problem are similar with those given in chapter 4 which requires no reiteration. We appraise the accuracy of our results with the numerical results of Evans & Ford (1996) which hold only for stationary nonlinear waves. The wave speeds for solitary waves of various amplitudes are compared for the two corresponding cases in table 8.1 for waves under what is commonly taken as an oceanic condition with $\sigma = 0.997$, $h_1 = 3\,h_2$.

Figure 8.2 shows the evolution of a solitary interfacial wave of amplitude $\alpha =$

α	0.2	0.4	0.6	0.8	0.9	0.95	0.99
c	0.050232	0.052267	0.053689	0.054534	0.054744	0.054797	0.054816
c_d	0.050237	0.052268	0.053689	0.054539	0.054761	0.054797	—

Table 8.1: Comparison of c: wave speed computed by Ford & Evans, with c_d: wave speed computed by the numerical method for FNFD unsteady theory over a range of wave of amplitudes for interfacial waves with oceanic condition $\sigma = 0.997$, $h_1 = 3h_2$.

$0.95\,h_2$ as computed with the initial wave profile and wave speed given by the numerical result obtained by using the method of Ford & Evans (1997). It is of importance to note that the initial amplitude $\alpha = 0.95h_2$ is already quite close to the maximum amplitude allowed for any stationary internal solitary wave to reach under the given condition ($\sigma = 0.997, h_1 = 3\,h_2$), which is $\alpha = .9985\,h_2$. In the case at hand, the effect of nonlinearity is very strong for a wave with this large amplitude.

In Figure 8.3 we show the difference between the tangential velocity components of the upper and lower layers at the interface for a solitary wave of amplitude $\alpha = 0.99$ under condition $\sigma = 0.997$, $h_1 = 3h_2$. The velocity jump at the interface can stimulate the Kelvin-Helmholtz instability. The numerical solution becomes unstable with respect to disturbances with wave length shorter than a threshold value λ_{kh}, say. The value of λ_{kh} increases with increasing velocity jump and σ. Figure 8.4 shows a result that may be ascribed to the effect of Kelvin-Helmholtz instability. In our computation for a solitary wave of initial amplitude $\alpha = .99\,h_2$, short waves are observed to be generated at the wave crest and washed down-stream along the current induced by the main long wave. The wave length of the short waves is very closed to the most unstable wave length, computed with the velocity jump at the crest by using the theory of Kelvin-Helmholtz, which suggest these short waves are due to the Kelvin-Helmholtz instability. However, more research will be needed to ascertain whether this set of short waves superposed on the primary long wave can definitely be attributed to the Kelvin-Helmholmz instability along the slowly vary slip-stream of the vortex sheet induced at the interface. Nevertheless, this set of wave train is found to maintain its constancy, both in space and time. This may therefore be regarded as a claim that this example shows that the numerical method developed for evaluating

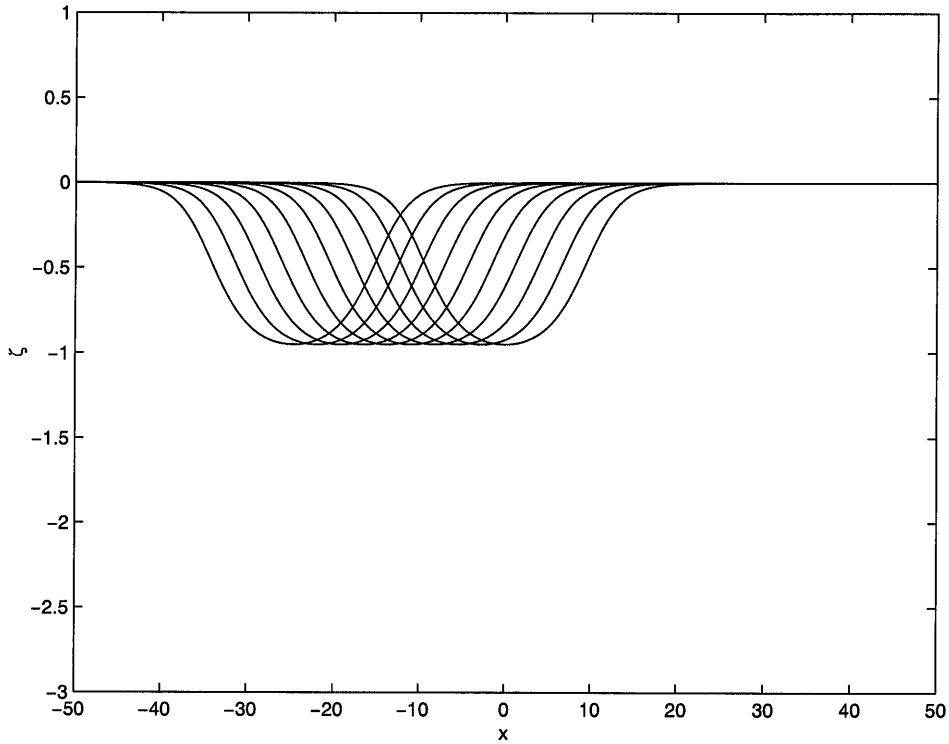

Figure 8.2: Evolution of an internal solitary wave of amplitude $\alpha = 0.95h_2$ under an oceanic condition $\sigma = .997$, $h_a = 3h_2$.

interfacial waves in a two-fluid system is stable and accurate.

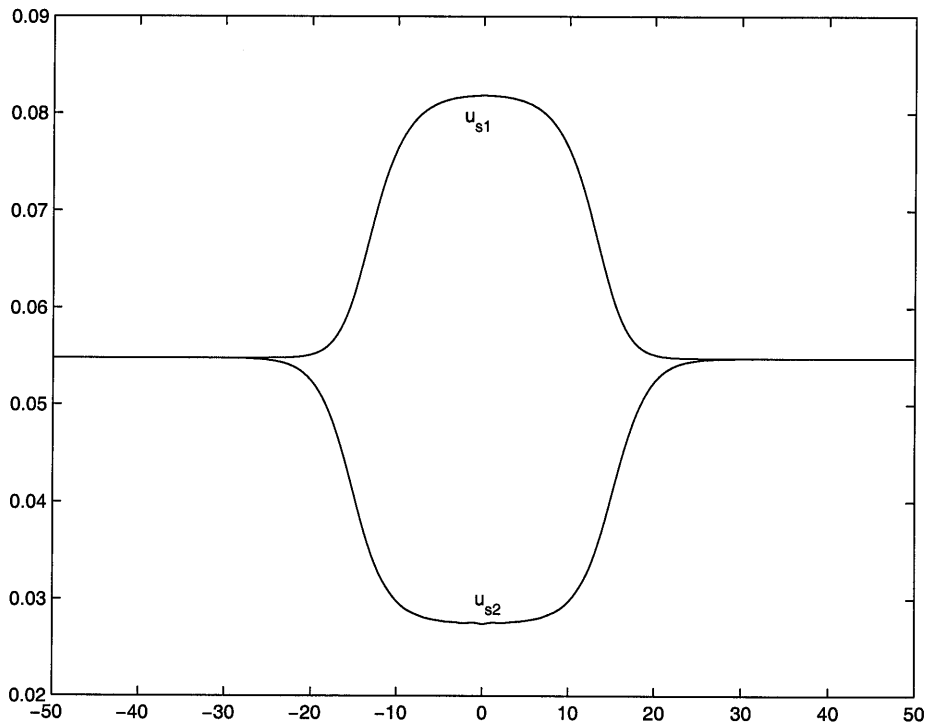

Figure 8.3: The jump in tangential velocity component at the interface for a solitary wave of amplitude $\alpha = 0.99h_2$ under an oceanic condition $\sigma = .997$, $h_1 = 3h_2$.

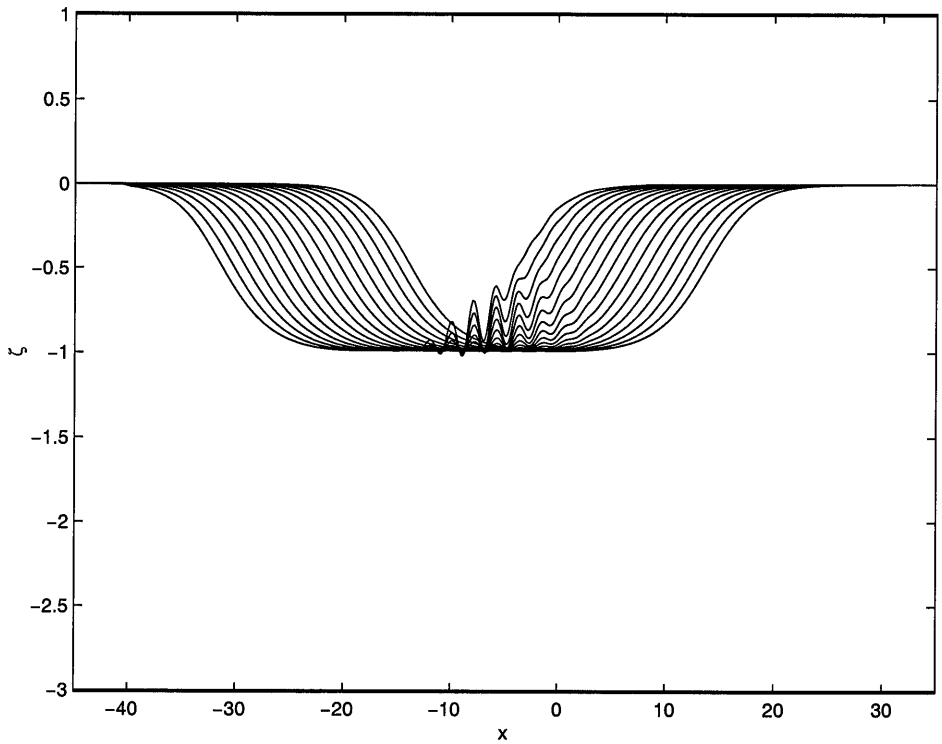

Figure 8.4: Evolution of an interfacial solitary wave of amplitude $\alpha = 0.99h_2$ under an oceanic condition: $\sigma = 0.997$, $h_1 = 3h_2$. A train of short waves are automatically generated and holding robust in space and time.

Chapter 9 Conclusion

In summary of the previous chapters, we may draw the following conclusions:

1. Wu's exact theoretical model for evaluating unsteady, fully nonlinear, fully dispersive, two-dimensional gravity waves on a single layer of water of uniform depth is reviewed in chapter 2. The system of model equations is reduced in spatial dimensions by one from the underlying Euler equations, but otherwise retains the full capacity of the primary system in every respect. The model equations are closed either in differential form, for facilitating theoretical studies and reductive analysis, or in integral form, for numerical computation of exact solutions. In exactness, this theory is fully established by the numerical results obtained in this study for the large time asymptotic wave profile and wave velocity of terminally evolving solitary waves in comparison with the exact solutions based on the permanent solitary wave formalism.

2. A reductive pertubation method is developed to provide higher-order asymptotic theory for solitary shallow water waves in chapter 3. This reductive method provides a constructive way to find higher-order asymptotic solutions for solitary waves. Higher-order perturbation solution up to 15th-order is obtained by asymptotic expansion analysis, and the solution is found to be an asymptotic series which diverge starting from the 12th-order. An optimum approximation to the exact theory is provided at the 11th-order with a maximum relative relative error generally negligible except when the wave amplitude is in a very small neighborhold.

3. Two stable, accurate, and efficient numerical methods, namely, the FNFD method and the Point-vortex method, are developed in chapter 4. The accuracy of the two methods is checked in chapter 5. The Point-vortex method has the advantage of using a self-adaptive mesh provided by Lagrange's markers and is more efficient for computing waves of small to moderate amplitudes. The disadvantage of the Point-vortex method is a result of the fact that Lagrange's markers tend to move

together about wave crests causing a mesh clustering at the wave crest and making the method difficult to compute waves of large amplitudes. The FNFD method, which uses an Euler mesh to avoid the clustering problem, is especially useful for computing evolutions of solitary waves of large amplitudes. The method has been applied to compute unsteady fully nonlinear solitary waves of amplitude up to 0.822 which is very close to the highest amplitude $(0.8331990\cdots)$ of solitary waves that has a cornered crest with a 120° interior angle and a wave speed $c = 1.2908904\cdots$ (Wu & Kao, 2000).

4. Interaction of solitary waves are numerically studied in chapter 6. The results are compared with those given by the asymptotic pertubation method, including the third-order results of Sue & Mirie (1980). The asymptotic perturbation results make good predictions for collisions between waves of small amplitude. Change of flow parter is found possible to occure during collisions between solitary waves of high amplitudes as indicated by the fully nonlinear numerical results.

5. The properties of capillary-gravity solitary waves on a layer of water of uniform depth is investigated both theoretically and numerically in chapter 7. Higher-order asymptotic theories show that the resulting solitary waves are elevation-polarized like solitary gravity waves, moving faster than linear waves, or depression-polarized and moving slower than linear waves according as the Bond number $\tau <$, or $> 1/3$. This is fully confirmed by the numerical computation based on the fully nonlinear model. Higher-order asymptotic theories provide approximations to the fully nonlinear theory with greater accuracy for waves of smaller amplitudes as indicated by comparisons between the two theories.

6. A stable and efficient numerical FNFD method is developed for computing evolutions of interfacial waves in a two-layer fluid system in chapter 8. Comparisons between the results of this FNFD method and those given by the stationary fully nonlinear method of Ford & Evans indicate a very high accuracy of present FNFD method.

In conclusion, it is hoped that the asymptotic theories and the numerical methods developed in this work based on Wu's FNFD model may offer opportunities for further

studies of these very interesting problems. It may also provide a sound starting point for making new advances in areas requiring considerations of other new physical effects that are of importance under differing premises.

Appendix A The Mathematica code used in chapter 3 and 7

Symbles :
Order : the Order of the pertubation equations
zt : ζ, z[i, x] : ζ_i, zpt : ζ', z2t : ζ''
vt : $\underline{u}$, v[i, x] : u_i
ut : $\hat{u}$, wt : $\hat{v}$
eqd : Surface projected dynamic equation
eqk : Kynematic condition at free surface

First Order

■ Settings

```
order = 1; n = order + 1;
zt = Sum[z[i, x] a^i, {i, 1, n}];
vt = Sum[v[i, x] a^i, {i, 1, n}];
zpt = D[zt, x]; z2t = D[zpt, x];
ct = Sum[m[i] a^i, {i, 0, n}];
kt = k0 * (1 + Sum[k[i] a^i, {i, 1, n}]);

ut = Sum[(-a)^i / (2 i)! (1 + zt)^(2 i) kt^(2 i) D[vt, {x, 2 i}], {i, 0, n}];
wt = Sum[(-1)^i a^(i - 1) / (2 i - 1)!
    (1 + zt)^(2 i - 1) kt^(2 i - 1) D[vt, {x, 2 i - 1}], {i, 1, n}];

eqd = Series[zt - ct *ut + ut^2 / 2 + a * kt^2 * (ut - ct)^2 * zpt^2 / 2 -
     τ a kt^2 z2t / (Sqrt[1 + a kt^2 zpt^2]^3), {a, 0, n}];
eqk = Series[wt - kt * (ut - ct) * zpt, {a, 0, n}];

rd0 = Simplify[SeriesCoefficient[eqd, 1]]
rk0 = Simplify[SeriesCoefficient[eqk, 1]]

rk1 = Integrate[rk0, x]

mtx[1] = {{Coefficient[rd0, z[1, x]], Coefficient[rd0, v[1, x]]},
  {Coefficient[rk1, z[1, x]], Coefficient[rk1, v[1, x]]}}
```

solutions

```
m[0] = 1
v[1, x] = z[1, x]
```

Second Order

■ Settings

```
order = 2; n = order + 1;
zt = Sum[z[i, x] a^i, {i, 1, n}];
vt = Sum[v[i, x] a^i, {i, 1, n}];
zpt = D[zt, x]; z2t = D[zpt, x];
ct = Sum[m[i] a^i, {i, 0, n}];
kt = k0 * (1 + Sum[k[i] a^i, {i, 1, n}]);

ut = Sum[(-a)^i / (2 i)! (1 + zt)^(2 i) kt^(2 i) D[vt, {x, 2 i}], {i, 0, n}];
wt = Sum[(-1)^i a^(i - 1) / (2 i - 1)!
    (1 + zt)^(2 i - 1) kt^(2 i - 1) D[vt, {x, 2 i - 1}], {i, 1, n}];

eqd = Series[zt - ct *ut + ut^2 / 2 + a * kt^2 * (ut - ct)^2 * zpt^2 / 2 -
    τ a kt^2 z2t / (Sqrt[1 + a kt^2 zpt^2]^3), {a, 0, n}];
eqk = Series[wt - kt * (ut - ct) * zpt, {a, 0, n}];
rd0 = Simplify[SeriesCoefficient[eqd, 2]];
rk0 = Simplify[SeriesCoefficient[eqk, 2]];
rk1 = Integrate[rk0, x];

tpv = Solve[rk1 == 0, v[2, x]];
v[2, x] = v[2, x] /. tpv[[1]][[1]]

sv0 = Simplify[rd0]

sv1 = Integrate[sv0 * 2 D[z[1, x], x], x]

sv2 = sv1 /. {z[1, x] → y[x], z^(0,1)[1, x] → y'[x]}
```

$$2\left(-m[1]\,y[x]^2+\frac{y[x]^3}{2}+\frac{1}{6}(1-3\tau)\,k_0^2\,y'[x]^2\right)$$

Execute one of the following step:

for τ>1/3:

```
tpc = Solve[(sv2 /. {y[x] → -1, y'[x] → 0}) == 0, m[1]]
```

for 0<τ<1/3:

```
tpc = Solve[(sv2 /. {y[x] → 1, y'[x] → 0}) == 0, m[1]]
```

```
m[1] = m[1] /. tpc[[1]][[1]]
```

$$-\frac{1}{2}$$

```
FullSimplify[sv2]
```

```
a0 = Coefficient[sv2, y[x]^2]
a1 = Coefficient[sv2, y[x]^3]
a2 = Coefficient[sv2, y'[x]^2]
```

```
sv3 = DSolve[c0 y[x]^2 + c1 y[x]^3 + c2 y'[x]^2 == 0, y[x], x] /. C[1] → 0
```

```
Simplify[sv3 /. {c0 → a0, c1 → a1, c2 → a2}]
```

$$\left\{\left\{y[x] \to -\text{Sec}\left[\frac{\sqrt{3}\,x}{2\sqrt{(1-3\tau)\,k_0^2}}\right]^2\right\}, \left\{y[x] \to -\text{Sec}\left[\frac{\sqrt{3}\,x}{2\sqrt{(1-3\tau)\,k_0^2}}\right]^2\right\}\right\}$$

$$k_0 = \frac{\sqrt{3}}{2\sqrt{-(1-3\tau)}}$$

$$\frac{\sqrt{3}}{2\sqrt{-1+3\tau}}$$

```
Simplify[sv3 /. {c0 → a0, c1 → a1, c2 → a2}]
```

$$\{\{y[x] \to -\text{Sech}[x]^2\}, \{y[x] \to -\text{Sech}[x]^2\}\}$$

Solutions

```
m[1]
z[1, x] = -Sech[x]^2
v[1, x] = z[1, x]
```

$$-\frac{1}{2}$$

$$-\text{Sech}[x]^2$$

$$-\text{Sech}[x]^2$$

```
v[2, x]
```

$$\frac{1}{6}\left(3\,\text{Sech}[x]^2 - 6\,\text{Sech}[x]^4 + 6\,z[2, x] + \frac{3\,z^{(0,2)}[1, x]}{4\,(-1+3\tau)}\right)$$

```
v[2, x] = Simplify[v[2, x] /. z^(0,2)[1, x] → D[z[1, x], {x, 2}]]
```

$$\frac{(5-9\tau+(-2+3\tau)\,\text{Cosh}[2x])\,\text{Sech}[x]^4 + 4\,(-1+3\tau)\,z[2, x]}{-4+12\tau}$$

■ Homogeneous solutions

```
y1 = Simplify[D[z[1, x], x]];
y2 = Simplify[y1 Integrate[1 / y1^2, x]];
wr = Simplify[Det[{{y1, y2}, { D[y1, x], D[y2, x]}}]];
```

Higher Orders

Successivly repeat this section with order=order+1

■ settings

```
order = 3;
n = order + 1;
zt = Sum[z[i, x] a^i, {i, 1, n}];
vt = Sum[v[i, x] a^i, {i, 1, n}];
zpt = D[zt, x]; z2t = D[zpt, x];
ct = Sum[m[i] a^i, {i, 0, n}];
kt = k0 * (1 + Sum[k[i] a^i, {i, 1, n}]);

ut = Sum[(-a)^i / (2 i)! (1 + zt)^(2 i) kt^(2 i) D[vt, {x, 2 i}], {i, 0, n}];
wt = Sum[(-1)^i a^(i - 1) / (2 i - 1)!
    (1 + zt)^(2 i - 1) kt^(2 i - 1) D[vt, {x, 2 i - 1}], {i, 1, n}];

eqd = Series[zt - ct * ut + ut^2 / 2 + a * kt^2 * (ut - ct)^2 * zpt^2 / 2 -
    τ a kt^2 z2t / (Sqrt[1 + a kt^2 zpt^2]^3), {a, 0, n}];
eqk = Series[wt - kt * (ut - ct) * zpt, {a, 0, n}];

rd0 = SeriesCoefficient[eqd, ttt];

rk0 = SeriesCoefficient[eqk, ttt];

rk1 = Integrate[rk0, x]

tpv = Solve[rk1 == 0, v[ttt, x]];

v[ttt, x] = v[ttt, x] /. tpv[[1]][[1]]

eq = rd0 /. {z[ttt - 1, x] → y[x], z^(0,2)[ttt - 1, x] → y''[x]};

F = FullSimplify[Coefficient[eq, y''[x]]]
G = FullSimplify[Coefficient[eq, y[x]]]
R = Simplify[F y''[x] + G y[x] - eq];
```

$$-\frac{1}{4}$$

$$1 - 3\,\mathrm{Sech}[x]^2$$

```
yp = TrigExpand[y2 Integrate[y1 R / F, x] - y1 Integrate[y2 R / F, x]];
```

```
Simplify[yp]
```

$$\frac{1}{40\,(1-3\,\tau)^2}\,(\text{Sech}[x]^4\,(21+30\,\tau-135\,\tau^2+40\,m[2]-240\,\tau\,m[2]+360\,\tau^2\,m[2]+$$
$$\text{Cosh}[2\,x]\,(-9+40\,m[2]-30\,\tau\,(3+8\,m[2])+45\,\tau^2\,(5+8\,m[2]))-x\,(-19+40\,k[1]+$$
$$40\,m[2]-30\,\tau\,(-1+8\,k[1]+8\,m[2])+45\,\tau^2\,(1+8\,k[1]+8\,m[2]))\,\text{Sinh}[2\,x]))$$

```
yp0 = FullSimplify[yp /. x → 0];
tpm = Solve[yp0 == 0, m[ttt - 1]]
m[ttt - 1] = m[ttt - 1] /. tpm[[1]][[1]]
```

$$\left\{\left\{m[2]\to\frac{1}{40}\left(-5-\frac{1}{(1-3\,\tau)^2}\right)\right\}\right\}$$

$$\frac{1}{40}\left(-5-\frac{1}{(1-3\,\tau)^2}\right)$$

```
tk = Coefficient[yp, x];
FullSimplify[tk];
tpk = Solve[tk == 0, k[ttt - 2]];
k[ttt - 2] = k[ttt - 2] /. tpk[[1]][[1]]
```

$$-\frac{-5+12\,\tau}{8\,(-1+3\,\tau)^2}$$

Solutions

```
k[ttt - 2]
m[ttt - 1]
z[ttt - 1, x] = FullSimplify[yp]
v[ttt - 1, x]
```

$$-\frac{-5+12\,\tau}{8\,(-1+3\,\tau)^2}$$

$$\frac{1}{40}\left(-5-\frac{1}{(1-3\,\tau)^2}\right)$$

$$\frac{3\,(-1+2\,\tau)\,(1+6\,\tau)\,\text{Sech}[x]^2\,\text{Tanh}[x]^2}{4\,(1-3\,\tau)^2}$$

$$\frac{1}{-4+12\,\tau}\left((5-9\,\tau+(-2+3\,\tau)\,\text{Cosh}[2\,x])\,\text{Sech}[x]^4+\frac{3\,(-1+2\,\tau)\,(-1+3\,\tau)\,(1+6\,\tau)\,\text{Sech}[x]^2\,\text{Tanh}[x]^2}{(1-3\,\tau)^2}\right)$$

```
v[ttt, x] = v[ttt, x] /. z^(0,2)[ttt - 1, x] → D[z[ttt - 1, x], {x, 2}]
```

$$\frac{1}{\sqrt{3}\,(-8+24\,\tau)}\left(16\,(-1+3\,\tau)^{3/2}\left(\frac{3\sqrt{3}\left(17-38\,\tau+24\,\tau^2+\frac{-5+12\,\tau}{(-1+3\,\tau)^2}-\frac{3\,\tau\,(-5+12\,\tau)}{(-1+3\,\tau)^2}\right)\text{Sech}[x]^4}{32\,(-1+3\,\tau)^{5/2}}-\frac{\sqrt{3}\,(53-144\,\tau+144\,\tau^2)\,\text{Sech}[x]^6}{32\,(-1+3\,\tau)^{5/2}}+\frac{1}{80\,(-1+3\,\tau)^{5/2}}\left(\sqrt{3}\,\text{Sech}[x]^2\left(-12+\frac{1}{(1-3\,\tau)^2}+30\,\tau+6\left(-5-\frac{1}{(1-3\,\tau)^2}\right)\tau-9\left(-5-\frac{1}{(1-3\,\tau)^2}\right)\tau^2-\frac{5\,(-5+12\,\tau)}{(-1+3\,\tau)^2}+\frac{15\,\tau\,(-5+12\,\tau)}{(-1+3\,\tau)^2}+\frac{60\,(-1+2\,\tau)\,(1+6\,\tau)\,\text{Sech}[x]^2\,\text{Tanh}[x]^2}{(1-3\,\tau)^2}-\frac{360\,\tau\,(-1+2\,\tau)\,(1+6\,\tau)\,\text{Sech}[x]^2\,\text{Tanh}[x]^2}{(1-3\,\tau)^2}+\frac{540\,\tau^2\,(-1+2\,\tau)\,(1+6\,\tau)\,\text{Sech}[x]^2\,\text{Tanh}[x]^2}{(1-3\,\tau)^2}\right)\right)-\frac{1}{16\,(-1+3\,\tau)^{3/2}}\left(\sqrt{3}\left(-\frac{3\,(-1+2\,\tau)\,(1+6\,\tau)\,\text{Sech}[x]^2\,\text{Tanh}[x]^2}{(1-3\,\tau)^2}+\frac{9\,\tau\,(-1+2\,\tau)\,(1+6\,\tau)\,\text{Sech}[x]^2\,\text{Tanh}[x]^2}{(1-3\,\tau)^2}-\frac{1}{4\,(1-3\,\tau)^2}\left(3\,(-1+2\,\tau)\left(-8\,(1+6\,\tau)\,\text{Sech}[x]^4\,\text{Tanh}[x]^2+(1+6\,\tau)\,\text{Sech}[x]^2\,(2\,\text{Sech}[x]^4-4\,\text{Sech}[x]^2\,\text{Tanh}[x]^2)+(1+6\,\tau)\,\text{Tanh}[x]^2\,(-2\,\text{Sech}[x]^4+4\,\text{Sech}[x]^2\,\text{Tanh}[x]^2)\right)\right)+8\,z[3,\,x]-24\,\tau\,z[3,\,x]\right)\right)\right)\right)$$

References

1. Baker, G.R., Meiron, D.I. & Orszag, S.A. (1982) Generalized vortex methods for free-surface flow problems. *J. Fluid Mech.* **123**, 477-501.

2. Beale, J.T., Hou, T.Y. & Lowengrub, J. (1996) Convergence of a boundary integral method for water waves. *SIAM J. Numer. Anal.* **33**, 1797-1843.

3. Benjamin, T.B. & Feir, J.E. (1967) The disintegration of wave trains in deep water. Part 1. Theory, *J. Fluid Mech.* **27**, 417-430.

4. Benjamin T.B. & Ursell, F. (1954) The stability of the plane free surface of a liquid in vertical periodic motion. *Proc. R. Soc. London Ser. A***225**, 505-515.

5. Benney, D.J. & Luke, J.C. (1964) On the interactions of permanent waves of finite amplitude. *J. Math. and Phys.* **43**, 309-313.

6. Boussinesq, J. (1871) Théorie de l'intumescence liquide appelee onde solitaire ou de translation se propageant dans un canal rectangulaire. *C.R. Acad. Sci. Paris* **72**, 755-759.

7. Boussinesq, J. (1872) Théorie des ondes et des remous qui se propagent le long d'un canal rectangulaire horizontal, en communiquant au liquide contenu dans ce canal des vitesses sensiblement pareilles de la surface au fond. *J. Math. pures appl. Ser. 2*, **17**, 55-108.

8. Byatt-Smith, J.G.B. (1971) An integral equation for unsteady surface waves and a comment on the Boussinesq equation. *J. Fluid Mech.* **49**, 625-633.

9. Camassa, R. (1990) Part 1. Forced generation and stability of nonlinear waves; Part 2. Chaotic advection in a Rayleigh-Benard flow. *Ph.D. thesis*, California Institute of Technology, Pasadena, California.

10. Camasa, R. & Wu, T.Y. (1989) The Kortweg–de Vries model with boundary forcing. *Wave Motion* **11**, 495–506.

11. Camassa, R. & Wu, T.Y. (1991a) Stability of forced steady solitary waves. *Phil. Trans. R. Soc. Lond.* A, **337**, 429-466.

12. Camassa, R. & Wu, T.Y. (1991b) Stability of some stationary solutions for the forced KdV equation. *Physica* D **51**, 295–307.

13. Chan, R. K.-C., Street, R.L. (1970) A computer study of finite-amplitude water waves. *J. Comput. Phys.* **16**, 68-94.

14. Chang, J.-H. (1997) Interaction of solitary waves with structures in viscous fluid. *Ph. D. Dissertation*, National Cheng-Kung University, Tainan, Taiwan.

15. Chappelear, J.E. (1962) Shallow water waves. *J. Geophys. Res.* **67**, 4693-4704.

16. Choi, W. (1993) Forced generation of solitary waves in a rotating fluid and their stability. *Ph.D. thesis*, California Institute of Technology, Pasadena, California.

17. Choi, W. (1995) Nonlinear evolution equations for two-dimensional surface waves in a fluid of finite depth. *J. Fluid Mech.* **295**, 381-394.

18. Choi, W. & Camassa, R. (1996) Weakly nonlinear internal waves in a two-fluid system. *J. Fluid Mech.* **313**, 83-103.

19. Cole, J. D. (1968) *Perturbation Methods in Applied Mathematics.* Waltham: Blaisdell Publ. Co.

20. Cole, S.L. (1985) Transient waves produced by flow past a bump. *Wave Motion* **7**, 579-587.

21. Cooker, M.J., Weidman, P.D. and Bale, D.S. (1997) Reflection of a high-amplitude solitary wave at a vertical wall. *J. Fluid Mech.* **342**, 141-158.

22. Craik, A.D.D. (1993) The stability of some three-dimensional and time-dependent flows. *Proc. IUTAM Symp. on Nonlinear Instability of Nonparallel Flows* (ed. S. P. Lin, W.R.C. Phillips, D.T. Valentine) 397-406, Springer-Verlag. Clarkson University, 26-31 July 1993.

23. Daily, J.W. and S.C. Stephan (1952) The solitary wave. *Proc. Third Conf. on Coastal Engrg.* ASCE, 13-30.

24. Ertekin, R. C., Webster, W. C. & Wehausen, J. V. (1984) Ship-generated solitons. In *Proc. 15th Symp. Naval Hydrodynamics*, 347-364. National Academy of Sciences. Washington, DC.

25. Ertekin, R.C., Webster, W.C. & Wehausen, J.V. (1986) Waves caused by a moving disturbance in a shallow channel of finite width. *J. Fluid Mech.* **169**, 275-292.

26. Faltinsen, O.M. (1977) Numerical solution of transient nonlinear free-surface motion outside or inside moving bodies. *Proc. 2nd Intern. Conf. Numer. Ship Hydrodyn., Berkeley, Calif.* 347-357.

27. Friedrichs, K.O. (1948) On the derivation of the shallow water theory. Appendix to The formation of breakers ans bores by J. J. Stoker. *Comm. Pure Appl. Math.* **1**, 81-85.

28. Friedrichs, K.O. & Hyers, D.H. (1954) The existence of solitary waves. *Comm. Pure Appl. Math.* **7**, 517-550.

29. Green, A.E. & Naghdi, P.M. (1976) A derivation of equations for wave propagation in water of variable depth. *J. Fluid Mech.* **78**, 237-246.

30. Grimshaw, R.H.J. (1971) The solitary wave in water of variable depth. *J. Fluid Mech.* **46**, 611-622.

31. Grimshaw, R.H.J. & Smyth, N.F. (1986) Resonant flow of a stratified fluid over topography. *J. Fluid Mech.* **169**, 429-464.

32. Grue, J., Friis, H.A., Palm, E. & Rusas, P.O. (1997) A method for computing unsteady fully nonlinear interfacial waves. *J. Flluid Mech.* **351**, 233-252.

33. Hirota, R. (1973) Exact N-soliton solutions of the wave equations of long waves in shallow-water and in nonlinear lattices. *J. Math. Phys.* **14**(7), 810-814.

34. Hou, T.Y., Teng, Z. & Zhang, P. (1996) Well-posedness of linearized motion for 3-D water waves far from equilibrium. *Comm. Partial Diff. Equat.* **21** (9 & 10) 1551-1585.

35. Huang, D.B., Sibul, O.J., Webster, W.C., Webausen, J.V., Wu, D.M. & Wu, T.Y. (1982) Ships moving in the transcritical range. *Proc. Conf. Behavior of ship in restricted waters.* Vol. 2, 26/1-26/10. Varna: Bulgarian Ship Hydrodynamics Center.

36. Hunter, J.K. & Vanden-Broeck, J.-M. (1983) Solitary and periodic gravity-capillary waves of finite amplitude. *J. Fluid Mech.* **134**, 205.

37. Isaacson, E. & Keller H. B (1966) *Analysis of Numerical Methods.* New York: Dover

38. Kadomtsev, B. B. & Petviashvili, V. I. (1970) The stability of solitary waves in weakly dispersing media. *Dokl. Akad. Nauk SSR* **192**, 753-756.

39. Kaup, D. J. (1975) A higher-order water-wave equation and the method for solving it. *Prog. Theor. Phys.* **54**, 396-408.

40. Keller, J. B. (1985) Soliton generation and nonlinear wave propagation. *Phil. Trans. R. Soc. Lond. A* **315**, 367-377.

41. Korteweg, D.J. & de Vries, G. (1895) On the change of form of long waves advancing in a rectangular channel, and on a new type of long stationary waves. *Philos. Mag.* **39**, 422-443.

42. Kupershmidt, B. A. (1985) Mathematics of dispersive water waves. *Comm. Math. Phys.* **99**, 51-73.

43. Laitone, E.V. (1960) The second approximation to cnoidal and solitary waves. *J. Fluid Mech.* **9**, 430-444.

44. Lax, P.D. (1968) Integrals of nonlinear equations of evolution and solitary waves. *Comm. Pure Appl. Math.* **21**, 467-490.

45. Lee, S.-J. (1985) Generation of long water waves by moving disturbances. *Ph.D. thesis*, California Institute of Technology, Pasadena, California.

46. Lee, S.-J. & Grimshaw, R.H.J. (1989) Precursor waves generated by three-dimensional moving diatrubances. In *Engineering Science, Fluid Dynamics* (ed. G. T. Yates) 59-74. Singapore: World Scientific.

47. Lighthill, J.M. (1978) *Waves in Fluids.* Cambridge: University Press.

48. Lin, C.C. & Clark, A. Jr. (1959) On the theory of shallow water waves. *Tsing Hua J. of Chinese Studies* Special **1**, 54-62; also in *Selected Papers of C.C. Lin*, 352-360. Singapor: World Scientific. (1987).

49. Liu, H. & Wu, T.Y. (1998) Some solitary wave solutions of fully nonlinear weakly dispersive wave models. *Postprint 3rd Intern. Conf. on Nonlinear Mechanics.* 17-20 Aug. 1998. Shanghai University, China.

50. Longuet-Higgins, M. S. & Cokelet, E.D. (1976) The deformation of steep surface waves on water I. A numerical method of computation. *Proc. R. Soc. Lond. A* **350**, 1-26.

51. Madsen, P.A., Banijamali, B., Schäffer, H.A. & Sorensen, O.R. (1996) Boussinesq type equations with high accuracy in dispersion and nonlinearity *Proc. 25th Intern. Conf. Coastal Engineering* ASCE 95-108.

52. Madsen, P.A., Murray, R. & Sorensen, O.R. (1991) A new form of the Boussinesq equations with improved linear dispersion characteristics. Part 1. *Coastal Engineering* **15**, 371-388.

53. Madsen, P.A. & Sorensen, O.R. (1992) A new form of the Boussinesq equations with improved linear dispersion characteristics. Part 2. A slowly varying bathymetry. *Coastal Engineering* **18**, 183-204.

54. Maxworthy, T. (1976) Experiments on collisions between solitary waves. *J. Fluid Mech.* **76**, 177-185.

55. Mei, C.C. (1983) *The applied dynamics of ocean surface waves.* New York: John Wiley.

56. Miles, J. W. (1984b) Parametrically excited solitary waves. *J. Fluid Mech.* **148**, 451-460; **154**, 535.

57. Nekrasov, A.I. (1921) On waves of permanent type. I. Izv. Ivanovo-Voznesensk. Politekhn. Inst. **3**, 52-65.

58. Nwogu, O. (1993) Alternative form of Boussinesq equations for nearshore wave propagation. *J. Wat. Ways, Port, Coastal Ocean Engng.* ASCE **119**(6), 618-638.

59. Ockendon, J.R. & Ockendon, H. (1973) Resonant surface waves. *J. Fluid Mech.*, **59**, 397-413.

60. Olver, P.J. (1986) *Applications of Lie Groups to Differential Equations.* Springer-Verlag.

61. Peregrine, D.H. (1968) Long waves in a uniform channel of arbitrary cross-section. *J. Fluid Mech.* **32**, 353-365.

62. Power, H. & Chwang, A.T. (1984) On the reflection of a planar solitary wave at a vertical wall. *Wave Motion* **6**, 183-195.

63. Prandtl, L. (1931) Abriss der Strömungslehre. Braunschweig, Vieweg.

64. Rayleigh, Lord (1876) On waves. *Phil. Mag.* **1**, 257-279; Reprinted in *Scientific papers*, vol.1, 251-271.

65. Rayleigh, Lord (1883) On maintained vibrations. *Phil. Mag.***15**, 229-235; On the crispations of fluid resting upon a vibrating support. *Phil. Mag.***16**, 50-58. Reprinted, 1990, in *Scientific Papers*, **2**, 188-193; 212-219. Cambridge: Univ. Press.

66. Russell, John Scott (1844) Report on waves. Rept. 14th Meeting of the British Association for the Advancement of Science, 311-390. London: John Murray.

67. Russell, John Scott (1865) The Modern System of Naval Architecture, Vol 1, Day and Son, London. p. 208.

68. Schäffer, H.A. & Madsen, P.A. (1995) Further enhancements of Boussinesq-type equations. *Coastal Engineering* **26**, 1-14.

69. Schember, H.R. (1982) A new model for three-dimensional nonlinear dispersive long waves. *Ph.D. thesis*, California Institute of Technology, Pasadena, California.

70. Shen, M.C. (1969) Asymptotic theory of unsteady three-dimensional waves in a channel of arbitrary cross section. *SIAM J. Appl. Maths.* **17**, 260-271.

71. Stokes, G.G. (1847) On the theory of oscillatory waves. Trans. Cambridge Phil. Soc. **8** 441-455. In *Math. Phys. Papers*, Vol 1, 197-229. Cambridge: Univ. Press. (1880)

72. Su, C.H. & Mirie, R.M. (1980) On head-on collisions between two solitary waves. *J. Fluid Mech.* **98**, 509-525.

73. Sun, M.G. (1981) Experimental photographs. (Private communication.)

74. Sun, S. M. (1991) Existence of a generalized solitary wave solution for water with positive Bond number less than 1/3. *J. Math. Anal. Appl.* **156**, 471.

75. Tang, C.J., Patel, V.C. & Landweber, L. (1990) Viscous effects on propagation and reflection of solitary waves in shallow water. *J. Comput. Phys.*, **88**, 86-113.

76. Temperville, A. (1979) Interactions of solitary waves in shallow water theory. *Arch. Mech.* **31**, 177-184.

77. Teng, M.H. & Wu, T.Y. (1992) Nonlinear water waves in channels of arbitrary shape. *J. Fluid Mech.* **242**, 211-233.

78. Teng, M.H. & Wu, T.Y. (1994) Evolutioon of long water waves in variable channels. *J. Fluid Mech.* **266**, 303-317.

79. Teng, M.H. & Wu, T.Y. (1997) Effects of channel cross-sectional geometry on long wave generation and propagation. *Phys. Fluids* **9**(11), 3368-3377.

80. Tsai, W. & Yue D.K.P. (1996) Computation of nonlinear free-surface flows. *Ann. Rev. Fluid Mech.* **28**, 249-278.

81. Vanden-Broeck, J.-M. & Shen, M.C. (1983) Z. *angew.* Math. Phys. **34**, 112.

82. Wehausen, J.V. & Laitone, E.V. (1960) Surface Waves. In Handbuch der Physik, Vol IX (ed. S. Flügge; co-ed. C. Truesdell) Springer Verlag.

83. Wei, G., Kirby, J.T., Grilli, S.T. & Subramanya, R. (1995) A fully nonlinear Boussinesq model for surface waves. Part 1. *J. Fluid Mech.* **294**, 71-92.

84. Weidman, P. D. & Maxworthy, T. (1978) Experiments on strong interactions between solitary waves. *J. Fluid Mech.* **85**, 417-431.

85. Whitham, G.B. (1974) *Linear and Nonlinear Waves.* New York: Wiley

86. Wu, D.M. and T.Y. Wu (1982) Three-dimensional nonlinear long waves due to moving surface pressure, *Proc. 14th Symp. on Naval Hydrodynamics*, 103-125. Washington, DC: National Academy Press.

87. Wu, D. M. & Wu, T.Y. (1988) Precursor solitons generated by three–dimensional disturbances moving in a channel. In *Nonlinear Water Waves* (ed. K. Horikawa and H. Maruo) 69–75. Springer–Verlag. IUTAM Symp. on Nonlinear Water Waves, 25-28 Aug. 1987, Tokyo, Japan.

88. Wu, J., Keolian, R. & Rudnick, I. (1984) Observation of a nonpropagating hydrodynamic soliton. *Phys. Rev. Lett.* **52**, 1421-1424.

89. Wu, T. Y. (1979) On tsunami propagation: Evaluation of existing models. *Tsunamis – Proc. National Science Foundation Workshop*, May 7-9, 1979, 110-149. Pasadena: Tetra Tech.Inc.

90. Wu, T. Y. (1981) Long waves in ocean and coastal waters. *J. Engng Mech. Div. ASCE* **107**, 501-522.

91. Wu, T.Y. (1987) Generation of upstream advancing solitons by moving disturbances. *J. Fluid Mech.* **184**, 75-99.

92. Wu, T.Y. (1988) Forced generation of solitary waves. In *Applied Mathematics, Astrophysics, A Symposium to Honor C. C. Lin, 22-24 June 1987*, MIT (ed. D.J. Benney, F.H. Shu & C. Yuan) 198-212. Singapore: World Scientific.

93. Wu, T.Y. (1993a) A bidirectional long-wave model. *Methods and Applications of Analysis* **1**(1), 108-117.

94. Wu, T.Y. (1993b) Stability of nonlinear waves resonantly sustained. *Proc. IUTAM Symp. on Nonlinear Instability of Nonparallel Flows* (ed. S. P. Lin, W.R.C. Phillips, D.T. Valentine) 367-381. Springer-Verlag. Clarkson University, 26-31 July 1993.

95. Wu, T.Y. (1995) Bidirectional soliton street - The Inaugural Pei-Yuan Chou Memorial Lecture (the 6th Asian Congress of Fluid Mechanics. 21-26 May 1995, Singapore). *Acta Mech. Sinica* **11**, 289-306.

96. Wu, T.Y. (1997) On modeling nonlinear water waves. *Proc. 12th Int'l Workshop on Water Waves and Floating Bodies* (Centennial Celebration of Georg Weinblum, March 16-20, 1997, Marseilles, France). 321-324.

97. Wu, T.Y. (1998a) Nonlinear waves and solitons in water. *Physica D* **123**, 48-63.

98. Wu, T.Y. (1998b) On fully nonlinear water waves. *Proc. 3rd Intern. Conf. on Nonlinear Mechanics.* (Ed.-in-Chief, Chien Wei-zang) 119-124. 17-20 Aug. 1998. Shanghai Univ. Press.

99. Wu, T.Y. (1998c) Modeling and computing nonlinear dispersive water waves. *Proc. 3rd Intern. Conf. on Hydrodynaics* (Eds. H. Kim, H.S. Lee and S.J. Lee) 3-9. Seoul, Korea, 12-15 Oct. 1998. Seoul:UIAM Publ.

100. Wu, T.Y. (1999a) Modeling nonlinear dispersive water waves. J. Engrg. Mech. Div. ASCE **125**, 747-755.

101. Wu, T.Y. (1999b) On modeling unsteady fully nonlinear dispersive interfacial waves. 13th U.S. National Congress of Appl. Mech. Yih Memorial Symp., 21–26 June 1998. Gainesville, FL. In *Fluid Dynamics at Interface* (ed. Wei Shyy), 171-178. Cambridge: Univ. Press.

102. Wu, T.Y. & Lin, D. M. (1994) Oceanic internal waves - their run-up on a sloping seabed. In *Physica D* **77**, 97-107.

103. Wu, T.Y. & Zhang, J.E. (1996a) On modeling nonlinear long waves. In *Mathematics is for solving problems: A Volume in honor of Julian Cole on his 70th brithday,* 233-247, SIAM.

104. Wu, T.Y. & Zhang, J.E. (1996b) Mass and energy transfer between unidirectional interacting solitons (A tribute to Prof. C.C. Yu in honor of his 80th Anniversary). *The Chinese Journal of Mechanics* **12**(1), 79-84.

105. Wu, T.Y. & Zhang, J.E. (1996b) Mass and energy transfer between unidirectional interacting solitons (A tribute to Prof. C.C. Yu in honor of his 80th Anniversary). *The Chinese Journal of Mechanics* **12**(1), 79-84.

106. Wu, T.Y. & Kao, J. (2000) Fully nonlinear stationary solitary wave. (to be published).

107. Yates, G. T. (1990) Some antisymmetric solutions with permanent form of the forced KdV equation. In *Engineering Science, Fluid Dynamics* 119-134. Singapore: World Scientific.

108. Yates, G. T. & Wu, T.Y. (1991) Stability of solitary waves under skewed forcing. Volume Festschrifft in honor of Marshall P. Tulin. In *Mathematical Aproaches in Hydrodynamics.* pp. 193-206, SIAM.

109. Yeung, R.W. (1982) Numerical methods in free-surface flows. *Ann. Rev. Fluid Mech.* **14**, 395-442.

110. Yih, C.S. & Wu, T.Y. (1995) General solution for interaction of solitary waves including head-on collisions. *Acta Mech. Sinica* **11**(3), 193-199.

111. Zabusky, N.J. (1967) A synergetic approach to problems of nonlinear dispersive wave propagation and interaction, in *Nonlinear Partial Differential Equations.* New York: Academic Press.

112. Zabusky, N.J. & Kruskal (1965) Interaction of "solitons" in a collisionless plasma and the recurence of initial states. Phys. Rev. Lett., **15**, 240-243.

113. Zakharov, V.E. (1968) Stability of periodic waves of finite amplitude on the surface of a deep fluid. *Z. Prik. Mek. Tekh. Fiziki* **9**, 86-94.

114. Zhang, D.H. & Chwang, A.T. (1996) Numerical study of nonlinear shallow water waves produced by a submerged moving disturbance in viscous flow. *Phys. Fluids*, bf 8, 147-155.

115. Zhu, J.L. (1986) Internal solitons generated by moving disturbances. *Ph.D. thesis*, California Institute of Technology, Pasadena, California.

116. Zhu, J.L., Wu, T.Y. & Yates, G.T. (1986) Generation of internal runaway solitons by moving disturbances. *Proc. 16th Symp. on Naval Hydrodyn. ONR* 186-197. Washigton, DC: National Academy Press.

117. Zhu, J.L., T.Y. Wu and G.T. Yates (1987) Internal solitary waves generated by moving disturbances. *Proc. Third Intl. Symp. Stratified Flows*, ASCE. (eds: E.J. List and G.H. Jirka) 74-83.